UNIVERSIDADE DE LISBOA

FACULDADE DE CIÊNCIAS

DEPARTAMENTO DE ESTATÍSTICA E INVESTIGAÇÃO OPERACIONAL

Uterine Contractions Clustering Based on Surface Electromyography: An Input for Pregnancy Monitoring

Filipa Esgalhado de Oliveira Gouveia Cardoso

Mestrado em Bioestatística

Dissertação orientada por:
Prof. Maria Helena Mouriño Silva Nunes
Prof. Arnaldo Guimarães Batista

2018

Acknowledgements

First and foremost, I must thank my loving family, mom, dad and sister. Thank you for all the support you gave me to complete my studies and for always believing in me. I want to thank my parents for never doubting me and giving me all the tools necessary to succeed. I'll be forever thankful for the enormous opportunity you gave me. To my little sis, a big thank you for your help and for your patience. I will always be here for you.

To my friends, I want to thank you from the bottom of my heart. I will cherish every single call we finally get to make, and I know this amazing friendship will remain even when we are a world apart.

I also want to thank Sara Russo and João Nunes for their contribution in this work, either with code developments or with deep conversations while eating ice cream.

I am grateful to Professor Helena Mouriño and Doctor Duarte Tavares, for the opportunity given to be a part of this project and the support and feedback throughout this thesis.

I am grateful to Professor Fátima Serrano and Doctor Catarina Reis from Maternidade Alfredo da Costa for the collaboration and the unique insight provided to improve this work.

A special thank you to Professor Arnaldo Batista, for the guidance and constant supervision. I am deeply grateful for all the advice, help and patience and to whom I wish all the success in this project.

Abstract

An innovative technique is introduced wherein where an unsupervised clustering method using as feature the whole spectrum of automatically detected contractions on the EHG (Electrohysterogram) is presented as a contribution to the automatic classification of the different uterine contractions, at least those that have been most recognized in the literature: Alvarez and Braxton-Hicks. It was expected to also be able to cluster the LDBF (*Longue Durée Basse Fréquence*) components, as these pose a fetal risk. The main task was to have the spectral contractions descriptions clustered and linked to the respective contraction type. That task was completed with positive identification of the Alvarez and Braxton-Hicks. The clustering process also provided clues regarding the missed Alvarez waves in the contraction detection algorithm, for which an alternative technique is suggested but not developed in this work. Regarding the LDBF they were found in the Braxton-Hicks cluster. It is suggested the LDBF´s to be detected based in their most prominent feature: the long duration. It is presented the rationale behind the selection of a cost function to be used in the spectral distance's algorithm. Spectral distances have been successfully used in audio recognition and this works represents an application to the EHG processing, for which the necessary adjustments have to be implemented. It was found that no single cluster pointed to the preterm cases, or indeed to the pre-labor subject recordings. It is hypothesized, based on previous studies in uterine electrophysiology, that the initiation of pre-term or term labor should be associated with triggering contraction sequences of different types, where the Alvarez waves play a major role. Alvarez and Braxton-Hicks, labeled as such, are not typically used in the clinical environment despite most of the Tocogram detected contractions being the latter. Alvarez waves are not usually detectable by the Tocogram. Alvarez were firstly detected invasively in the early fifties, and Braxton-Hicks in 1872 using routine palpation techniques. The interest in Alvarez components declined rapidly since being practically undetectable by the de facto reference in the contraction detection: the Tocogram. The EHG capabilities and resolution made it possible to revive the research on the most subtle uterine contractions, Alvarez included and this work is a contribution in this research area.

Keywords: Electrohysterogram, Uterine Electromyography, Clustering, Hierarchical Clustering, Preterm labor

Resumo

Inicialmente a investigação da contratilidade uterina recorria à utilização de dois métodos: o tocograma externo e o cateter de pressão intrauterino. Ambos os métodos apresentam limitações ao nível da avaliação do risco de parto prematuro e na monitorização da gravidez. O EHG (Electrohisterograma) é um método alternativo ao tocograma externo e ao cateter de pressão intrauterino. Este método pode ser aplicado de forma invasiva no músculo uterino, ou de forma não invasiva através de elétrodos colocados no abdómen. O EHG tem sido considerado uma ferramenta adequada para a monitorização da gravidez e do parto. O índice de massa corporal tem um impacto quase impercetível no EHG, sendo esta uma das principais características deste método. O EHG pode também ser utilizado para identificar as mulheres que vão entrar em trabalho de parto e ainda auxiliar na tomada de decisão médica quanto à utilização da terapia tocolítica (antagonista da oxitocina), evitando deste modo a ingestão de medicação desnecessária e os consequentes efeitos secundários.

Na literatura existem apenas cinco casos publicados em que foi realizada uma separação dos principais eventos do sinal EHG: contrações, movimentos fetais, ondas Alvarez e ondas LDBF (*Longue Durée Basse Fréquence*). Em três das publicações a separação dos eventos foi feita manualmente e nos restantes casos algoritmos, como redes neuronais, foram aplicados ao EHG. As ondas Alvarez e as Braxton-Hicks são as mais reconhecidas. As ondas Alvarez foram descritas pela primeira vez nos anos cinquenta e as Braxton-Hicks foram descritas pela primeira vez em 1872 sendo detetadas através de palpação. As ondas Alvarez são ocasionalmente sentidas pela mulher. Estas ondas estão localizadas numa pequena área do tecido uterino sem propagação e podem levar a contrações com maior intensidade e, consequentemente, ao parto pré-termo. As Braxton-Hicks são contrações ineficientes registadas a partir da 20ª semana de gravidez que se tornam mais frequentes e intensas com o decorrer da gravidez. Estas contrações são menos localizadas que as ondas Alvarez e, durante o parto, propagam-se por todo o tecido uterino num curto período de tempo. As Braxton-Hicks estão associadas a uma diminuição do ritmo cardíaco fetal. As ondas LDBF são contrações de longa duração associadas a hipertonia uterina, quando há contração do tecido uterino sem retorno ao relaxamento muscular, o que representa um risco na gravidez.

Neste trabalho foram utilizadas duas bases de dados. Na base de dados da Islândia existem 122 registos de 45 mulheres, dos quais apenas 4 correspondem a partos pré-termo. Na base de dados TPEHG (*Term-Preterm EHG*) existem 300 registos, dos quais 38 correspondem a partos pré-termo. Neste trabalho foram escolhidos canais bipolares, visto que estes reduzem o ruído idêntico, como o ECG (Eletrocardiograma) materno ou movimentos respiratórios. Para ambas as bases de dados os sinais originais de EHG foram processados e filtrados.

Na estimação espetral foram considerados dois métodos: paramétricos e não paramétricos. O método Welch foi escolhido pois representa um bom compromisso entre ambos. Este método foi utilizado para calcular o espectro de cada evento detetado no sinal EHG. Para detetar os eventos no sinal EHG foram considerados cinco métodos baseados na energia ou amplitude. O método Wavelet foi o escolhido pois após uma inspeção visual, este era o método que delineava melhor as contrações.

Na base de dados da Islândia foram identificadas 3136 contrações e na TPEHG foram encontradas 4622 contrações. O objetivo principal desta tese é obter *clusters* de contrações detetadas no sinal EHG. No entanto, as contrações são séries temporais não estacionárias, e a sua classificação visual é inviável a longo termo e também difícil de aplicar na prática clínica. Existem vários parâmetros que

podem ser extraídos do sinal EHG, mas o espectro das contrações foi o método escolhido visto que este representa o sinal EHG e tem sempre a mesma dimensão, independentemente da duração da contração.

As distâncias espetrais têm sido utilizadas com sucesso no reconhecimento áudio. Neste trabalho foi realizada uma aplicação desse método ao processamento do EHG, no qual foram realizados os ajustes necessários. Para comparar os espectros foram estudadas 8 distâncias diferentes: Itakura-Saito, COSH, Itakura, Itakura simétrica, Kullback-Leibler, Jeffrey, Rényi e Jensen-Rényi. Apenas as distâncias simétricas foram selecionadas para um estudo mais detalhado visto que estas são, segundo a literatura, as distâncias mais adequadas aquando do *clustering*. Após comparação das distâncias simétricas, a divergência de Jeffrey foi a selecionada para a comparação dos espectros.

Nesta tese foram avaliados três métodos diferentes de *clustering*: o linkage, o K-means e o K-medoids. O linkage é um método hierárquico. Os *clusters* que resultam do agrupamento hierárquico estão organizados numa estrutura chamada dendrograma. No agrupamento hierárquico, não é necessário predeterminar o número de *clusters*, o que torna este um método ideal na exploração dos dados. O K-means e o K-medoids são métodos de partição, nos quais os dados são separados em k *clusters* decididos previamente. Os *clusters* são definidos de forma a otimizar a função da distância. No algoritmo K-means, os *clusters* baseiam-se na proximidade entre si de acordo com uma distância predeterminada. A diferença entre o K-medoids e o K-means é que o K-medoids escolhe pontos de dados como centros, chamados de medoides, enquanto K-means usa centróides. Após uma comparação dos diferentes métodos de *clustering* foi escolhido neste trabalho foi o *average linkage*, visto que este apresentava melhores resultados quer na separação dos espectros quer na silhueta.

É então apresentado um método inovador no qual se utiliza todo o espectro das contrações detetadas automaticamente no EHG para o *clustering* não supervisionado. Esta técnica é uma contribuição para a classificação automática das diferentes contrações, especialmente aquelas mais reconhecidas na literatura: Alvarez e Braxton-Hicks. Era expectável encontrar um *cluster* isolado com as ondas LDBF, visto que estas representam um risco para o feto. O principal objetivo era juntar num *cluster* os espectros semelhantes das contrações, e relacioná-lo com o respetivo tipo de contração. Essa tarefa foi concluída através da identificação positiva de Alvarez e Braxton-Hicks. O *clustering* forneceu ainda algumas pistas sobre ondas Alvarez que não foram encontradas com o algoritmo de deteção de contrações, situação para a qual um método alternativo é apresentado. É sugerido que as ondas Alvarez sejam detetadas com métodos baseados na frequência, como, por exemplo, a frequência instantânea, no entanto este método não foi desenvolvido neste trabalho. Em relação às ondas LDBF, estas foram encontradas no *cluster* das Braxton-Hicks. É sugerido que a deteção das ondas LDBF seja baseada na sua caraterística mais distinta: a longa duração. Verificou-se que os casos pré-termo e os registos pré-parto não ficaram isolados num *cluster*, não se tendo encontrado uma relação entre a idade gestacional e o tipo de contração. Conclui-se que as contrações mais curtas apresentam maior amplitude do que as contrações com maior duração. Baseado em estudos anteriores sobre a eletrofisiologia do útero, supõem-se que o início do trabalho de parto pré-termo e termo esteja associado a sequências específicas de diferentes tipos de contrações, nas quais as ondas Alvares desempenham um papel importante. As contrações identificadas como Alvarez e Braxton-Hicks não são usadas como tal na prática clínica apesar de a maioria das contrações detetadas pelo tocograma serem Braxton-Hicks. O interesse pelas ondas Alvarez diminuiu rapidamente visto que estas ondas são praticamente indetetáveis pelo método de referência de deteção de contrações: o tocograma. As capacidades e a resolução do EHG levaram à renovação do estudo das contrações mais subtis, incluindo as Alvarez. Este trabalho é uma contribuição para a investigação nesta área.

Palavras-chave: Electrohisterograma, Electromiografia Uterina, *Clustering*, *Clustering* hierárquico, Parto Pré-termo

Contents

List of figures

List of tables

List of Attachments

Acronyms

AAR – Adaptive Autoregressive

AR – Autoregressive

ANN - Artificial Neural Network

AUC – Area Under Curve

BMI – Body Mass Index

ECG - Electrocardiogram

EHG – Electrohysterogram

EMG – Electromyography

FECG – Fetal Electrocardiogram

FFT – Fast Fourier Transform

GA – Gestational Age

H^2 – Nonlinear Correlation coefficient

HR – Heart Rate

IS – Itakura-Saito

IUP - Intrauterine Pressure

IUPC – Intrauterine Pressure Catheter

KL – Kullback-Leibler

LAHF – Low Amplitude High Frequency

LDBF – *Longue Durée Basse Fréquence*

LDA – Linear Discriminant Analysis

PCA – Principal Component Analysis

PSD – Power Spectral Density

QDA – Quadratic Discriminant Analysis

RBF – Radial Basis Function

RMS – Root Mean Square

ROC – Receiver Operating Characteristic

SE – Sample Entropy

SMOTE - Synthetic Minority Over-sampling Technique

SVM – Support Vector Machine

TOCO – Tocodynamometry

TPEHG – Term-Preterm EHG

TR – Time Reversibility

USCM – Unsupervised Statistical Classification Method

UPGMA – Unweighted Pair Group Method with Arithmetic Mean

UPGMC – Unweighted Pair Group Method Centroid

VarEn – Variance entropy

WT – Wavelet Transform

WPGMA – Weighted Pair Group Method with Arithmetic Mean

WPGMC – Weighted Pair Group Method with Arithmetic Centroid

Chapter 1 - Introduction

The EHG (Electrohysterogram) has been presented as modern method for pregnancy and labor monitoring. External TOCO (Tocography) and IUPC (Intrauterine Pressure Catheter) are the classic techniques in pregnancy monitoring. TOCO is widely used in labor monitoring but this method has low accuracy and limited conveyed information.[1] The golden standard for measuring the uterine pressure is the IUPC but this method is invasive can be only used in women with ruptured membranes, so not adequate for continuous pregnancy monitoring. The Tocogram acquisition pose a problem for subjects with high BMI (Body Mass Index). Both IUPC and TOCO have very limited application in preterm risk evaluation. Since the uterine contractibility is electrical triggered in the myometrium tissue, an EMG (Electromyography) signal is generated, and named EHG. The EHG signal accurately represents the contractile uterine activity and can be non-invasively recorded at the abdominal surface.[2] The BMI impact on the EHG amplitude is practically negligible, and this feature is one of the flagships of this technique.[3]

In recent times the EHG has been considered the adequate tool for pregnancy and labor monitoring. Research work is progressing regarding the use of this tools for this task as well as preterm risk evaluation.[1]

Preterm birth, defined as occurring before 37 weeks of gestation, is a major cause of infant mortality and morbidity worldwide. According to the World Health Organizations the prevalence of preterm birth is 1 in 10 babies, 15 million babies per year, which presents a public health problem.[4] Premature babies have a higher risk for short and long-term complications, like cerebral palsy, breathing and hearing problems, development delay and vision difficulties.[5] In Portugal, between 2011 and 2016 the preterm birth rate as increased from 7.4% to 7.8% and in 2015 was registered the highest value, 8.0%.[6]

Labor monitoring may also benefit from the EHG technique. True labor detection may be a challenging task and the EHG has been reported as having a positive contribution. It is a technique that can be used to identify subjects that will enter the labor phase within 24-72 hours as well as those requiring augmentation of labor (oxytocin administration).[7]

The EHG can also contribute to improve the medical decision for the administration of tocolytic therapy (oxytocin antagonist). In both cases it can be avoided unnecessary drug therapy and its side effects.

Either preterm risk evaluation or labor monitoring using the EHG must deal with the fact that this is a complex electrical signal conveying information regarding uterine contractibility characteristics namely contraction features. In many instances the EHG has been used as a contraction detector likewise the tocogram. However, the signal itself should have embedded the different uterine contractions types that are currently accepted to exist, namely Braxton-Hicks and Alvarez. The idea behind this work project is to automatic detect these features or possibly additional ones. Ideally these unsupervised clustering process could lead to earlier preterm risk and true labor warnings.

In this work the EHG signals from the TPEHG database[8] and the Icelandic 16-electrode database[9] will be analyzed. Both databases will be submitted to algorithms of contraction detection and spectral analysis. New databases will be created with the features extracted from the EHG signal and hierarchical clustering will be implemented. The main goals of this work are:

- Isolate contractions in the EHG signal;

- Distinguish spectra of contractions through the cluster analysis;
- Determine if there is a relation between contractions, preterm birth and true labor;
- Contribution to the understanding of uterine electrophysiology mechanisms.

Regarding the EHG application several electrode applications are being used by the research community. Figure 1.1[10–12] represents just a few of them.

(a)

(b)

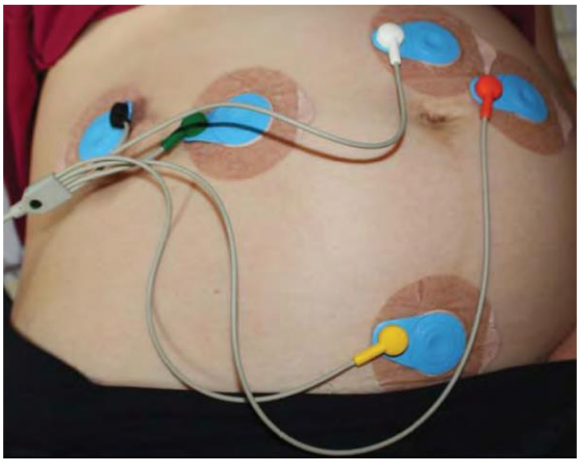

(c)

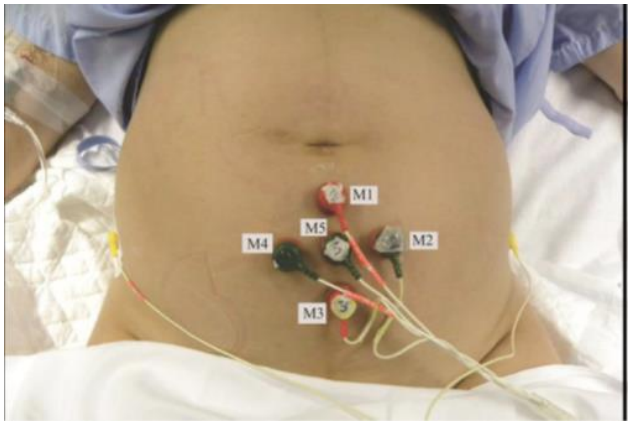

Figure 1.1: Electrodes localizations in different researches. (a) – Ye-Lin et al.[10] (b) – Hayes-Gill et al.[11] (c) – Garfield et al.[12]

1.1 State of the art

The research of uterine contractibility started with two possible ways of recording: external measurement with a tocotransducer, that is positioned on the abdominal wall or intrauterine pressure measurement by means of a catheter. In 1931 the first EHG signal was recorded with abdominal electrodes and internal electrodes.[13]

Marque et al. recorded 14 women with electrodes placed in the abdominal wall. The researchers concluded that the pregnancy EHG characterized by low frequencies and a long duration and the labor EHG presented higher frequencies. The high frequencies in EHG are related to a coordinated labor uterine activity.[13]

Newman et al. studied the low amplitude high frequency contractions referred by Alvarez and Caldeyro. Recordings were made in 142 women with external tocodynamometry, 92 of them were at high risk of premature labor. From the 142 women, 136 presented the low amplitude high frequency contractions on at least one occasion. The greater prevalence of this type of contraction among the women that developed preterm labor and the reduction of this pattern after the initiation of tocolytics seems to support the idea that the uterus of these women is predisposed to premature synchronization of uterine activity.[14] Roberts et al. reached a similar conclusion to Newman stating that women that experience uterine irritability have a higher risk of occurrence of preterm birth.[15]

Khalil et al. analyzed synthetic EHG signals and EHG signals from 32 women. Experts identified four different events: contractions, fetus motions, Alvarez waves and LDBF (*Longue Durée Basse Fréquence*) waves, Figure 1.3[16]. To detect these events Wavelet Transform, Neural Networks and Dynamic Cumulative Sum were applied to the EHG signal. The algorithm detection presented satisfactory results. This study was the first to classify events in the EHG signal.[16] It should be noticed that the signals shown from Figure 1.3 to Figure 1.7 do not clearly show the respected time features. An effort is being made in this work to show the EHG signals with great detail. This led to eventually being able to visually identify the Alvarez components.

Chendeb, M. analyzed 50 events for each class identified by the experts. The classes were: contractions, fetus motions, Alvarez waves, LDBF waves and baseline activity. SVM (Support Vector Machines) algorithms were used to perform the classification. An example of Alvarez waves can be observed in Figure 1.4.[17]

Marque et al. recorded 9 pregnant women for the contraction evaluation and the recordings of fetal movements, Figure 1.5[18], were performed in 8 women. The EHG signal and the ultrasound were recorded at the same time. Every time the women felt a contraction or a fetal movement a recording was made. These makers serve as a reference during the analysis of the EHG signal as an indicator of the presence of a contraction. Only 55 contractions were registered of which 51 were pointed out by the women. The bursts associated with contractions from the 23rd week of gestation have a duration longer than 2 minutes and the bursts associated with contractions closer to term have a duration inferior to 2 minutes. The Alvarez waves, Figure 1.6 top[18], frequent contractions with low amplitude, were registered in 3 women. No relation between the uterine activity and the pregnancy term could be established at the time of this study. Two types of spontaneous contractile activities during pregnancy than can be recorded by EHG since the 23rd week of pregnancy. The spectral characteristics of the contractions change during pregnancy. The fetal movements recorded from pregnancies longer than 28 weeks seem to have different characteristics than the contractions recorded at the same time. Typically, the spectrum of the

contractions is obtained using the PSD (Power Spectral Density) which describes how the power of a time series is distributed along the frequency. The units are V^2/Hz.[18]

Sousa, C. analyzed the EHG signals from the Icelandic 16-electrode EHG database and found the following events: Alvarez waves, Contractions, Early and Late Labor Contractions, Fetal Movements, LDBF waves, Fetal Hiccups and Basal Uterine Activity. The spectral analysis and power estimation were used in the evaluation of events.[19]

Chendeb et al. analyzed 100 real events for each class identified by the experts. The classes were: contractions, fetus motions, Alvarez waves, LDBF waves and noise. The researchers used Neural Networks and SVM algorithms to perform the classification. They reported a success rate of 85%. An example of the separated events can be observed in Figure 1.7.[20]

Neither of the studies referred above included in their classification Braxton-Hicks contractions, reported by Braxton-Hicks[21] in 1872. These contractions were the first to be described in literature however, most of the studies do not include the classification Braxton-Hicks contractions.

In the last decades research in this field as grown with the introduction of new methods powered by a development of computational power. Ample research using EHG signals has been done, especially in the last decade. These studies can be divided in two groups: when the research includes the complete EHG signal, presented in Attachment 1, and when the research only includes segmented bursts of the EHG signal, presented in Attachment 2. The studies that included spectral features are highlighted in grey.

Nowadays, there is pregnancy monitoring equipment available to the public based in the EHG signal.[11] These systems have the American Food and Drug administration clearance and European Commission mark. Four different devices are already in the market: OB-Tools, Monica *Novii* monitors from Monica Healthcare®, Figure 1.2 left[22], PUREtrace from NEMO Healthcare®, Figure 1.2 right[23], and SureCALL® Labor Monitor®. These systems have been used mainly to detect contractions and FECG (Fetal Electrocardiogram). However, they are not wide spread used in the clinical environment. The flagship of these systems is being able to monitor the uterine contractions in a subject with a high BMI. As far as it has been investigated, none of these systems provide contractions identification. Manly they seem to aim to replace the tocogram and perform FECG.

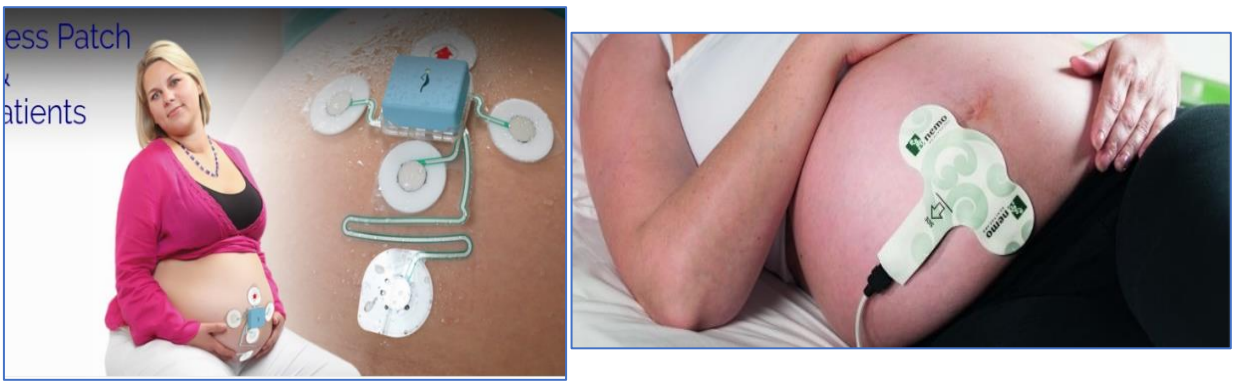

Figure 1.2: Pregnancy monitoring devices based on EHG signal. Left: Monica *Novii* monitors from Monica Healthcare® [22]; Right: PUREtrace from NEMO Healthcare® [23]

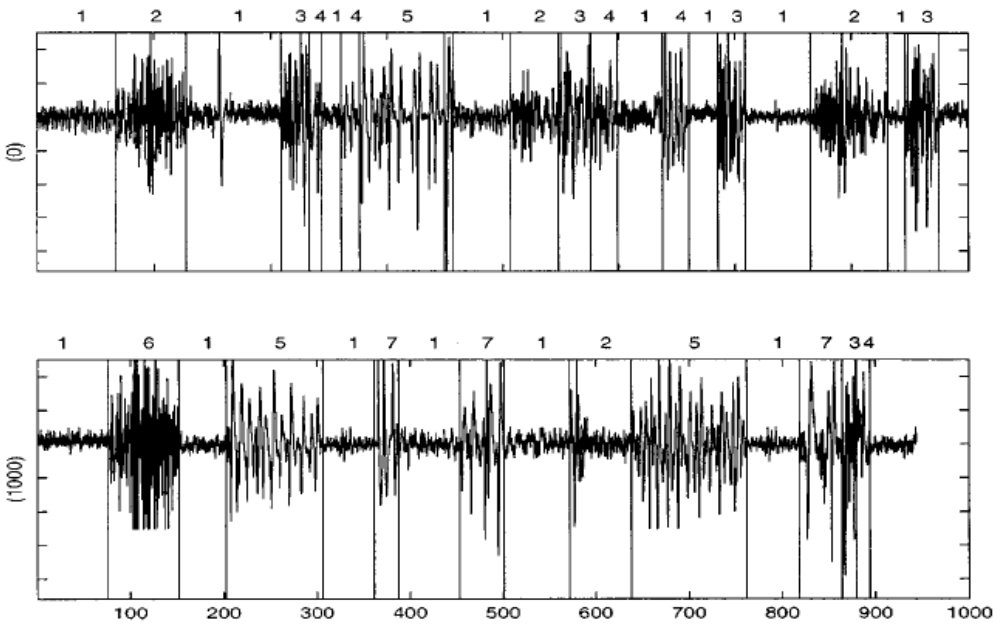

Figure 1.3: Detection and classification of events in uterine EHG. Label: 1- Background activity, 2 and 6- Contractions, 4 and 7- Fetus motions, 5- LDBF waves, 3- Alvarez waves.[16]

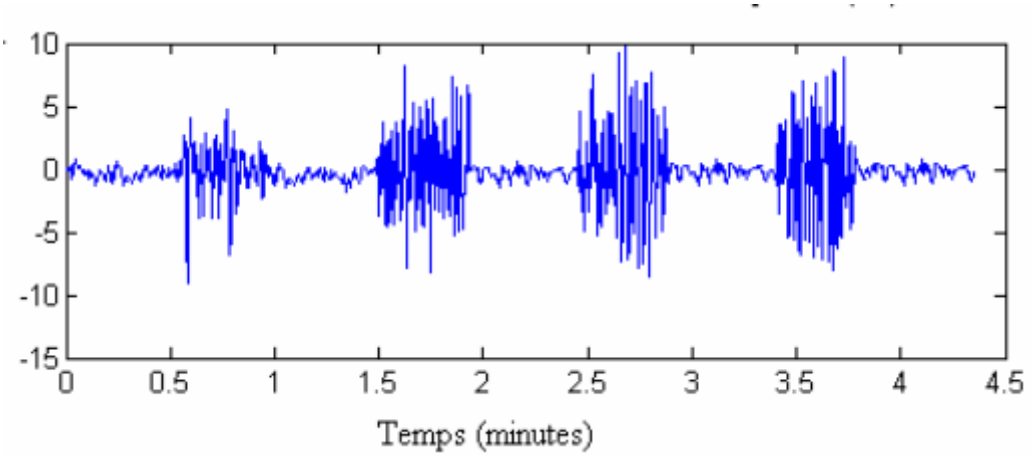

Figure 1.4: EHG signal with detected Alvarez waves. The X axis represents the time in minutes and the Y axis represents the amplitude scale in arbitrary units.[17]

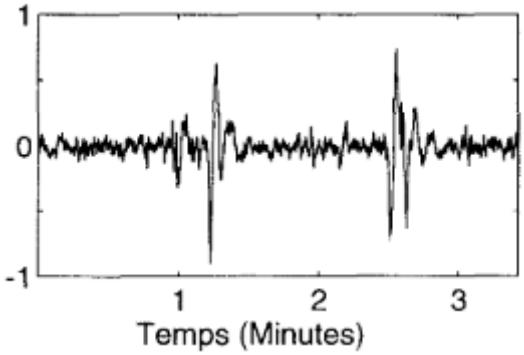

Figure 1.5: Fetal movement detected in the EHG at the 33rd week of gestation. The signal was filtered between 0.02 to 6 Hz. The X axis represents the time in minutes and the Y axis represents the amplitude scale in arbitrary units.[18]

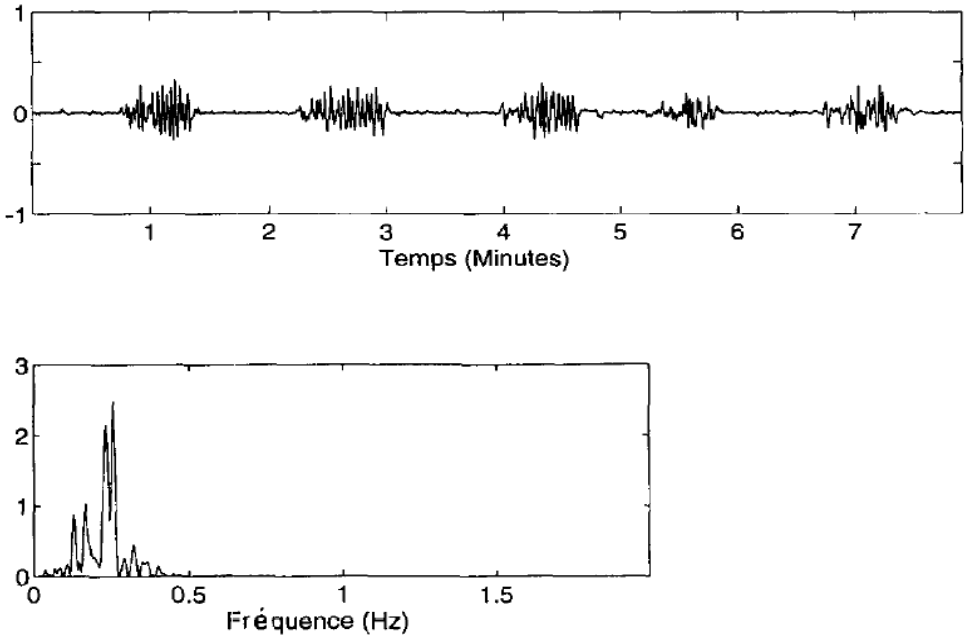

Figure 1.6: Top: EHG signal in which Alvarez waves are represented. The signal was filtered between 0.02 to 6 Hz. The X axis represents the time in minutes and the Y axis represents the amplitude scale in arbitrary units. Bottom: PSD of the first Alvarez wave represented above. The X axis represents the frequency in Hz.[18]

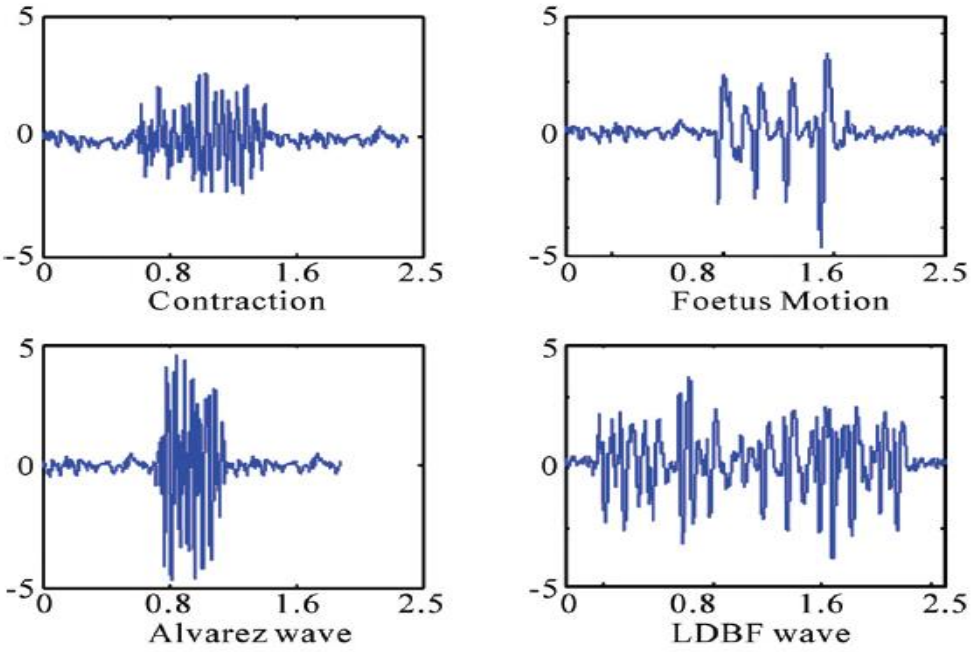

Figure 1.7: Classification of events in the uterine EHG. The X axis represents the time in minutes and the Y axis represents the amplitude scale in arbitrary units.[20]

1.2 Thesis organization

The thesis outline is:

- Chapter 1: Introduction of the theme, state of the art and thesis outline.
- Chapter 2: Brief description of uterine anatomy and physiology and definition of preterm birth.
- Chapter 3: Description of the methods used to monitor uterine activity, with emphasis in electrohysterography. The EHG signal and its main components are presented.
- Chapter 4: Description of the methods used in the EHG signal processing and filtering. The method used in spectral analysis is also contemplated in this chapter.
- Chapter 5: Contraction detection methods.
- Chapter 6: Theoretical basis of different distances applied to the spectra of the separated contractions.
- Chapter 7: Theoretical basis of clustering analysis.
- Chapter 8: Clustering results of the Icelandic and TPEHG databases.
- Chapter 9: Principal conclusions, achievements of this work and proposals for future work.

Chapter 2 – Uterus's anatomy and physiology

2.1 Anatomy of the uterus

The uterus, Figure 2.1[24], is a pear-shaped organ and is entirely located in the lesser pelvis, between the bladder and the rectum. In the non-pregnant state the uterus has 7.5 cm in length, 4 to 5 cm in width at its upper portion, 2 to 3 cm in thickness and weights between 30 and 80g.[24,25]

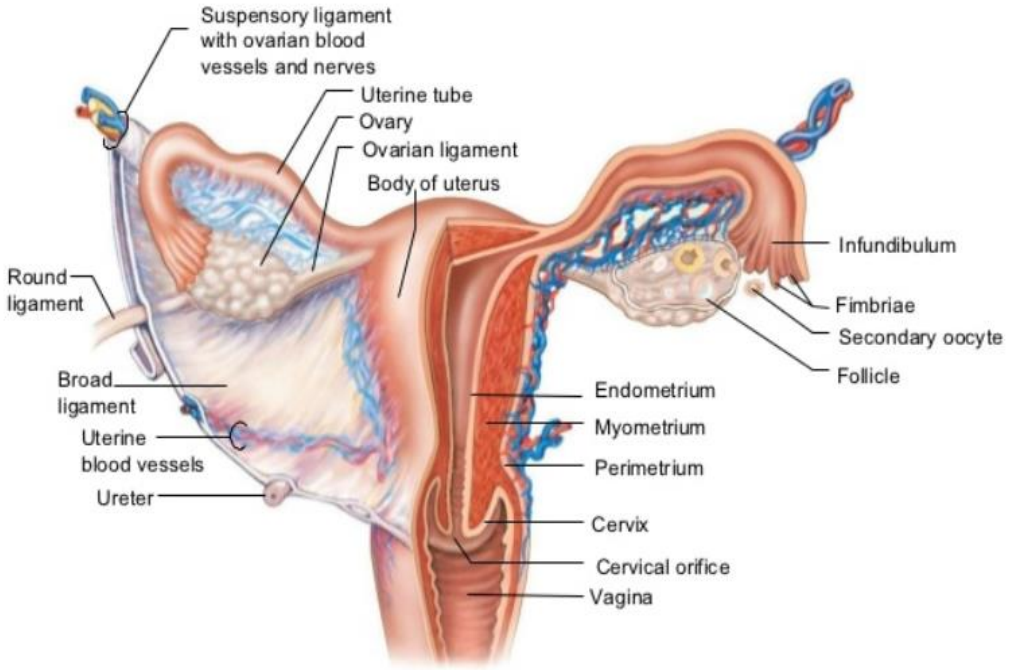

Figure 2.1: Anatomy of the uterus.[24]

This complex muscular organ is essential to reproduction since it receives the embryo and sustains its development.[24] The uterus is composed by the fundus, upper portion of the uterus, the corpus, also called body of the uterus, and the cervix, a narrow caudal portion composed of dense fibrous connective tissue and muscle cells. The uterus is suspended by several supporting ligaments called endopelvic fascia. The uterine wall is part of this organ and is composed of three layers. The perimetrium consists of an outer serosal layer, that supports and covers the body of the uterus and part of the cervix. The endometrium, the inner mucosal layer, is covered with columnar epithelium and contains tubular glands. It is thickness changes throughout the menstrual cycle and it is thickest during the ovulation period since is preparing for the implantation of a fertilized egg. The myometrium, the middle muscular layer, composed by smooth muscle fibers in longitudinal, circular, and spiral patterns. This layer is thickest and during the pregnancy it increases due to hypertrophy of the existing cells and increase of the cell number. [25–27] Through the pregnancy the uterus enlarges and no longer stays confined to the pelvic cavity, it extends upwards, Figure 2.2[28]. The uterus grows during the pregnancy increasing its weight around 1.4kg.[29,30]

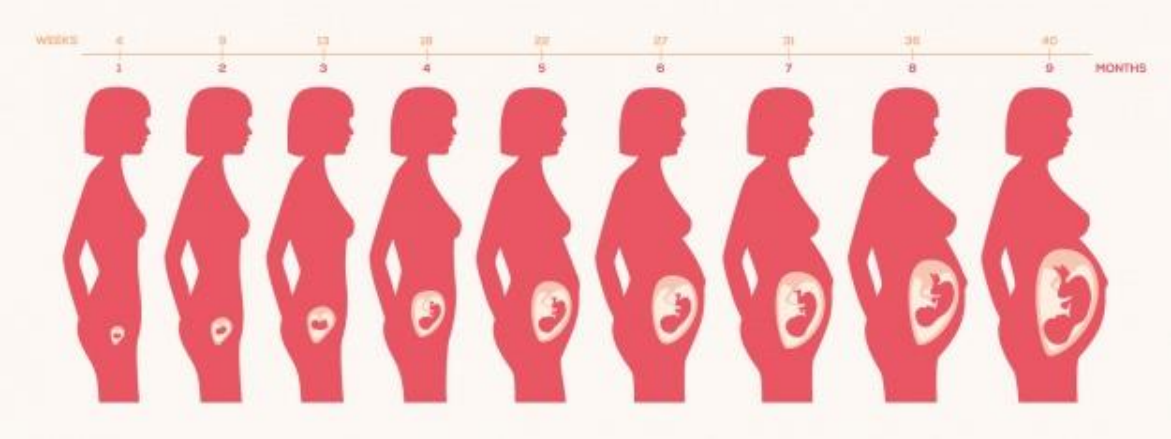

Figure 2.2: Development of the uterus during pregnancy.[28]

2.2 Physiology of the uterus

The uterus activity and growth is under hormonal control.[30] The physiology of uterine contractibility appears to be different in the non-pregnant from pregnant state. Through life uterine contractions play an important role in reproduction facilitating the journey of sperm to the fallopian tubes and during menstruations, helping expel the shed inner of the endometrium.[31] Abdominal surface recording of uterine electrical events is representative of the activity generated by the muscle cells of the uterus. During term and preterm labor uterine electrical activity and intrauterine pressure achieve maximum activity.[32] Electrical activity in the myometrium is low and uncoordinated during the early stages of pregnancy, but intense and synchronized as delivery approaches.[3]

The myometrium is composed by smooth muscle fibers. Smooth muscle contains actin fibers attached to the dense bodies and myosin filaments, represented in Figure 2.3[29]. The contractile process of smooth muscle is activated by an increase of intracellular calcium ions prevenient of extracellular fluid. The calcium ions bind with calmodulin's fibers to form the calmodulin-calcium complex. This complex connects and activates with a phosphorylating enzyme that phosphorylate one of the light chains of the myosin head. The phosphorylated myosin has the capacity of binding with the actin filament leading to the contraction of smooth muscle. When the calcium levels start to decrease, the phosphate split of the myosin and the contraction ceases. [29,31,33]

This process is extremely important in uterus contractions and birth. Toward the end of pregnancy, the uterus becomes progressively more excitable due to hormonal and mechanical changes that allow the strong rhythmical contractions during the parturition. The hormonal factors include: the increase of the ratio estrogens/progesterone that contributes to a higher uterine contractility; oxytocin that stimulates the uterine contractions especially toward the end of gestation by a positive feedback mechanism; fetal hormones, such as, oxytocin, cortisol, prostaglandins, that increase the intensity of uterine contractions. The mechanical factors are also responsible for the increased contractility of the uterus. The mechanical factors include the mechanical stretch of uterine musculature and the stretch or irritation of uterine cervix.[29]

An important type of contraction during pregnancy are the Braxton Hicks contractions. These contractions are weak and present a slow rhythm but become progressively stronger toward the end of pregnancy. Then the Braxton Hicks contractions become extremely strong and start stretching the

cervix. The later force the baby through the birth canal, causing parturition. The mechanism that suddenly changes the Braxton Hicks contractions is unknown, but the *positive feedback* theory has been suggested. The positive feedback theory proposes that the stretching of the cervix caused by the fetus's head provokes a strong reflex increasing the contractility of the uterine body. This contractility pushes the baby forward, stretching even more the cervix causing more positive feedback to the uterine body. The *positive feedback* theory is represented in Figure 2.4[29].

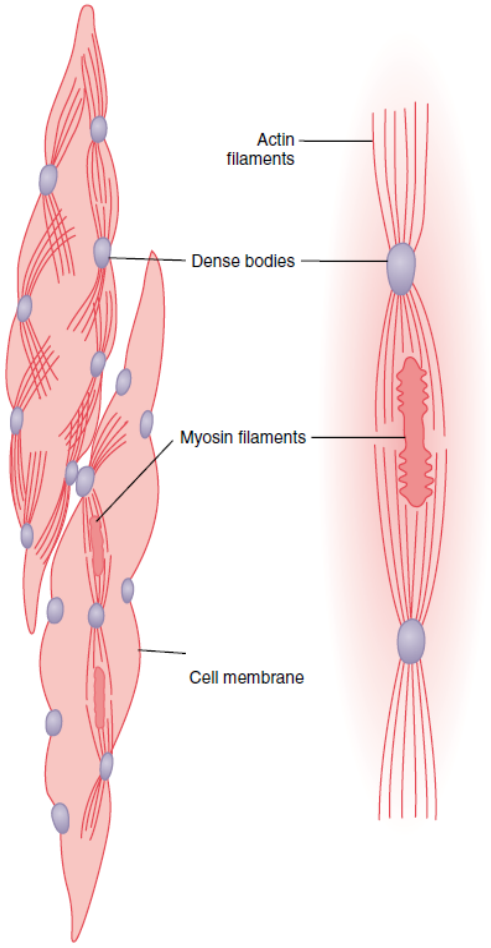

Figure 2.3: Representation of smooth muscle. The actin fibers are attached to the dense bodies and relation of myosin filaments to actin filaments is illustrated.[29]

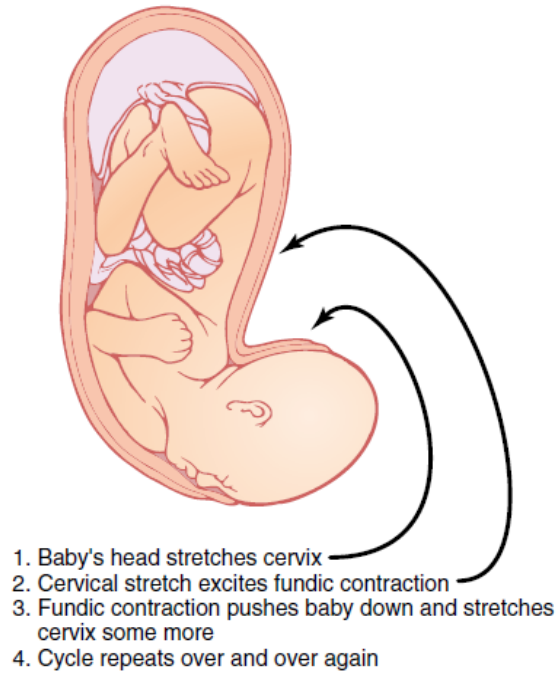

Figure 2.4: Representation of the *positive feedback* theory.[29]

2.3 Preterm birth

Preterm birth is defined as all births before 37th week of gestation.[34] Based on the gestational age it is possible to divide pregnancy into the following categories, represented in Attachment 3[35]:

- Extremely preterm – babies born before the 28th weeks of pregnancy are considered extremely preterm. These babies frequently present long-term health problems and disabilities. To avoid labor, tocolytics may be administered.[36]
- Very preterm – children born between 28 and 32 weeks of gestation. They present higher survival rate. Tocolytics can be administered.[4]
- Moderate or late preterm – between 33 and 37 weeks of gestation. Moderate preterm babies have higher rates of morbidity and mortality when compared to those born at term. Induction or caesarean birth should not be planned before 39 completed weeks unless medically indicated.[4,37]
- Term – pregnancy lasts between 38 and 42 weeks of gestation. This is considered the normal length of pregnancy.[38]
- Post-Term – Pregnancy that extents to 43 weeks of gestation and beyond. Post term pregnancies are associated with an increased risk of fetal and maternal morbidity. Obesity, hormonal and genetic factors have been implicated to be the root of this problem.[39]

To prevent premature labor tocolytic treatments can be administered, ideally between 24th and 32nd week of gestation. Tocolytic drugs delay preterm birth giving the baby the opportunity to develop more thus increasing the survival hypothesis. An example of a tocolytic drug is oxytocin antagonists. Since preterm labor is related with an increase of myometrial oxytocin receptors, oxytocin antagonists are given to the pregnant woman to inhibit those receptors and decrease myometrial contractility.[40,41] Attachment 3[19] represents the pregnancy evolution and its main events.

Chapter 3 - Monitoring uterine activity

As far as uterine contractibility is concerned the most used method in the clinical sector used are external TOCO and IUPC. Electrohysterography is also used but it is a new technique found in the hospital.

3.1 External Tocography

The common practice to evaluate uterine contractibility is the external TOCO (Tocography). TOCO can be used in all stages of pregnancy and labor. This method is non-invasive and is a simple measurement technique in which the contractions are recorded by tocodynamometers.[1,42] Tocodynamometers are external pressure measurement devices that are attached to subject's abdomen and held in place with stretch belt, as depicted in Figure 3.1[43]. These devices are used to detect changes in abdominal wall as an indication of uterine contractions.[44] This method presents low accuracy and sensibility, which can affect the estimation accuracy of the contraction. Another disadvantage of TOCO is that it only provides a single measure of local uterine pressure.[44,45]

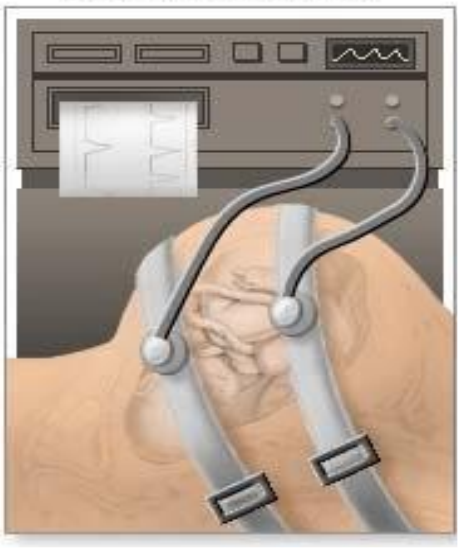

Figure 3.1: Monitoring uterine activity with the external monitor (TOCO).[43]

3.2 Intrauterine Pressure Catheter

The IUPC (Intrauterine Pressure Catheter) is the golden standard for uterine contraction monitoring. In this method a catheter is inserted in the uterus as displayed in Figure 3.2[46]. The IUPC provides the best information concerning uterine contractions since it provides the exact quantification of the mechanical effect of contractions. However the insertion of the catheter in the IUPC requires the rupture of membranes which can increase the risk of infection or accidentally induce labor.[25,47] Moreover the IUPC cannot be used in monitoring uterine activity since can only be used when the

membranes are ruptured. It is manly used in selected cases, such as when the woman is obese or is already in labor.[46]

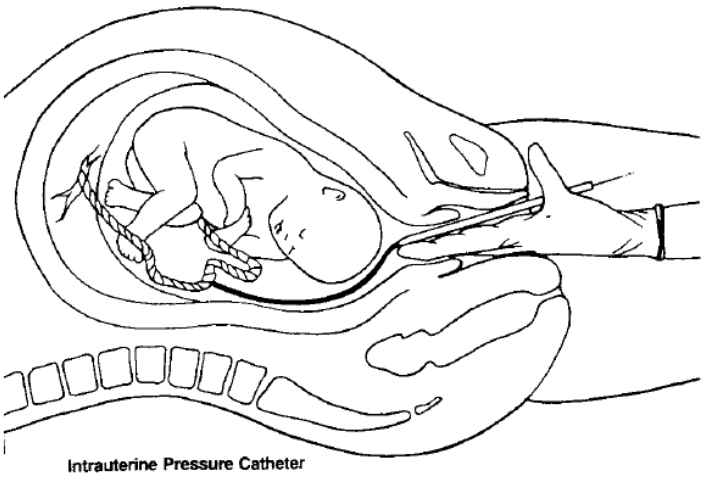

Figure 3.2: Monitoring uterine activity with IUPC.[46]

3.3 Electrohysterography

Electrohysterography is a promising alternative method to TOCO and IUPC. This method can be applied invasively into the uterine muscle or non-invasively through electrodes attached to abdominal wall, represented in Figure 3.3[9].[48] The non-invasive method has been widely used since it provides quantitative measurement and a topographic characterization of uterine electrical activity. The non-invasive EHG has a higher correlation with IUPC than TOCO for contraction detection. Recent data suggest that non-invasive EHG is as good as IUPC for monitoring uterine contractility and that extracting information from EHG signals provide a strong basis to predict and diagnose preterm births.[1,49] Several studies have shown that the EHG signal, Figure 3.4, may vary depending on whether the woman is in true labor or false labor and whether she will have term delivery or preterm delivery.[50] Great efforts are been made in research to differentiate between effective contractions and non-effective contractions and between term and preterm EHG signals.[8,50] A shift of the energy content toward higher frequencies as labor approaches has been identified in the literature.[13,51] However the EHG can be disturbed by physiologic interferences such as the maternal ECG (Electrocardiogram) or the maternal respiration. These artifacts can make the extraction of information from the EHG signal a complex task. Therefore this method is not commonly used in the clinic setup.[49]

Figure 3.3: Location of abdominal electrodes (in white) from the Icelandic database. It is also represented the tocogram belt in black.[9]

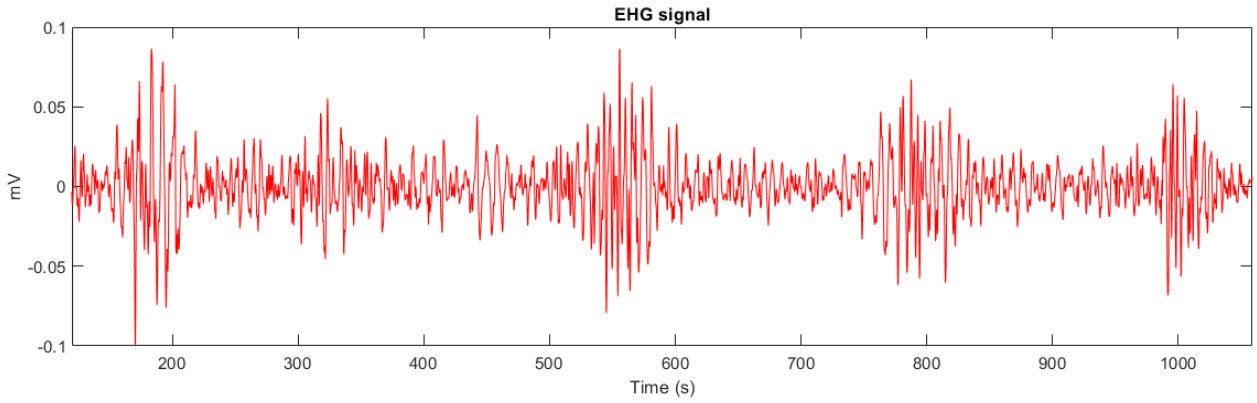

Figure 3.4: EHG signal from the Icelandic database

3.4 EHG signal

The EHG signal is composed by the Slow Wave and Fast Wave. The Slow wave is related to skin stretching and electrode movement and has a frequency between 0.01 and 0.3 Hz. The Fast Wave represent the individual electrical signals firing and its frequency ranges from 0.2 to 3.0 Hz. The Fast Wave can be divided in two: FWL (Fast Wave Low) and FWH (Fast Wave High). The FWL is always present in uterine electrical recordings and its frequency gets higher along the pregnancy. The FWH is related to efficient labor contractions.[16,48,52] The major components in the EHG signal are:

- Alvarez waves: also referred as uterine irritability or LAHF **(**Low Amplitude High Frequency**)** were first described by Alvarez and Caldeyro in 1950.[53] These waves have low amplitude and short duration, occur with a frequency of 1-2 per minute and they are occasionally felt by the woman.[52,54] The Alvarez waves have the same frequency contents as a contraction, between 0-1 Hz, but the length of a contraction is superior than that of an Alvarez wave.[20] Alvarez waves are localized in a small part of

uterine tissue without propagation and can lead to a development of more synchronous contractions with superior intensity and subsequently to preterm birth. [52,54,55]

- Braxton-Hicks contractions: first described by Braxton-Hicks in 1872[21], this inefficient contractions begin around the 20th week of gestation and become more frequent and stronger when term approaches. Braxton-Hicks contractions have high amplitude. Researchers present different conclusions regarding Braxton-Hicks contractions. Some authors report that a Braxton-Hicks contractions occur every 3 or 4 hours[56,57] and for others this event is more common, happening at least once in an hour.[58] Braxton-Hicks contractions are less localized than Alvarez waves and at parturition it is considered to fully "propagate" to the whole uterus in a short amount of time.[52,56,58] More research is needed regarding this event.
- LDBF waves: LDBF waves have long duration and low frequency that ranges from 0 to 1 Hz. Their duration is several minutes long. LDBF waves are rare and are associated with uterine hypertonia, when there is a contraction of the uterus without the return to muscle relaxation, which pose a pregnancy risk.[16,20,52,59]
- Contractions: There are several other contractions that may not be included in the above-mentioned contraction types and that require further investigation. It might represent labor contractions or pre-labor contractions or even false labor contractions. The duration of the contractions is inferior to the duration of LDBF wave and superior to the amplitude of an Alvarez wave.[17] They are good candidates to be classified as belonging to the Braxton hicks contraction family. They might also represent labor contractions, however, in both reviewed database no records were made during labor. [20,6061]
- Leman waves: Described only in one study as contractions of low amplitude (Alvarez waves). These waves are often overlooked in the detection process due to poor signal-to-noise ratio.[17]

As far as research was possible only four illustrations (time series) of these components in the EHG signal were found in the bibliography and are presented in the Figure 1.3, Figure 1.4, Figure 1.6 and Figure 1.7. One would expect some more representations of these EHG events. A sum of the contractions characteristics mentioned above can be found in Attachment 4[62].

The EHG can also contain noise from several sources like motion artifacts or physiological interferences. The question arises whether these interferences appear in the bandwidth of work which is 0.1 to 1 Hz. The principal artifacts are:

- Maternal ECG: its energy content is mostly distributed between 1.38 to 1.5 Hz, so out of our work band. It is mostly constant throughout the recording sessions and it's usually present in all channels.[52]
- Maternal respiration: the maternal respiration has a frequency within 0.20 and 0.34 Hz. It partially overlaps with uterine electrical activity which makes it a very disturbing artefact. In the bipolar montages these interferences usually cancelled out to a reasonable degree.[10,52]
- Motion artifacts: are unavoidable in the EHG signal since uterine contraction can induce movement artifacts due to forced respiration patterns or pain. Motion artifacts typically do not propagate and are associated with a rise in energy between 1 and 4 Hz.[10,52]
- Fetal ECG: usually detected in the EHG signal despite the electrode location not being optimized for this task. This signal has low amplitude and a bandwidth that does not overlap with the work one.[52]
- Fetal movements: the EHG signal contains components triggered by the fetal movements. Contractions containing fetal movements were eliminated from the analysis. An example of fetal movements is presented in Figure 1.5[18].

Chapter 4 – Pre-processing, database and electrode setup

The used platform in this work was MATLAB® (The MathWorks Inc, 2018).

For this thesis the Icelandic 16-electrode EHG Database[9] and the TPEHG database[8] were used. The databases are available at PhysioNet.[9,63]

The Icelandic database has 122 recordings from 45 pregnant women, several of those did more than one recording. This database has 4 cases of preterm birth. The recordings were performed in the third trimester. The data recorded using 16 electrodes in a 4-by-4 grid, Figure 4.1[8,9] This database also includes annotations and obstetric information on the participants. The women were only admitted to the study if they had normal singleton pregnancies and no known risk factors for preterm birth.[9]

The TPEHG database has 300 recordings that were clustered into four groups depending to the time of recording: 143 records were early term (before the 26th week of gestation), 119 records were later term (during or after the 26th week of gestation), 19 records were early preterm (before the 26th week of gestation) and 19 records were later preterm (during or after the 26th week of gestation). This database has 38 cases of preterm birth. For the recordings four electrodes configuration was used resulting in three bipolar channels, Figure 4.2. The records of pregnancies containing no electrical activity or containing excessive noise, those ended in C-sections and those ended in induced delivery were excluded from the database.[8]

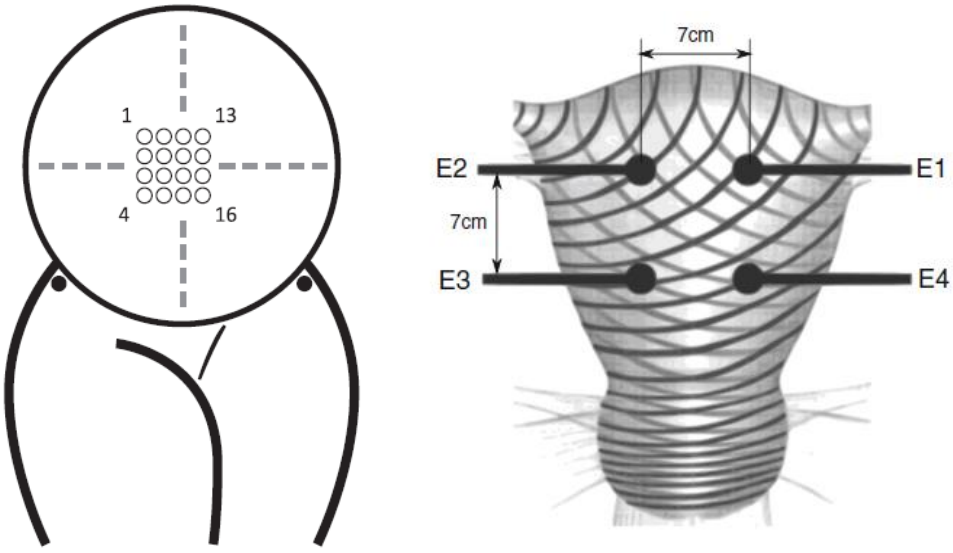

Figure 4.1: On the left: Electrodes placement in the recordings of the Icelandic database in a 4-by-4 grid.[9] On the right: Electrodes placement in the recordings of the TPEHG database. The bipolar channels are E2-E1, E2-E3 and E4-E3.[8]

To have a better understanding of the data, the Figure 4.2 and Figure 4.3 depict the delivery week and the gestational week at recording of the Icelandic and TPEHG databases, respectively. The blue line represents the 37th week of gestation, the dots below the line are the preterm cases. It is possible to detect in Figure 4.3 that the TPEHG database shows two separated groups, indicating that the recordings were not continuous throughout pregnancy. Those two distinct groups of recordings can lead to a biased analysis since there is a lack of data between the 26th and 29th week of gestation. The Icelandic database also presents an unevenly distributions of records regarding gestational week.

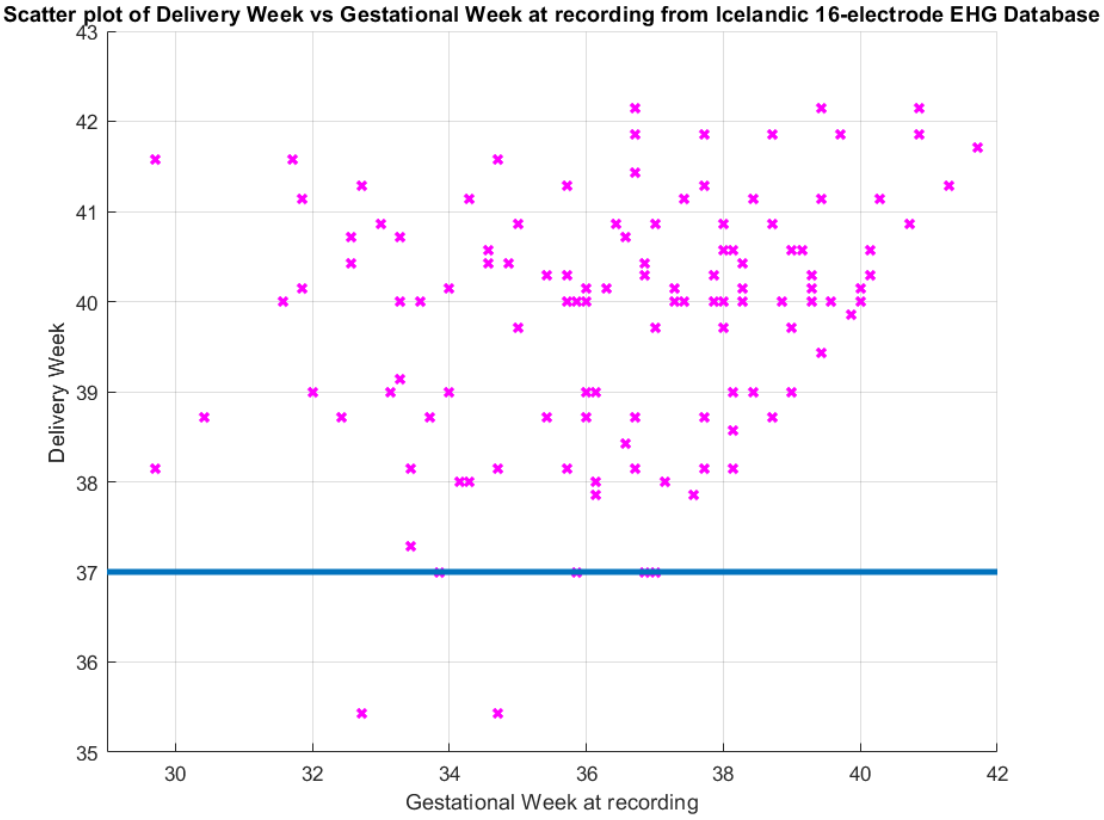

Figure 4.2: Icelandic database: Delivery week vs Gestational week of the recordings. The blue line represents the 37th week of gestation.

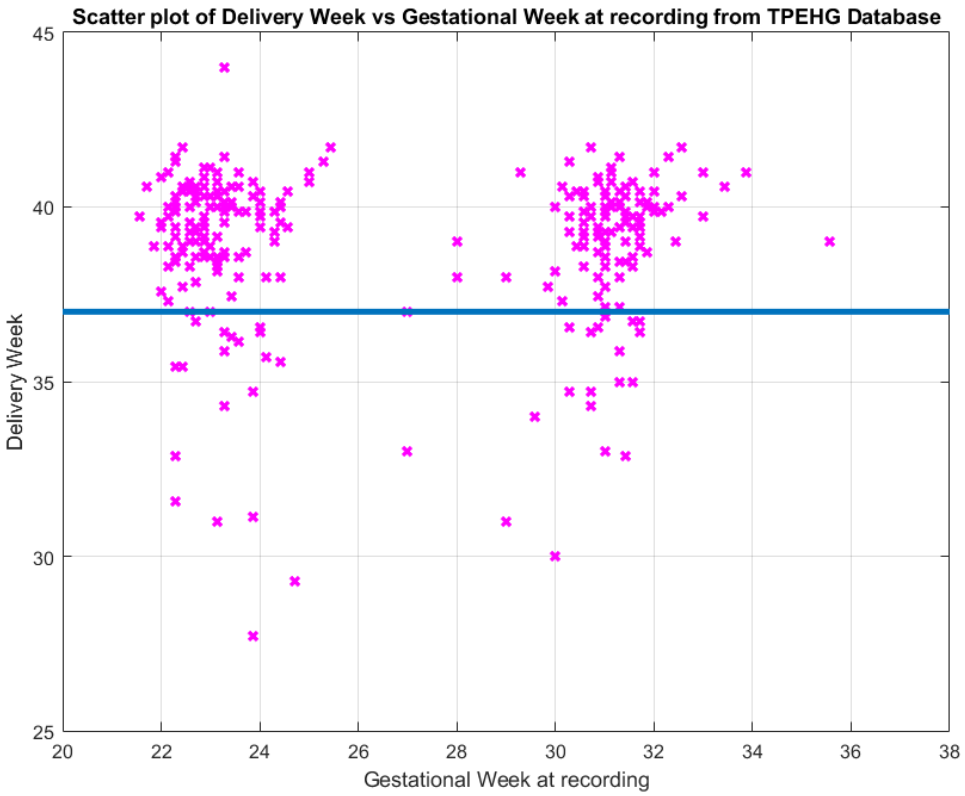

Figure 4.3: TPEHG database: Delivery week vs Gestational week of the recordings. The blue line represents the 37th week of gestation.

4.1 Pre-processing and filtering

In both databases the original EHG was processed and filtered. In the top plot of Figure 4.4 an original EHG signal is represented. There is a significant variation in the EHG signal in the beginning of the recording due to equipment electronic startup transient. The following baseline fluctuation can be explained as a normal response of the skin/electrode interface. The abrupt signal feature present in the end of the recording also represents the equipment electronic transient when it is switched off.

In the Icelandic database 200 samples were removed from the beginning and the end of the signal and in the TPEHG database the first 2000 samples and the last 200 samples were removed from the original signal. This was to remove the abrupt variations seen at the beginning and the end of the signal as depicted in Figure 4.4. Next, the first value of the signal was subtracted to the whole EHG signal and decimation was applied. In the Icelandic database the original signal sampling rate of the EHG signal was 200 Hz and a decimation factor of 50 was applied resulting in a new sampling rate of 4 Hz. In the TPEHG database the original signal sampling was 20 Hz and a decimation factor of 5 was applied resulting in a new sampling rate of 4 Hz. The signal was posteriorly filtered between 0.1 Hz to 1 Hz by a Wavelet filtering method. Figure 4.4 bottom represents the resulted signal without decimation. Figure 4.5 bottom shows a detailed zoom of the original signal where the maternal ECG is clearly present along with background noise. A flowchart with the pre-processing and filtering is presented in Figure 4.6.

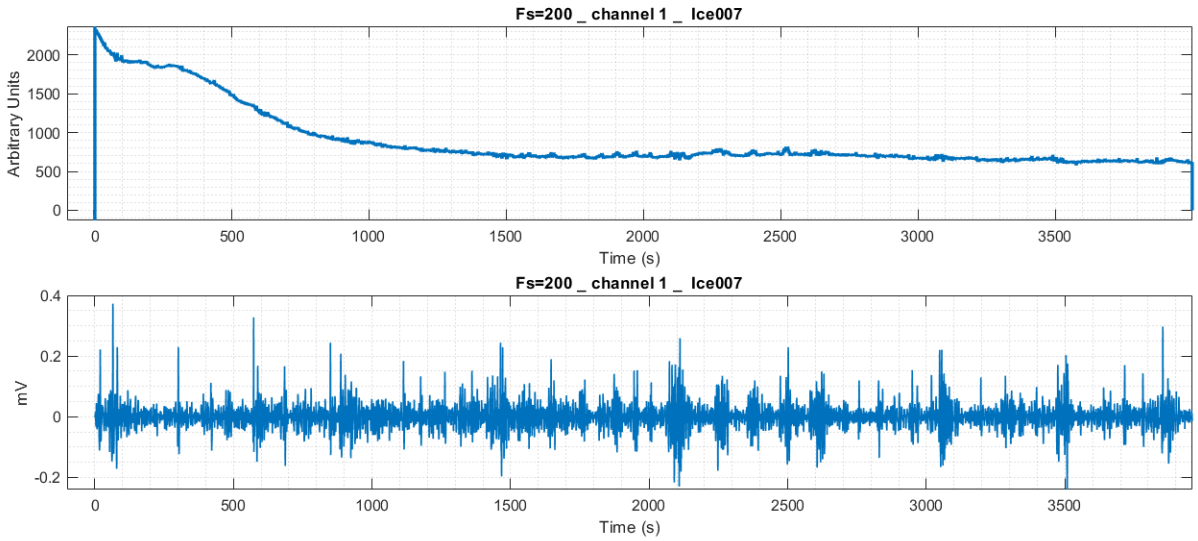

Figure 4.4: On top: Original EHG signal from the subject 7 of the Icelandic database. On bottom: EHG signal after the first two steps of pre-processing.

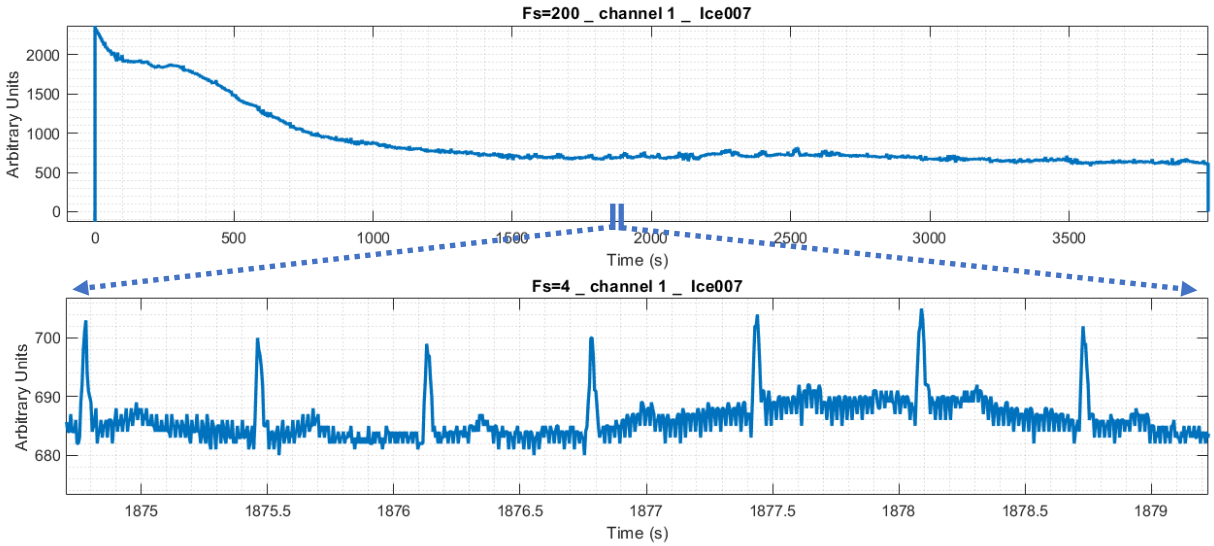

Figure 4.5: On top: Original EHG signal from the subject 7 of the Icelandic database. On bottom: EHG signal after three steps of pre-processing. The blue arrows represent the zoom done in the top plot where maternal ECG and interference is clearly seen.

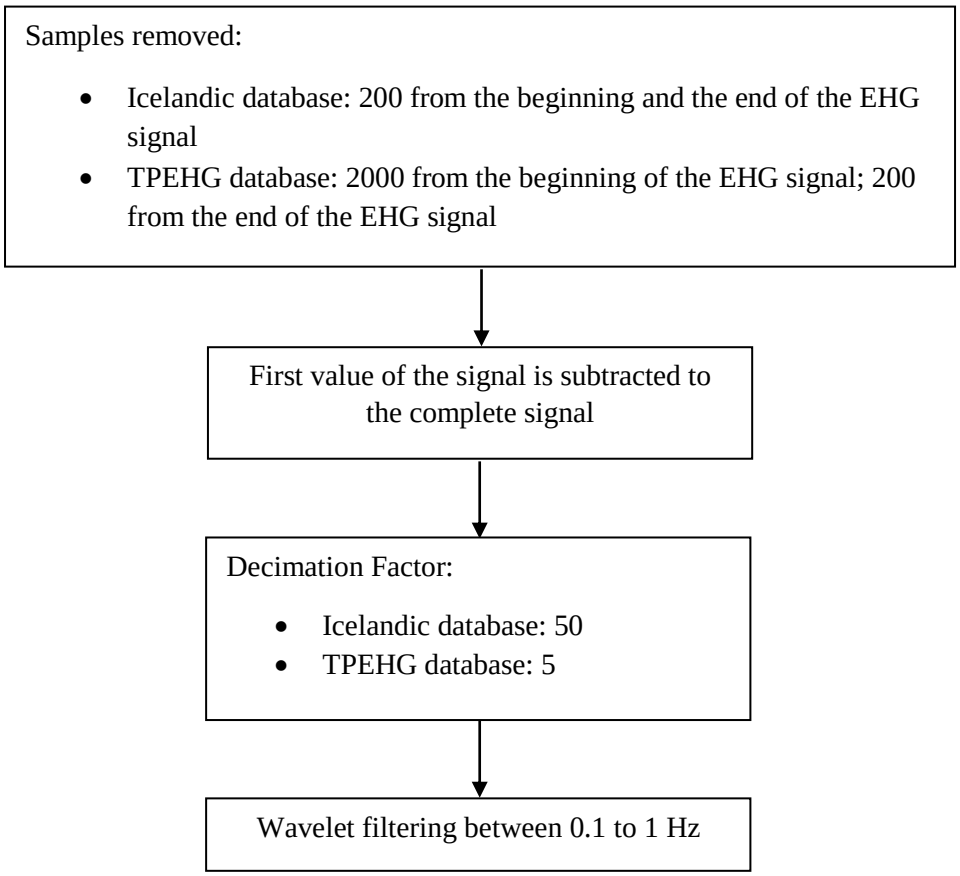

Figure 4.6: Flow chart of the pre-processing and filtering applied to the Icelandic and the TPEHG database

4.2 Monopolar vs bipolar channels

The databases used in this work have different channel configurations: in the Icelandic database there is 16 monopolar channels and in the TPEHG database there is 3 bipolar channels.

Bipolar channels are obtained subtracting two different monopolar channels. Bipolar channels have lower spatial resolution (from 16 to 12 channels in the Iceland database). The advantage is reducing common noise in the resulted bipolar channel, like the maternal electrocardiogram, electrode movements or respiratory movements, as represented below.

$$S_1 = S'_1 + r \tag{4.1}$$

$$S_2 = S'_2 + r \tag{4.2}$$

$$S_b = S_1 - S_2 \tag{4.3}$$

where S_1 and S_2 represent monopolar signals, r represents the signal noise and S_b represents the bipolar signal. If the noise of the monopolar signals is identical, then in the bipolar signal the noise is eliminated. The bipolar recording affects the EHG spectral content and can induce a bias to the propagation direction of the EHG signal by forcing the direction of the electrodes chosen. Another effect of the bipolar recordings is the high-pass filtering outcome resulting in the elimination of the lower frequencies.[25,56,58] Most authors chose bipolar channels over monopolar ones.[3,56,64]

In this thesis, bipolar channels for both databases were chosen. In the TPEHG database the chosen channel was the E2-E3 since the vertical signal presents a higher variation of signal potential, and in the Icelandic database the selected channel was the channel 4-channel 13 since it covers all the area of the abdomen. An illustration of the chosen channel is represented in Figure 4.7.

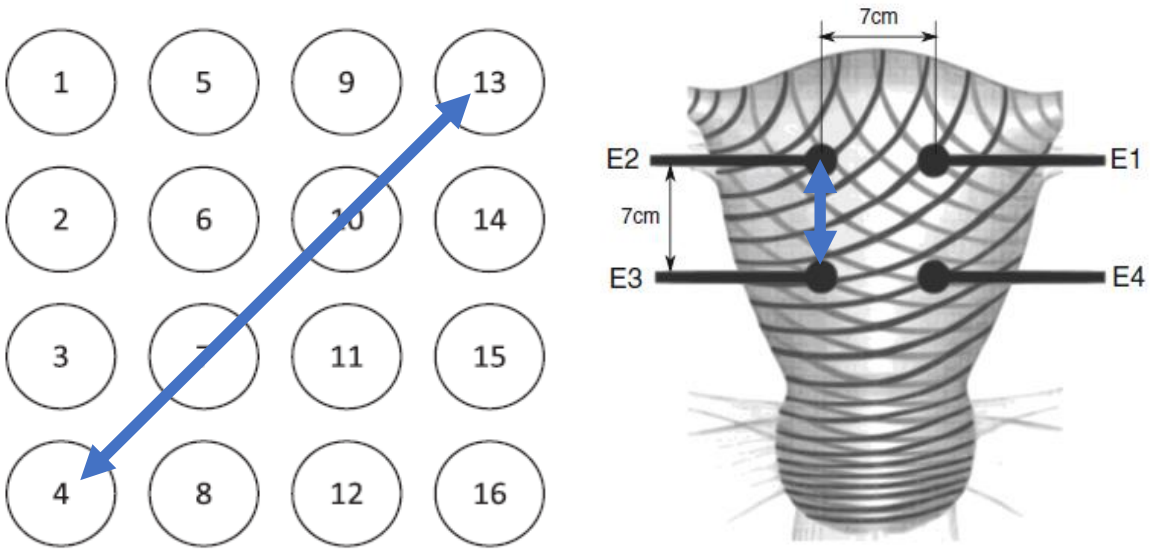

Figure 4.7: The blue arrow represents the channel chosen in this thesis for the Icelandic database[9] (left) and for the TPEHG database[8] (right)

4.3 Spectral Analysis

The PSD methods can be divided in two groups: parametric and non-parametric. Parametric methods match the signal with a model. If the selected model is wrong, the PSD estimation may contain invalid frequency peaks. Non-parametric methods main advantage methods is its robustness, however the disadvantage of this method is the use of data windowing, that can lead to a distortion of the PSDs.[50,65–68]

In this work the following PSD methods were calculated:

- Wavelet Marginal (non-parametric method);
- FFT (Fast Fourier Transform) (non-parametric method);
- FFT Windowed (non-parametric method);
- Welch (non-parametric method);
- Covariance (parametric method);
- Burg (parametric method);
- Modified Covariance (parametric method);
- Yuelear (parametric method);
- AR (parametric method).

The created databases include all the above-mentioned PSD estimations. The FFT method, used regularly in literature, was not applied in this work since this PSD estimation has several peaks. In contrast, most of the parametric methods present a smooth estimation of the PSD. The Welch method is a compromise between the non-parametric methods and the parametric ones being this the reason behind the choice of the Welch method. The Wavelet method PSD estimation is quite attractive as far as smoothness and resolution is concerned. However, for lack of time it was not used in this work.

The Welch method, also called average periodogram, is non-parametric and includes the periodogram technique. The main steps of the Welch method are represented in Figure 4.9. First this method divides the input signal into overlapping segments, as represented in Figure 4.8[69]. A window is the applied to each segment, in this work the window chosen was the *Hanning* window. The next step in the Welch method is to apply the FFT to the segments already windowed and then periodograms are obtained. The last step is to obtain the average of the periodograms.[65,69–71] The Welch method is used to determine the power spectral of each burst. The PSD has been used by researchers to analyze the EHG signal and to evaluate if changes of the power spectra may indicate premature delivery.[72] A study using PSD analysis revealed that as labor induction progresses there was a shift of the energy content toward higher frequencies.[51]

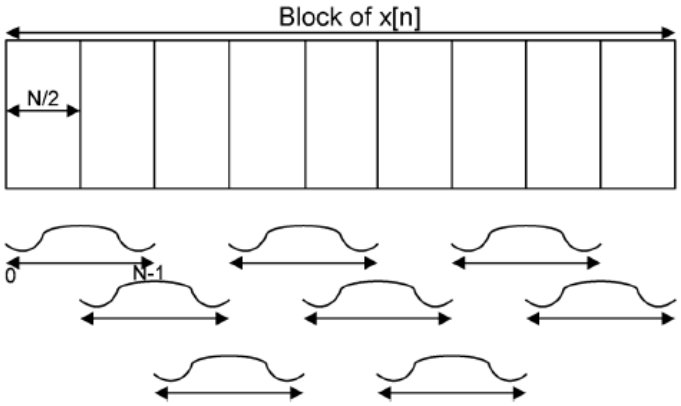

Figure 4.8: Overlapping segments used in welch method. N represents the number of samples of the window. The overlap is 50%.[69]

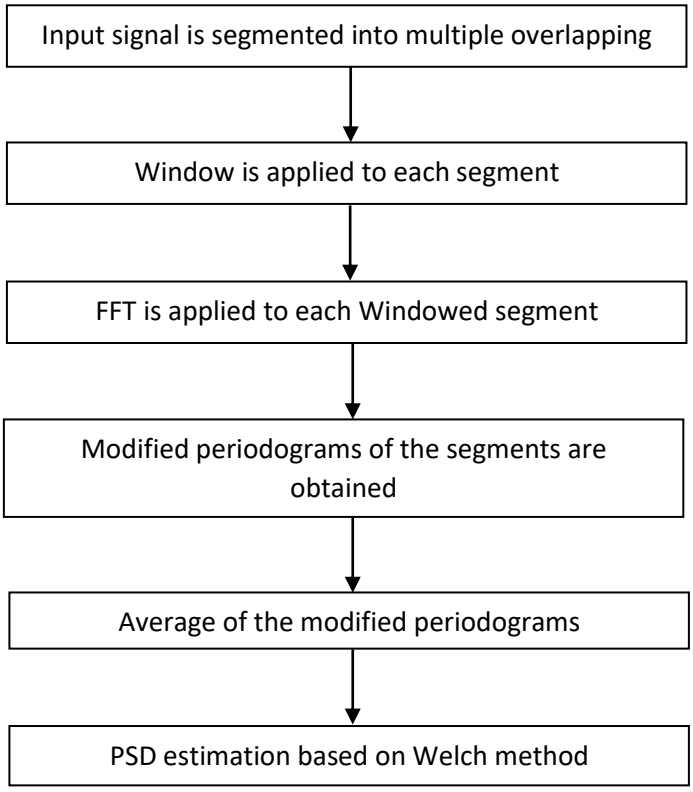

Figure 4.9: Flow chart of the Welch method

4.4 Building the Databases

Since the created data is similar for the Icelandic and the TPEHG databases only the results of the Icelandic database will be mentioned. In Figure 4.11 is represented the original format of the data of the Icelandic database. The original format contains the original EHG signal in which each row represents a signal recorded by one electrode. An application was designed for this purpose. That function was updated, tested, debuged and named:

read_Iceland_Database_v13_append_psd_contract_fm_v9_bipolar, Figure 4.10.

```
>> read_Iceland_Database_v13_append_psd_contract_fm_v9_bipolar(data_folder,{'all'},.1,1)
```

Figure 4.10: Command line of function *read_Iceland_Database_v13_append_psd_contract_fm_v9_bipolar*

The inputs of the *read_Iceland_Database_v13_append_psd_contract_fm_v9_bipolar* are:

- *data_folder:* string with the folder of the original database;
- *selected_cases:* the selected cases to be included in the database, i.e. if {'all'} were selected then the database would include all cases available;
- *f_min*: minimum frequency for filtering;
- *f_max*: maximum frequency for filtering.

This function builds and saves in a MATLAB® file the table represented in Figure 4.12. Some of the parameters included on the table are:

- filtered signal;
- all the information provided in the header files;
- separated contractions with different detection methods (see Chapter 5).

val

16x746000 double

	39806	39807	39808	39809	39810	39811	39812	39813	39814	39815	39816	39817	39818
1	-2	3	-4	0	0	4	-4	0	0	5	-4	0	-2
2	1608	1607	1607	1609	1608	1607	1606	1609	1608	1607	1606	1609	1607
3	1800	1800	1799	1802	1801	1800	1798	1802	1800	1799	1798	1801	1799
4	2768	2764	2770	2769	2769	2764	2769	2769	2769	2763	2768	2768	2767
5	2002	2001	2002	2004	2003	2002	2001	2005	2002	2001	2001	2004	2001
6	1922	1922	1924	1925	1923	1922	1923	1926	1923	1921	1923	1925	1921
7	2569	2561	2574	2566	2571	2560	2574	2566	2569	2560	2574	2565	2570
8	2218	2214	2219	2217	2217	2214	2218	2217	2218	2214	2218	2217	2217
9	1982	1986	1982	1986	1983	1986	1981	1987	1983	1986	1981	1986	1981
10	2812	2815	2811	2814	2812	2815	2811	2815	2812	2815	2811	2813	2811
11	1462	1468	1464	1466	1462	1467	1463	1466	1462	1467	1463	1465	1461
12	3362	3353	3361	3354	3362	3353	3360	3353	3362	3353	3360	3353	3362
13	2621	2624	2621	2623	2622	2623	2620	2624	2621	2623	2620	2623	2620
14	2894	2886	2892	2885	2894	2886	2893	2885	2894	2886	2892	2885	2894
15	3045	3042	3043	3040	3045	3041	3042	3040	3045	3041	3042	3039	3045
16	2601	2589	2602	2592	2601	2589	2603	2592	2601	2589	2602	2591	2602

Figure 4.11: Original files from the Icelandic 16-Electrode Database available in PhysioNet. Each row represents the recording of one channel.

63x1 table

	1 Ice004_P_1of1m_decimated
1 Data	*16x15720 double*
2 Filtered Data	*16x15720 double*
3 Gestational Weeks	36.7143
4 Record Type	'Pregnancy'
5 Delivery Week	41.4286
6 Type of Delivery	'Vaginal/Induction'
7 Oxytocin in Labour	'No'
8 Epidural	'No'
9 IBM before	31
10 IBM at recording	35.8000
11 Age	'30'
12 Gravidity	'4'
13 Parity	'2'
14 Previous Caesarean	'Posterior'
15 Placental Position	'No'
16 Comments for recording	*1x2 cell*
17 Comments for delivery	*1x1 cell*
18 Frequency	4
19 Filter wavelength	[0.1000 1]
20 fetal_movements_boundaries_final	*10x5 cell*
21 index_contraction_boundaries_final	*10x5 cell*
22 separated_fetal_movements	*10x5 cell*
23 separated_contractions	*10x5 cell*
24 nor_contraction_neither_fetal_index	*10x5 cell*
25 label_energy	*1x5 cell*
26 uterine_basal_activity_signals	*10x5 cell*
27 model_order_contraction	*1x5 cell*
28 freq_axis_for_wavelet_marginal_contraction	*1x5 cell*
29 freq_axis_cov_contraction	*1x5 cell*
30 psd_matrix_contraction	*1x5 cell*

63x1 table

	1 Ice004_P_1of1m_decimated
31 ps_matrix_contraction	*1x5 cell*
32 lsd_matrix_contraction	*1x5 cell*
33 ls_matrix_contraction	*1x5 cell*
34 cumsum_matrix_contraction	*1x5 cell*
35 freq_axis_for_fft_contraction	*1x5 cell*
36 signal_power_contraction	*1x5 cell*
37 spectral_methods_names_contraction	*1x5 cell*
38 bw_flo_fhi_matrix_contraction	*1x5 cell*
39 locs_peaks_psd_cell_contraction	*1x5 cell*
40 locs_peaks_ps_cell_contraction	*1x5 cell*
41 locs_peaks_lsd_cell_contraction	*1x5 cell*
42 locs_peaks_ls_cell_contraction	*1x5 cell*
43 id_for_locs_peaks_ps_lsd_ls_cell_contraction	*1x5 cell*
44 id_for_locs_peaks_psd_cell_contraction	*1x5 cell*
45 model_order_fetal	*1x5 cell*
46 freq_axis_for_wavelet_marginal_fetal	*1x5 cell*
47 freq_axis_cov_fetal	*1x5 cell*
48 psd_matrix_fetal	*1x5 cell*
49 ps_matrix_fetal	*1x5 cell*
50 lsd_matrix_fetal	*1x5 cell*
51 ls_matrix_fetal	*1x5 cell*
52 cumsum_matrix_fetal	*1x5 cell*
53 freq_axis_for_fft_fetal	*1x5 cell*
54 signal_power_fetal	*1x5 cell*
55 spectral_methods_names_fetal	*1x5 cell*
56 bw_flo_fhi_matrix_fetal	*1x5 cell*
57 locs_peaks_psd_cell_fetal	*1x5 cell*
58 locs_peaks_ps_cell_fetal	*1x5 cell*
59 locs_peaks_lsd_cell_fetal	*1x5 cell*
60 locs_peaks_ls_cell_fetal	*1x5 cell*
61 id_for_locs_peaks_ps_lsd_ls_cell_fetal	*1x5 cell*
62 id_for_locs_peaks_psd_cell_fetal	*1x5 cell*
63 channels_order	*10x1 struct*

Figure 4.12: Table with processed (step1) unipolar data from the Icelandic database. Each column represents the recording of each pregnancy visit. All the information of the header files was included as well as other parameters such as separated contractions and the filtered data. The figure on the right is the continuation of the left one.

After the table development, Figure 4.12, and since the parameters of contraction detection and PSD method were already chosen, new databases were built. To create these new databases the functions, *create_database_cont_bipolar_v2,* and *create_database_cont_bipolar_v2_tpehg* were used for the Icelandic and the TPEHG databases, respectively.

```
>> create_database_cont_bipolar_v2('C:\Users\Filipa Esgalhado\Documents\mt\Ice_new',{'all'},10,'wavelet')
>> create_database_cont_bipolar_v2_tpehg('C:\Users\Filipa Esgalhado\Documents\mt\tpehg',{'all'},2,'wavelet')
```

Figure 4.13: Command line of function *create_database_cont_bipolar_v2* and *create_database_cont_bipolar_v2_tpehg*

The inputs of these functions are:

- *data folder*: string with the folder of the complete database;
- *selected cases*: the selected cases to be included in the database, i.e. if {'all'} were selected then the database would include all cases available;
- *channel*: number between 1 to 10 for the *create_database_cont_bipolar*_v2 and a number between 1 and 3 for the *create_database_cont_bipolar_v2_tpehg*;
- *method name*: selected method for the detection of contractions, i.e. 'wavelet'.

This are the name references of the obtained databases:

- for the Icelandic database: *method_wavelet_channel_ch4-ch13_with_header*;
- for the TPEHG database: *method_wavelet_channel_E2-E3_tpegh.*

The functions built a database of a bipolar channel that contains all the separated contractions, the PSD of each burst and also all the information provided in the header files of the original databases. The header files of the Icelandic database include[9]:

- Participant ID
- Record number
- Record type (labor, pregnancy)
- Age of participant (years)
- BMI (body mass index) of participant before pregnancy
- BMI of participant at time of recording
- Gravidity (number of times participant has been pregnant, including current pregnancy)
- Parity (previous births after 22 weeks gestation)
- Previous caesarean (Yes, No)
- Placental position
- Gestational age at recording (weeks/days), according to a first trimester ultrasound
- Gestational age at delivery (weeks/days)

- Mode of delivery (Vaginal, Vaginal/Induction, Elective caesarean, Emergency caesarean due to slow progress, Emergency caesarean due to other than slow progress). Vaginal delivery indicates spontaneous onset unless appended with /Induction.
- Synthetic oxytocin use in labor (Yes, No)
- Epidural during labor (Yes, No)
- Comments for recording
- Comments for delivery

The header files of the TPEHG database include[63]:

- record number;
- pregnancy duration;
- gestation duration at the time of recording;
- maternal age;
- number of previous deliveries (parity);
- previous abortions;
- weight at the time of recording;
- hypertension;
- diabetes;
- placental position;
- bleeding first trimester;
- bleeding second trimester;
- funneling;
- smoker

An example of the output of *create_database_cont_bipolar_v2* function is shown in Figure 4.14. With these functions two databases were created which contained all the separated contractions, PSD methods and all the header information. In the Icelandic database 3136 contractions were detected and in the TPEHG database 4622 contractions were identified.

The database with the separated contractions, Figure 4.14, is the foundation of this work since all the posterior analysis will be made from this database. The separated contraction method will be explained in the next chapter. Each line represents one contraction, with the 9 PSD estimation methods and all the information provided in the subject's header. A table with the database detailed information is presented below, Table 4.1.

Table 4.1: Table with the information provided in the separated contractions database

Number of the database column (Figure 4.14)	Contents
1	Identification of the subject, the visit and the number of the contraction
2	Separated contraction
3	Index of the contraction in the EHG signal
4 and 5	Frequency axis
6 to 14	9 PSD estimation methods
15 to 29	Header information
30	Classification of the contraction (not implemented)

database_bipolar

3136x30 cell

	1	2	3	4	5	6	7	8	9	10	11	12	13	14
1	'id'	'sep_contractions'	'index_cont'	'freq_axis_for_wavelet_...	'freq_axis_for_fft'	'wavelet'	'FFT'	'FFT_windo...	'welch'	'cov'	'burg'	'mcov'	'yuelear'	'ar'
2	'Ice001_L_1of1m_decimated_1of2'	*1x1 cell*	[248 315]	*1x1 cell*	*1x1 cell*	*1024x1 dou...*	*1x513 doub...*	*1x513 doub...*	*1x513 doub...*	*1x513 doub...*	*1x513 doub...*	*1x513 doub...*	*1x513 doub...*	*1x513 doub...*
3	'Ice001_L_1of1m_decimated_2of2'	*1x1 cell*	[1149 1193]	*1x1 cell*	*1x1 cell*	*1024x1 dou...*	*1x513 doub...*	*1x513 doub...*	*1x513 doub...*	*1x513 doub...*	*1x513 doub...*	*1x513 doub...*	*1x513 doub...*	*1x513 doub...*
4	'Ice002_P_1of3m_decimated_1of17'	*1x1 cell*	[1655 1850]	*1x1 cell*	*1x1 cell*	*1024x1 dou...*	*1x513 doub...*	*1x513 doub...*	*1x513 doub...*	*1x513 doub...*	*1x513 doub...*	*1x513 doub...*	*1x513 doub...*	*1x513 doub...*
5	'Ice002_P_1of3m_decimated_2of17'	*1x1 cell*	[2746 2916]	*1x1 cell*	*1x1 cell*	*1024x1 dou...*	*1x513 doub...*	*1x513 doub...*	*1x513 doub...*	*1x513 doub...*	*1x513 doub...*	*1x513 doub...*	*1x513 doub...*	*1x513 doub...*
6	'Ice002_P_1of3m_decimated_3of17'	*1x1 cell*	[4714 4820]	*1x1 cell*	*1x1 cell*	*1024x1 dou...*	*1x513 doub...*	*1x513 doub...*	*1x513 doub...*	*1x513 doub...*	*1x513 doub...*	*1x513 doub...*	*1x513 doub...*	*1x513 doub...*
7	'Ice002_P_1of3m_decimated_4of17'	*1x1 cell*	[5324 5445]	*1x1 cell*	*1x1 cell*	*1024x1 dou...*	*1x513 doub...*	*1x513 doub...*	*1x513 doub...*	*1x513 doub...*	*1x513 doub...*	*1x513 doub...*	*1x513 doub...*	*1x513 doub...*
8	'Ice002_P_1of3m_decimated_5of17'	*1x1 cell*	[5775 5889]	*1x1 cell*	*1x1 cell*	*1024x1 dou...*	*1x513 doub...*	*1x513 doub...*	*1x513 doub...*	*1x513 doub...*	*1x513 doub...*	*1x513 doub...*	*1x513 doub...*	*1x513 doub...*
9	'Ice002_P_1of3m_decimated_6of17'	*1x1 cell*	[6231 6559]	*1x1 cell*	*1x1 cell*	*1024x1 dou...*	*1x513 doub...*	*1x513 doub...*	*1x513 doub...*	*1x513 doub...*	*1x513 doub...*	*1x513 doub...*	*1x513 doub...*	*1x513 doub...*
10	'Ice002_P_1of3m_decimated_7of17'	*1x1 cell*	[7215 7422]	*1x1 cell*	*1x1 cell*	*1024x1 dou...*	*1x513 doub...*	*1x513 doub...*	*1x513 doub...*	*1x513 doub...*	*1x513 doub...*	*1x513 doub...*	*1x513 doub...*	*1x513 doub...*
11	'Ice002_P_1of3m_decimated_8of17'	*1x1 cell*	[8108 8367]	*1x1 cell*	*1x1 cell*	*1024x1 dou...*	*1x513 doub...*	*1x513 doub...*	*1x513 doub...*	*1x513 doub...*	*1x513 doub...*	*1x513 doub...*	*1x513 doub...*	*1x513 doub...*
12	'Ice002_P_1of3m_decimated_9of17'	*1x1 cell*	[8574 8649]	*1x1 cell*	*1x1 cell*	*1024x1 dou...*	*1x513 doub...*	*1x513 doub...*	*1x513 doub...*	*1x513 doub...*	*1x513 doub...*	*1x513 doub...*	*1x513 doub...*	*1x513 doub...*

database_bipolar

3136x30 cell

	15	16	17	18	19	20	21	22	23	24	25	26	27	28	29	30
1	'Gestational Weeks'	'Record Type'	'Delivery Week'	'Type of Delivery'	'Oxytocin in Labour'	'Epidural'	'IBM before'	'IBM at recording'	'Age'	'Gravidity'	'Parity'	'Previous Caesarean'	'Placental Position'	'Comments ...	'Comments ...	'Classification'
2	39.4286	'Labour'	39.4286	'Vaginal'	'No'	'No'	23.3000	27.6000	'31'	'3'	'2'	'No'	'Fundus'	*1x2 cell*	*1x1 cell*	NaN
3	39.4286	'Labour'	39.4286	'Vaginal'	'No'	'No'	23.3000	27.6000	'31'	'3'	'2'	'No'	'Fundus'	*1x2 cell*	*1x1 cell*	NaN
4	38.1429	'Pregnancy'	40.5714	'Vaginal'	'No'	'No'	20.7000	25.9000	'38'	'4'	'1'	'No'	'Posterior'	'#The partici...	*1x1 cell*	NaN
5	38.1429	'Pregnancy'	40.5714	'Vaginal'	'No'	'No'	20.7000	25.9000	'38'	'4'	'1'	'No'	'Posterior'	'#The partici...	*1x1 cell*	NaN
6	38.1429	'Pregnancy'	40.5714	'Vaginal'	'No'	'No'	20.7000	25.9000	'38'	'4'	'1'	'No'	'Posterior'	'#The partici...	*1x1 cell*	NaN
7	38.1429	'Pregnancy'	40.5714	'Vaginal'	'No'	'No'	20.7000	25.9000	'38'	'4'	'1'	'No'	'Posterior'	'#The partici...	*1x1 cell*	NaN
8	38.1429	'Pregnancy'	40.5714	'Vaginal'	'No'	'No'	20.7000	25.9000	'38'	'4'	'1'	'No'	'Posterior'	'#The partici...	*1x1 cell*	NaN
9	38.1429	'Pregnancy'	40.5714	'Vaginal'	'No'	'No'	20.7000	25.9000	'38'	'4'	'1'	'No'	'Posterior'	'#The partici...	*1x1 cell*	NaN
10	38.1429	'Pregnancy'	40.5714	'Vaginal'	'No'	'No'	20.7000	25.9000	'38'	'4'	'1'	'No'	'Posterior'	'#The partici...	*1x1 cell*	NaN
11	38.1429	'Pregnancy'	40.5714	'Vaginal'	'No'	'No'	20.7000	25.9000	'38'	'4'	'1'	'No'	'Posterior'	'#The partici...	*1x1 cell*	NaN
12	38.1429	'Pregnancy'	40.5714	'Vaginal'	'No'	'No'	20.7000	25.9000	'38'	'4'	'1'	'No'	'Posterior'	'#The partici...	*1x1 cell*	NaN

Figure 4.14: Output of the function *create_database_cont_bipolar_v2*. This database was constructed from the Icelandic database and contains all the separated contractions and all the subject's information provided in the header files. Bottom figure is the continuation of the top one.

Chapter 5 – Contraction Detection

Contraction detection can be manual or automatic. Most researchers use manual segmentation of the EHG signal, however, in this work an automatic detection was performed to avoid the time consuming and error prone manual segmentation task. To detect the contractions a method based on energy was chosen since in a first instance was considered that contractions would exhibit an energy increase. In this work the following methods were calculated:

- Wavelet Energy;
- Teager Energy;
- RMS (Root Mean Square);
- Squared RMS;
- Hilbert Envelop.

It is beyond the scope of this work to compare the detection methods. A paper is being submitted about this subject. It is also beyond the scope of this work to provide a detailed explanation about the above-mentioned methods.

In the contraction detection algorithm, the first event was always ignored. Contractions with amplitude above 0.3 mV were also eliminated since do not represent physiologic activity.

A visual validation of the contractions was required. For that, an application tool was developed to represent the contractions along the EHG signal, the ***Uterine Inspector***. This would confirm if the contractions were well defined and perfectly overlapped with the EHG signal. At the same time the user could assess the contraction detection accuracy. The user selects the database and the recorded visit. The generated table in Figure 5.1 represents the contractions and fetal movements for each method and each channel, Table 5.1. In the visual inspection, there was a perfect overlap of the contractions and the EHG signal. Under visual inspection by several subjects the contraction detection rate was considered very good. The ***Uterine Inspector*** software is a tool to be used for expert validation of the contraction detector. In Figure 5.2 an output of this application is represented.

This tool was based in the research of Oliveira et al.[73] This work have been further developed, tested and debugged.

Table 5.1: Interpretation of table presented in ***Uterine Inspector***, Figure 5.1

	Detection Method
Wavelet_cont	Contractions detected with Wavelet method
Wavelet_fm	Fetal Movements detected with Wavelet method
Teager_cont	Contractions detected with Teager method
Teager_fm	Fetal Movements detected with Teager method
RMS_cont	Contractions detected with RMS method
RMS_fm	Fetal Movements detected with RMS method
RMS_Squared_cont	Contractions detected with Squared RMS method
RMS_Squared_fm	Fetal Movements detected with Squared RMS method
Hilbert_Envelope_cont	Contractions detected with Hilbert Envelop method
Hilbert_Envelope_fm	Fetal Movements detected with Hilbert Envelop method
PDE_Inst_Freq_cont	Contractions detected with Phase Difference Instantaneous Frequency method. Was not implemented at this stage
PDE_Inst_Freq_fm	Fetal Movements detected with Phase Difference Instantaneous Frequency method. Was not implemented at this stage

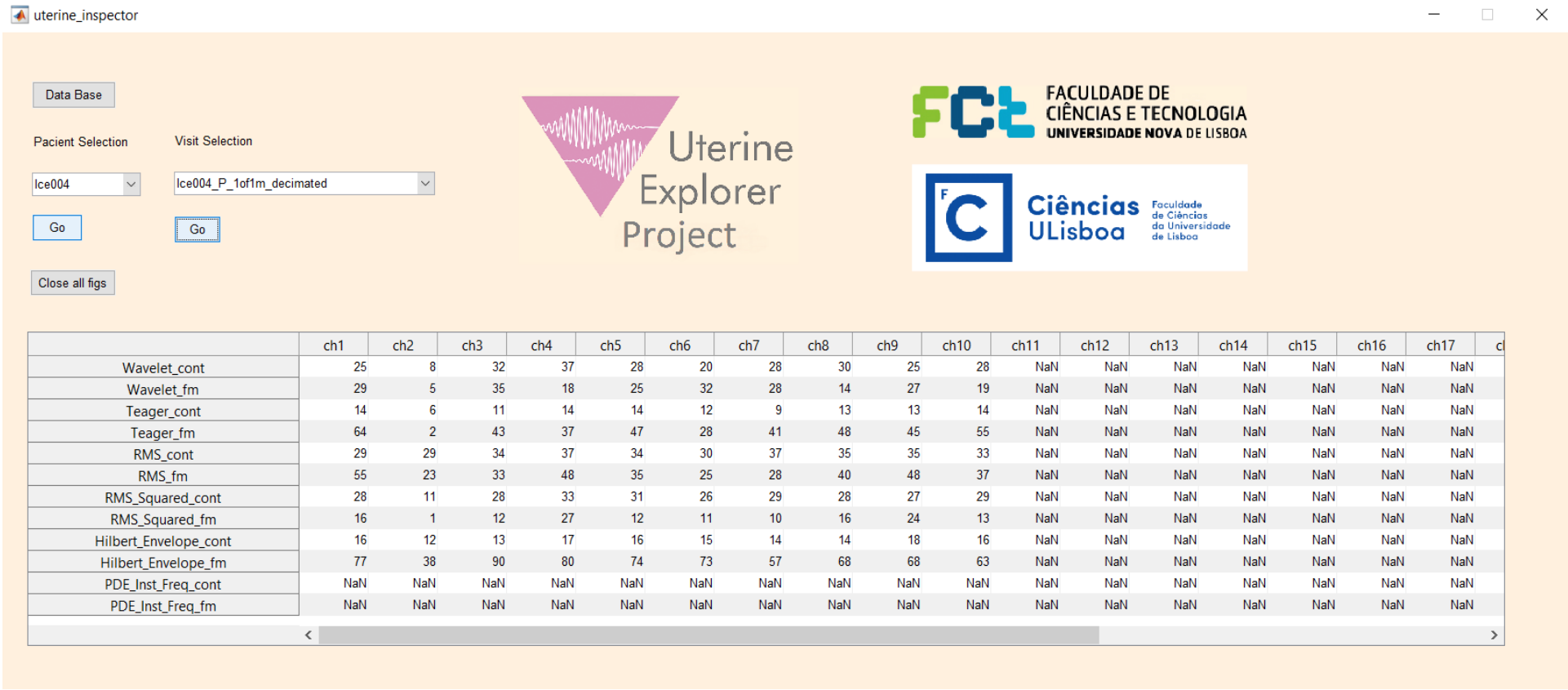

	ch1	ch2	ch3	ch4	ch5	ch6	ch7	ch8	ch9	ch10	ch11	ch12	ch13	ch14	ch15	ch16	ch17	ch
Wavelet_cont	25	8	32	37	28	20	28	30	25	28	NaN	NaN	NaN	NaN	NaN	NaN	NaN	
Wavelet_fm	29	5	35	18	25	32	28	14	27	19	NaN	NaN	NaN	NaN	NaN	NaN	NaN	
Teager_cont	14	6	11	14	14	12	9	13	13	14	NaN	NaN	NaN	NaN	NaN	NaN	NaN	
Teager_fm	64	2	43	37	47	28	41	48	45	55	NaN	NaN	NaN	NaN	NaN	NaN	NaN	
RMS_cont	29	29	34	37	34	30	37	35	35	33	NaN	NaN	NaN	NaN	NaN	NaN	NaN	
RMS_fm	55	23	33	48	35	25	28	40	48	37	NaN	NaN	NaN	NaN	NaN	NaN	NaN	
RMS_Squared_cont	28	11	28	33	31	26	29	28	27	29	NaN	NaN	NaN	NaN	NaN	NaN	NaN	
RMS_Squared_fm	16	1	12	27	12	11	10	16	24	13	NaN	NaN	NaN	NaN	NaN	NaN	NaN	
Hilbert_Envelope_cont	16	12	13	17	16	15	14	14	18	16	NaN	NaN	NaN	NaN	NaN	NaN	NaN	
Hilbert_Envelope_fm	77	38	90	80	74	73	57	68	68	63	NaN	NaN	NaN	NaN	NaN	NaN	NaN	
PDE_Inst_Freq_cont	NaN	NaN	NaN	NaN	NaN	NaN	NaN	NaN	NaN	NaN	NaN	NaN	NaN	NaN	NaN	NaN	NaN	
PDE_Inst_Freq_fm	NaN	NaN	NaN	NaN	NaN	NaN	NaN	NaN	NaN	NaN	NaN	NaN	NaN	NaN	NaN	NaN	NaN	

Figure 5.1: ***Uterine Inspector*** software developed in MATLAB® to evaluate the contraction detection.

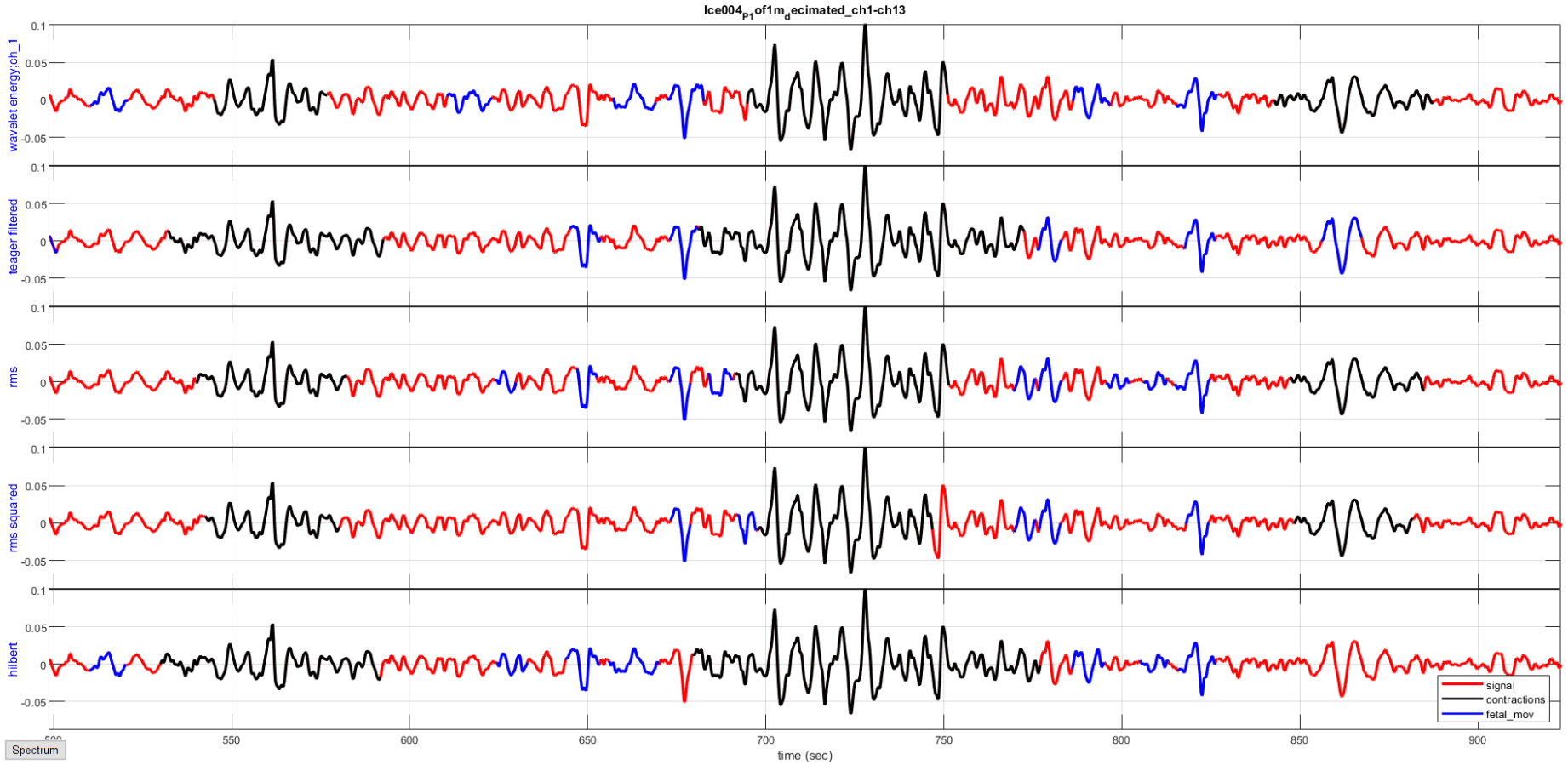

Figure 5.2: Example of an output from the ***Uterine Inspector***. The EHG signal is represented in red. The contractions detected by each method are represented in black and the fetal movements are represented in blue. Each plot represents a different method of detection.

Chapter 6 – Spectral Distance's Analysis and Evaluation

In this thesis, the main goal is to cluster contractions from EHG signals. However, contractions, as represented on Figure 6.1, are non-stationary time series and their visual classification is challenging and not viable in long term or in the clinical practice. There are several features that can be extracted from the EHG signal but the power spectra of the contractions, Figure 6.2, were chosen since the spectra accurately represents the EHG signal and it has the same length independently of the number of samples of the contraction.

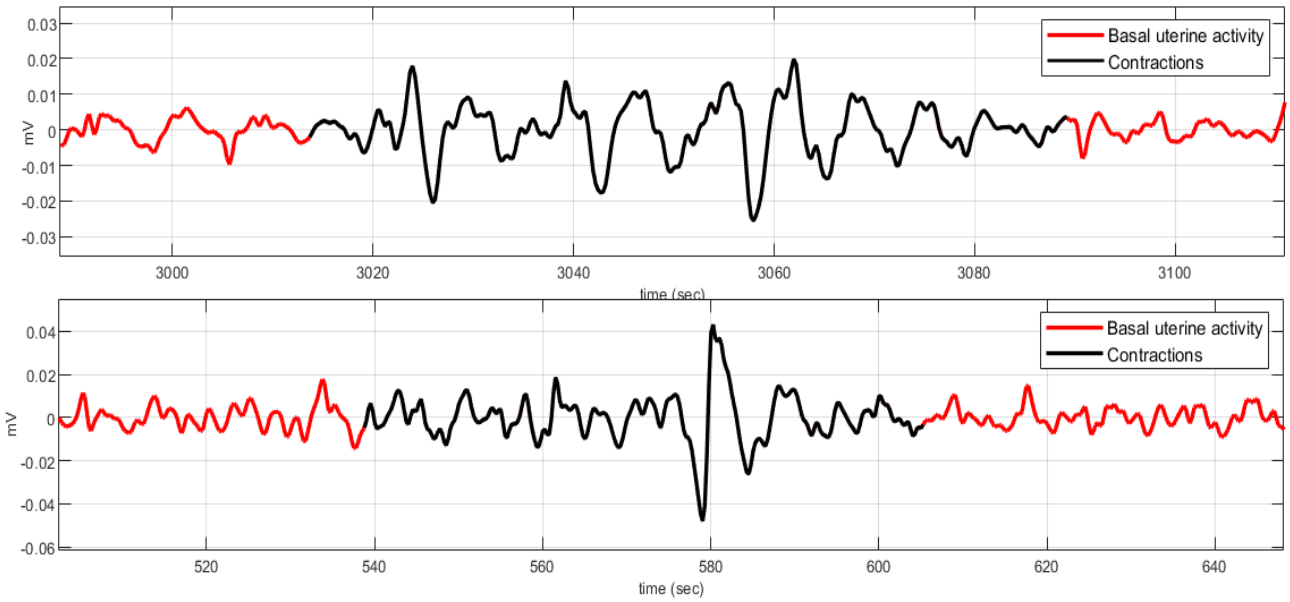

Figure 6.1: Two plots of contractions from EHG signal. The subject was the Ice004 from the Icelandic database. Visually is hard to compare the two contractions since the signal is non-stationary. Also, the contractions can have different number of samples which present a problem when determining a distance.

Power spectra were firstly used by *Itakura, F.* and *Saito, S.*[74] in the 1968 for speech recognition. Speech recognition is being able to identify spoken words and transform it into machine readable format. Since the 1970s this field has progressed, mostly due to the advances of digital signal processing and the increase of processing speed.[75] Nowadays there are several software applications available on the market that can differentiate words, recognize speakers, emotions and detect disordered or pathological voices.[76] Several researchers have used successfully power spectra for speech recognition. For example, researchers are now able to use the Automatic Speech Recognition to recover speech from noisy environments.[75,77] Power spectra have also been widely used with EHG and contractions analysis. Power spectra are used as a feature to choose the best parameters to classify contractions from the EHG signal and also to determine the power spectra peaks and the expected frequency band of the EHG.[67,78] Studying power spectra some researchers found that the amplitude of the power spectrum increased prior to the delivery but other studies came to the conclusion that amplitude did not had a substantial relation to the gestational age or delivery.[32,50,79,80]

So far, EHG researchers have used some features of the PSD estimations such as frequency peaks, median frequency and peak amplitudes. It is quite debatable if this is the best procedure for a

multicomponent spectrum as those shown in Figure 6.2. So, in this work it was decided to use the whole spectrum. This innovative approach has the drawback of higher computational demands. For instance, the 4622 (TPEHG database) spectra with 513 samples each and are all fed to the classification algorithm. There was a risk of being unable to process this data within a reasonable time span using a common computation platform.

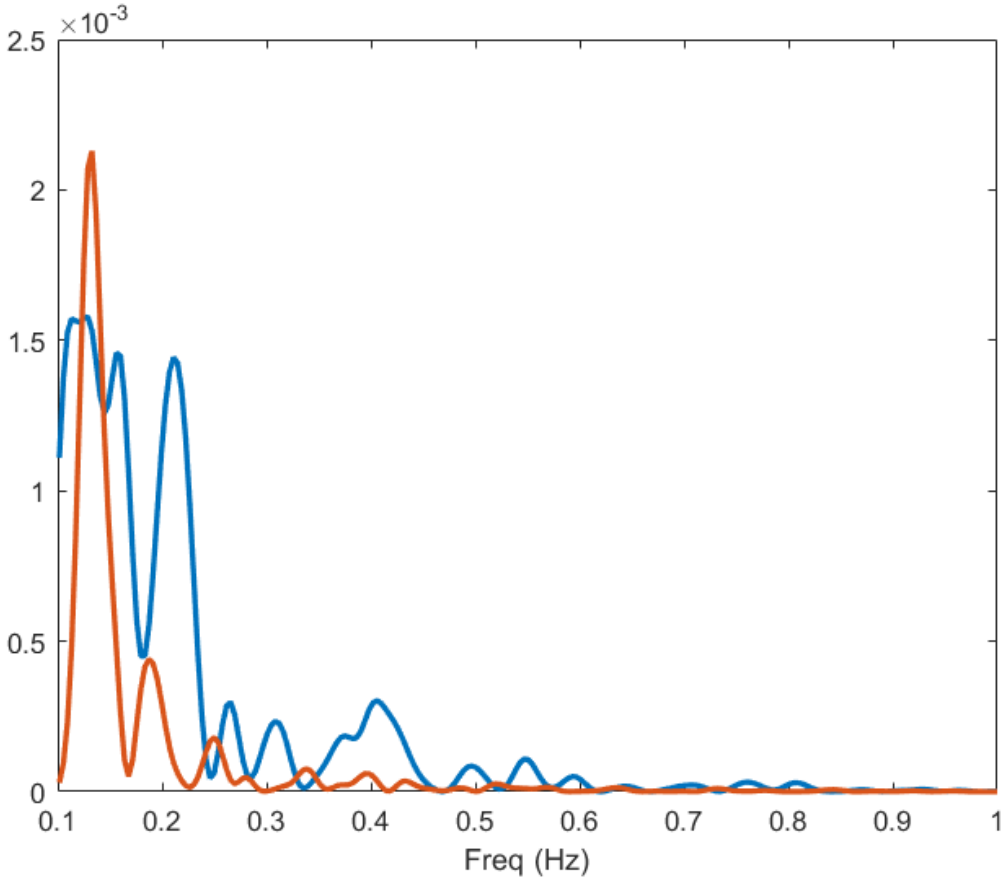

Figure 6.2: Power Spectrum of the two contractions shown in Figure 6.1. The power spectrums have the same dimension independently of the number of samples of the contractions making it a more suitable feature to work with when calculating a spectral distance.

To compare the power spectra of the contractions was necessary to use an adequate metric. There are many metrics however to it is necessary to understand their proprieties to choose the most suitable for clustering. A *metric* ρ on a set of *X*, associates to each pair of points in *X* a non-negative real number $\rho(x, y)$. Metrics should satisfy the following [81,82]:

1. $\rho(x, y) = 0$ when $x = y$

2. $\rho(x, y) = \rho(y, x)$

3. $\rho(x, z) \leq \rho(x, y) + \rho(y, z)$

The pair (X, ρ) is then called a *metric space* and the number $\rho(x, y)$ is called the *distance* between the points x and y. These axioms express that metrics are symmetrical (axiom 2) and satisfy the triangle inequality property (axiom 3).[81,83,84] Usually these two axioms are not respected. For clustering purposes, however, it is more convenient to use the symmetric divergences.[85] *Gray* and *Markel* refer that "true metrics satisfy the triangle inequality in addition to being symmetrical and

positive definite"[82] but this designation is not always respected. For example, the Itakura-Saito distance and the Itakura distance do not respect axioms 2 and 3 however they are referred in most articles as distances. In this thesis, *j* is the imaginary unit, such that $j^2 = -1$.

6.1 Itakura-Saito Distance and COSH Distance

The IS (Itakura-Saito) distance was created by *Itakura, F.* and *Saito, S.*[74] in 1968 from the maximum likelihood estimation of short-time speech spectra under autoregressive modeling. It is defined as "a measure of the goodness of fit between two spectra" and is a common measure for representing the difference between two signals in frequency domain.[74,86] It is represented as[43–45]:

$$d_{IS}(X,Y) = \int_{-\pi}^{\pi} \left[\frac{|X(\omega)|^2}{|Y(\omega)|^2} - log\left(\frac{|X(\omega)|^2}{|Y(\omega)|^2} \right) - 1 \right] \frac{d\omega}{2\pi} \quad (6.1)$$

Where $X(w)$ and $Y(\omega)$ represent the spectral estimations under comparison. For instance $|Y(w)|^2$ is represented using the following AR model[87]:

$$|Y(\omega)|^2 = \frac{\sigma^2}{|1 + a_1 e^{-j\omega} + a_2 e^{-j2\omega} + \ldots + a_p e^{-jp\omega}|^2} \quad (6.2)$$

Here σ and a_i (i=1, ..., *p*) are, respectively, the gain and the i[th] prediction coefficient of the Linear Predictive Coding (LPC) model of order p. This distance is not symmetric, is mostly concave and does not fulfil the triangle inequality.[90,91] The IS distance is a Bregman divergence generated from a convex function.[90,92] The Bregman divergences, named after *Bregman, L.M.*,[93] are a class of distortion functions and can be generated from convex functions. The Bregman divergences are not symmetrical and do not satisfy the triangle inequality property hence they are not a metric.[84,90,94] To calculate this distance the function *distispf* was used. This function can be found in the *voicebox* toolbox for MATLAB® and was created by Brooks,M.[95]. The cost function from IS distance, Figure 6.3, from *distispf* function is:

$$F(x) = pf1/pf2 - log(pf1/pf2) - 1 \quad (6.3)$$

Where $pf1$ and $pf2$ are the power spectra to be compared.

The COSH distance is the symmetric version of the Itakura-Saito distance and is defined[82]:

$$V(\theta) = ln\left[\frac{\sigma^2}{|X|^2}\right] - ln\left[\frac{\sigma'^2}{|Y|^2}\right] \quad (6.4)$$

$$\Omega = \int_{-\pi}^{\pi} \{cosh[V(\theta)] - 1\} \frac{d\theta}{2\pi} \quad (6.5)$$

Where θ is a normalized frequency plane, $\frac{\sigma^2}{|X|^2}$ and $\frac{\sigma\prime^2}{|Y|^2}$ represent the spectral models and Ω is the COSH distance.[82] To calculate this distance the function *distchpf* from the *voicebox* toolbox was used.[95] The cost function from COSH distance, Figure 6.4, from *distchpf* function is:

$$F(x) = (p1/p2 + p2/p1)/2 - 1 \quad (6.6)$$

Where $p1$ and $p2$ are the power spectra to be compared.

Figure 6.3 represent the cost function of the IS distance in 2D and 3D. Both plots show clearly the non-symmetrical nature of cost function representation. In the 2D plot, the displayed density of the contour lines also shows the increasing slope of the cost function towards the low frequencies in both frequency axis. Figure 6.4 represents the cost function for COSH distance where symmetricity is clearly displayed.

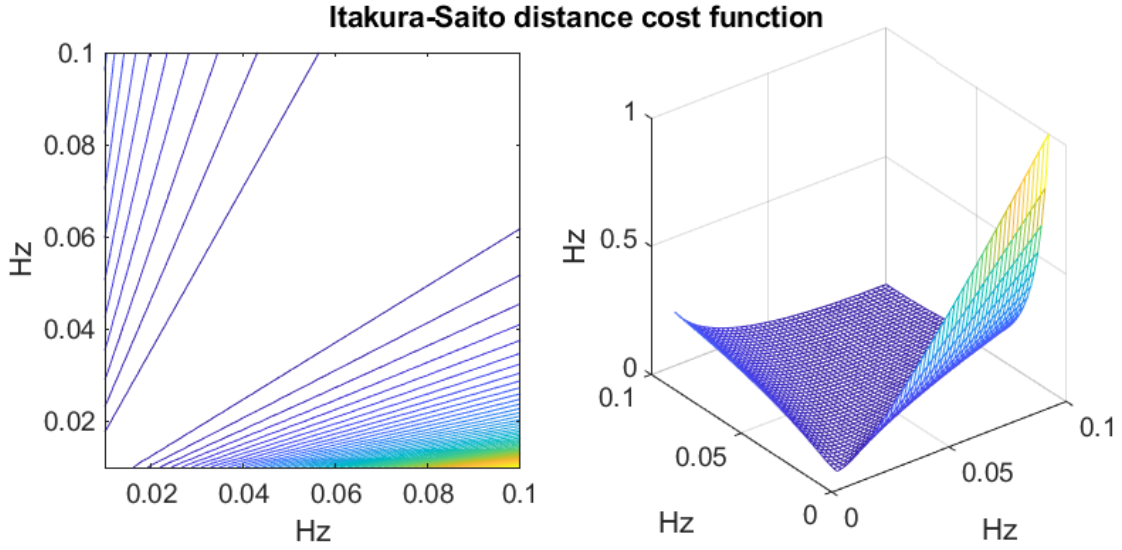

Figure 6.3: Cost function of Itakura-Saito distance: 2D contour (left) and respective 3D plot (right). The contour lines join points of equal value and between the lines there is an equal increment of height.

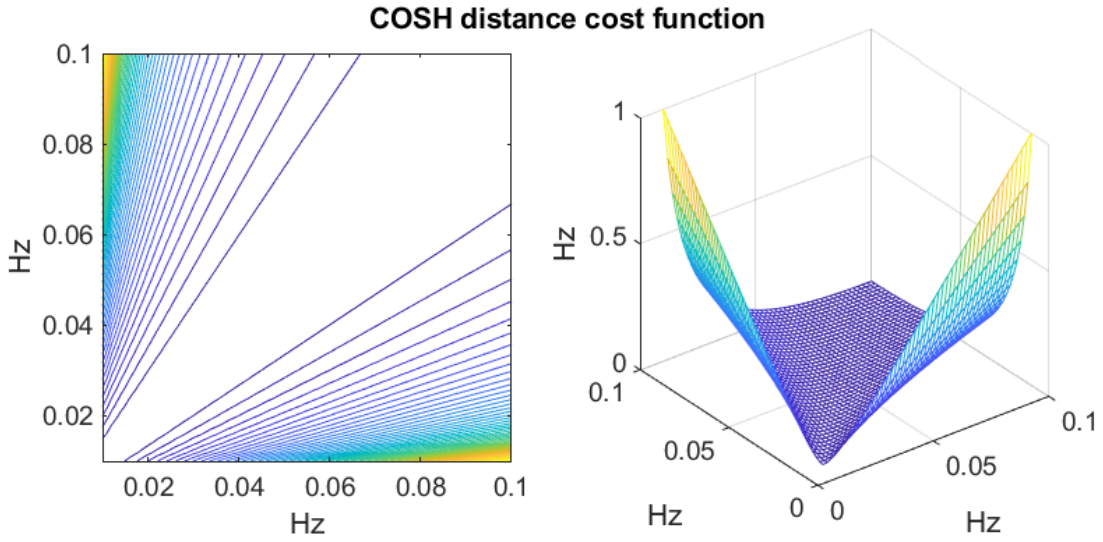

Figure 6.4: Cost function of COSH distance: 2D contour (left) and respective 3D plot (right).

6.2 Itakura Distance and Symmetrical Itakura Distance

The Itakura distance[96] is a distortion of the Itakura-Saito distance and it was created to minimize the gain sensibility. This distance is also known as *log likelihood ration distortion*[87] and is defined by:

$$d_I(X,Y) = log\left(\frac{1}{2\pi}\int_{-\pi}^{\pi}\frac{|X(\omega)|^2}{|Y(\omega)|^2}\,d\omega\right) \tag{6.7}$$

where $\frac{\sigma_X^2}{|X|^2}$ and $\frac{\sigma_Y^2}{|Y|^2}$ represent the spectra of the AR models[87,89,96]. This measure is gain independent and is not symmetrical. However we can obtain the symmetrical Itakura distance by doing[97]:

$$d_{Symetrical\,I}\,(X,Y) = \frac{d_{I(X,Y)} + d_{I(Y,X)}}{2} \tag{6.8}$$

To calculate this distance the function *distitpf* from the *voicebox* toolbox was used.[95] The cost function from Itakura distance, Figure 6.5, from *distitpf* function is:

$$F(x) = \frac{|X(\omega)|^2}{|Y(\omega)|^2} \tag{6.9}$$

Where $X^{\omega}$and Y^{ω} are the power spectra to be compared. It is clearly not symmetrical and with a quadratic slope.

The cost function from the symmetrical Itakura distance, Figure 6.6, is:

$$F_s(x) = 0.5 \times \left(\frac{|X(\omega)|^2}{|Y(\omega)|^2} + \frac{|Y(\omega)|^2}{|X(\omega)|^2}\right) \tag{6.10}$$

Although F_s being a symmetrical function the quadratic slope is obviously present.

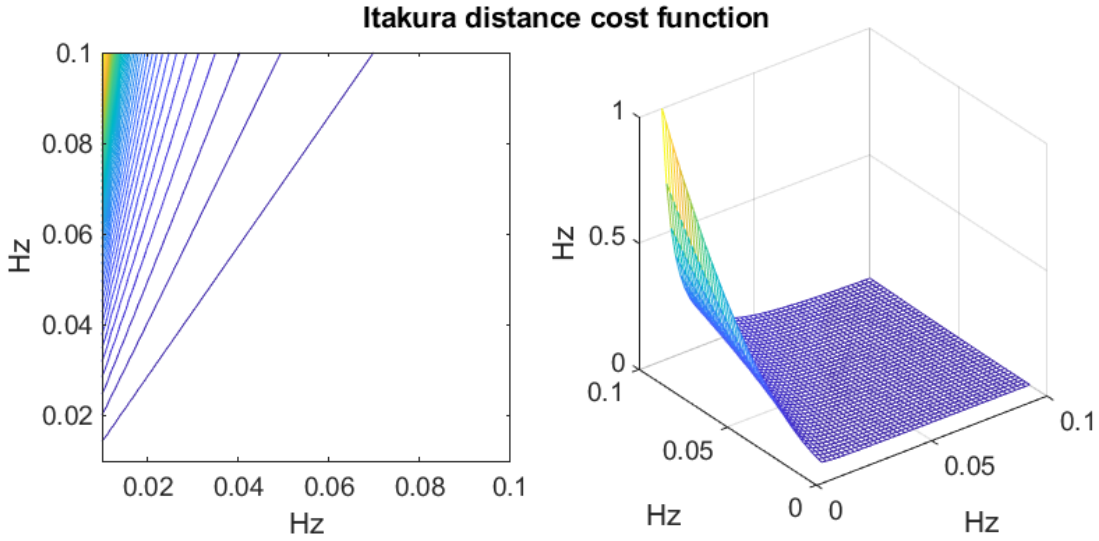

Figure 6.5: Cost function of Itakura distance: 2D contour (left) and respective 3D plot (right). The contour lines join points of equal value and between the lines there is an equal increment of height.

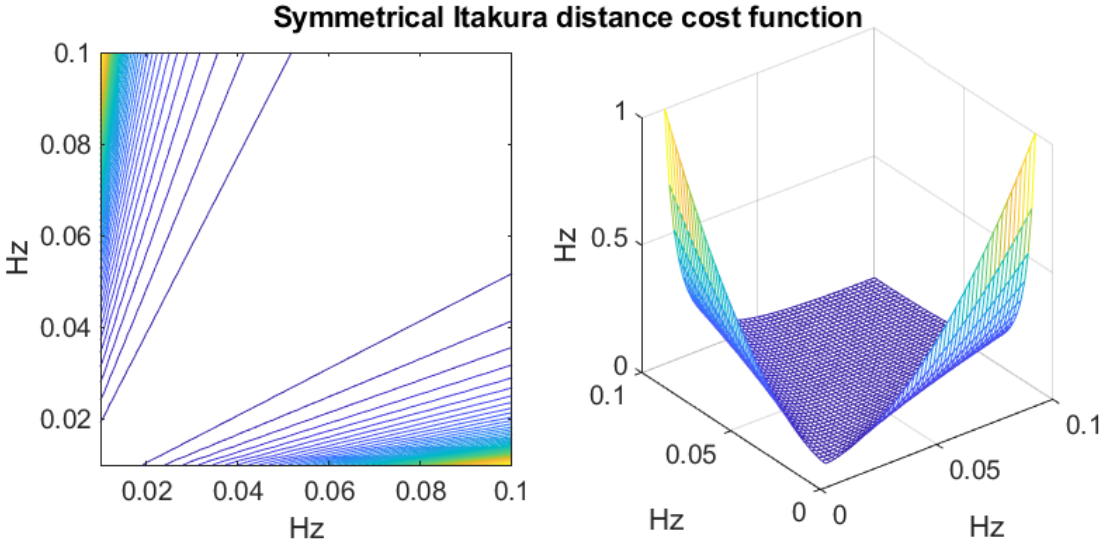

Figure 6.6: Cost function of the symmetrical Itakura distance: 2D contour (left) and respective 3D plot (right).

6.3 Kullback-Leibler Divergence and Jeffrey Divergence

The KL (Kullback-Leibler) Divergence, also called *relative entropy*, *information gain or I-divergence* is an information theoretic measure of the divergence between two probability distributions. The KL divergence is defined [86,98]:

$$D_{KL}\,(P||Q) = = \int_{-\infty}^{\infty} p(x)\, log\left(\frac{q(x)}{p(x)}\right) \mathrm{d}x \tag{6.11}$$

for continuous distributions P and Q and where p and q denote the probability densities of P and Q. This measure is non-negative, asymmetrical, convex and does not fulfil the triangle inequality property.[91,99,100] The KL divergence can also be used as a distance measure between two spectral density functions.[101,102] The KL divergence is a Bregman divergence generated from a convex function.[90,92] A typical problem of the KL divergence happens when $p(x)$ is very low for a particular x so the specific term $\frac{q(x)}{p(x)}$ can dominate the result.[103]

The Jeffrey divergence is a way of making the KL divergence symmetrical, that can be used for AR models and is given by[104–106]:

$$d_{JD}\,(P||Q) \;=\; d_{KL(P||Q)} + \; d_{KL(Q||P)} \tag{6.12}$$

To calculate this distance the function *KLDiv* was used. This function was created by David Fass for MATLAB®.[107] The cost function from KL divergence, Figure 6.7, from *KLDiv* function is:

$$F_{KL}(x) = p(x)\, log\left(\frac{q(x)}{p(x)}\right) \tag{6.13}$$

Where $p(x)$ and $q(x)$ are the power spectra to be compared. The cost function from Jeffrey divergence, Figure 6.8, is:

$$F_{JD}(x) = p(x)\, log\left(\frac{q(x)}{p(x)}\right) \;+\; q(x)\, log\left(\frac{p(x)}{q(x)}\right) \tag{6.14}$$

Figure 6.7 shows that the KL function is not symmetrical and displays a soft slope in the low frequency. Figure 6.8 represents the symmetrical nature of the Jeffrey divergence. The slope it is more evenly distributed between the bisector frequency line and the limit frequency axis.

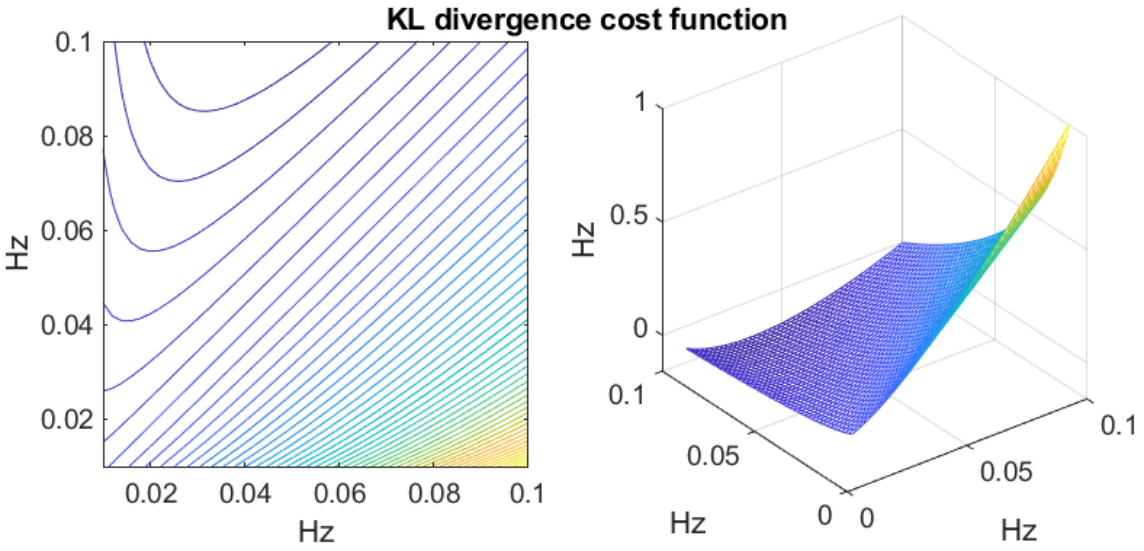

Figure 6.7: Cost function of KL divergence: 2D contour (left) and respective 3D plot (right). The contour lines join points of equal value and between the lines there is an equal increment of height.

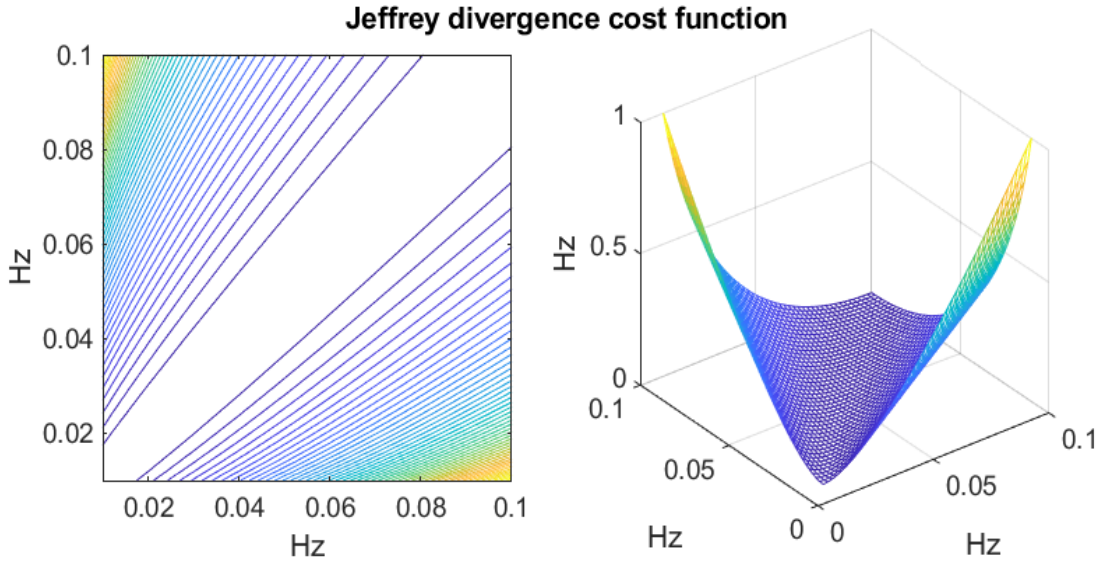

Figure 6.8: Cost function of Jeffrey divergence: 2D contour (left) and respective 3D plot (right).

6.4 Rényi Entropy, Rényi Divergence and Jensen-Rényi Divergence

In 1961 *Rényi, A*[108] introduced the *entropy of order* α of a discrete probability distribution $\{pi\}$, $i = 1, \ldots, n$:

$$d_{Re}\,(p) = \frac{1}{1-\alpha}\,\log_2 \sum_{i=1}^{n} p_i(x)^{\alpha} \tag{6.15}$$

The Rényi Divergence *of order* α is defined as the number of bits by which a mixture of two codes can be compressed. The expression of this divergence is[109]:

$$D_{\alpha}\,(P||Q) = \frac{1}{1-\alpha}\,\log\left(\int p(x)^{\alpha} q(x)^{1-\alpha}\,\mathrm{d}x\right) \tag{6.16}$$

where P and Q are different continuous distributions, with probability densities respectively equal to p and q and $\alpha \neq 1$. The Rényi divergence is positive and is not symmetrical. The Rényi divergence can also be used as a distance measure between two spectral information functions.[102,110,111] When $\alpha = 1$ the KL Divergence is obtained and when $\alpha = \frac{1}{2}$ the Rényi divergence is symmetrical. [109] The Jensen-Rényi divergence is symmetrical version of the Rényi divergence for any positive value of α and is given by:

$$D_{JRD}\,(P,Q) = d_{Re}\left(\sqrt{PQ}\right) - \frac{d_{Re}\,(P) + d_{Re}\,(Q)}{2} \tag{6.17}$$

where $P\ and\ Q$ are the power spectra and d_{Re} represents the Rényi entropy also defined on the power spectra.[52–55] To calculate this distance the functions *K_q_renyi* was used. This function was created by Guan Wenye for MATLAB®.[116] The cost function from Rényi divergence from *K_q_renyi* function, Figure 6.9 (α=0.45) and Figure 6.11 (α=0.5), is:

$$F(x) = p_i(x)^{\alpha} q_i(x)^{1-\alpha} \tag{6.18}$$

where $p_i(x)$ and $q_i(x)$ are the power spectra to be compared. [116] The cost function from Jensen-Rényi divergence, Figure 6.10 (α=0.45) and Figure 6.12 (α=0.5), is:

$$F_{JRD}(x) = p_i(x)^{\alpha} q_i(x)^{1-\alpha} + q_i(x)^{\alpha} p_i(x)^{1-\alpha} \tag{6.19}$$

Inspecting the symmetrical cost functions (Figure 6.10, 6.11 and 6.12) the following comments apply: Jensen-Rényi with α=0.45 (Figure 6.10) shows a saddle-like zone around the bisector frequency axis which represents lower sensitivity in this area which eliminates this cost function in this work. Figure 6.11 and 6.12 are equivalent and represent the Rényi divergence and the Jensen-Rényi divergence with α=0.5. The slope is smother compared to Jeffrey divergence in Figure 6.8. this makes this cost function a candidate for this work.

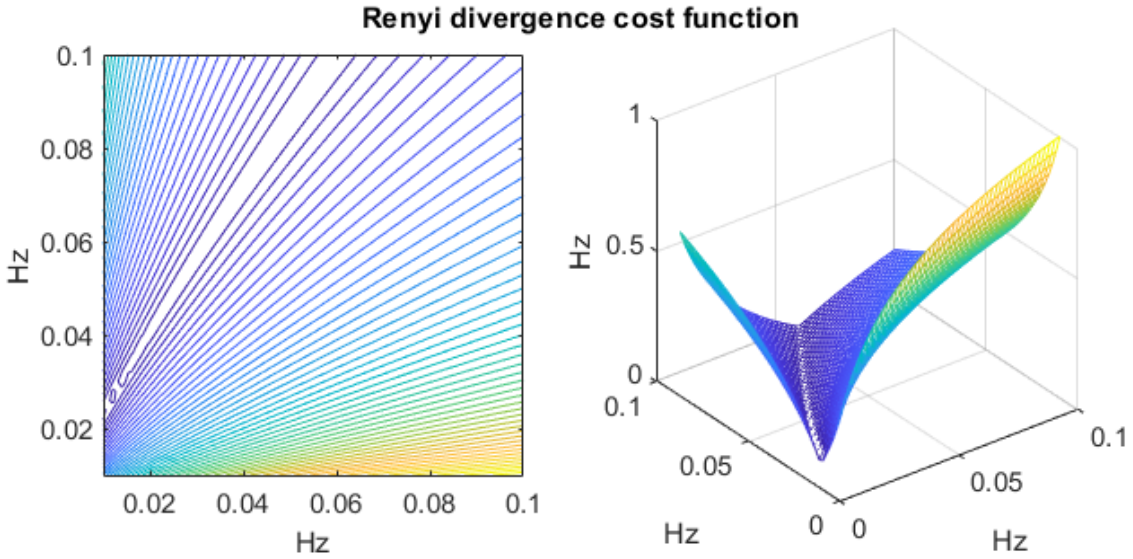

Figure 6.9: Cost function of Rényi divergence: 2D contour (left) and respective 3D plot (right) with α=0.45. The contour lines join points of equal value and between the lines there is an equal increment of height.

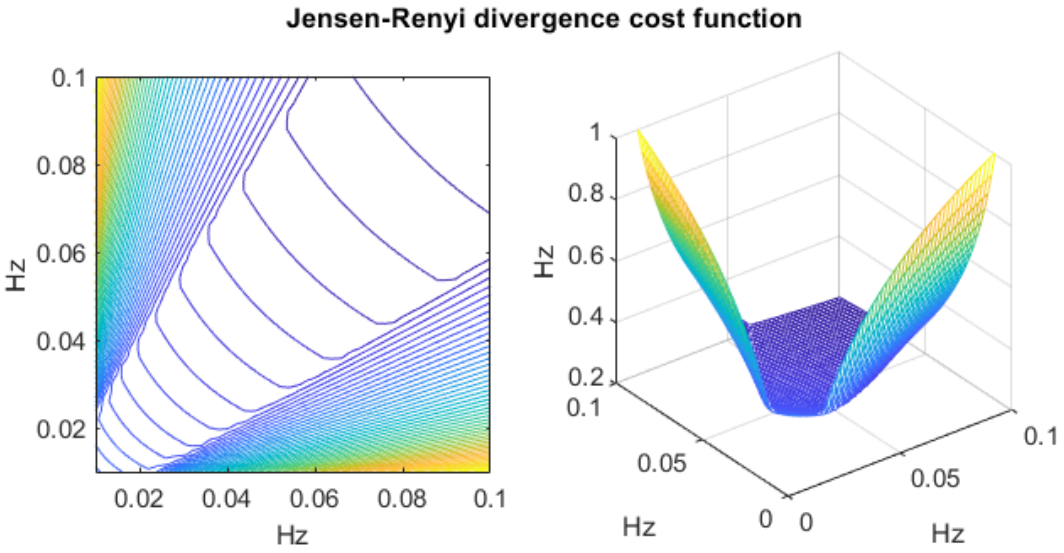

Figure 6.10: Cost function of Jensen-Rényi divergence: 2D contour (left) and respective 3D plot (right) with α=0.45

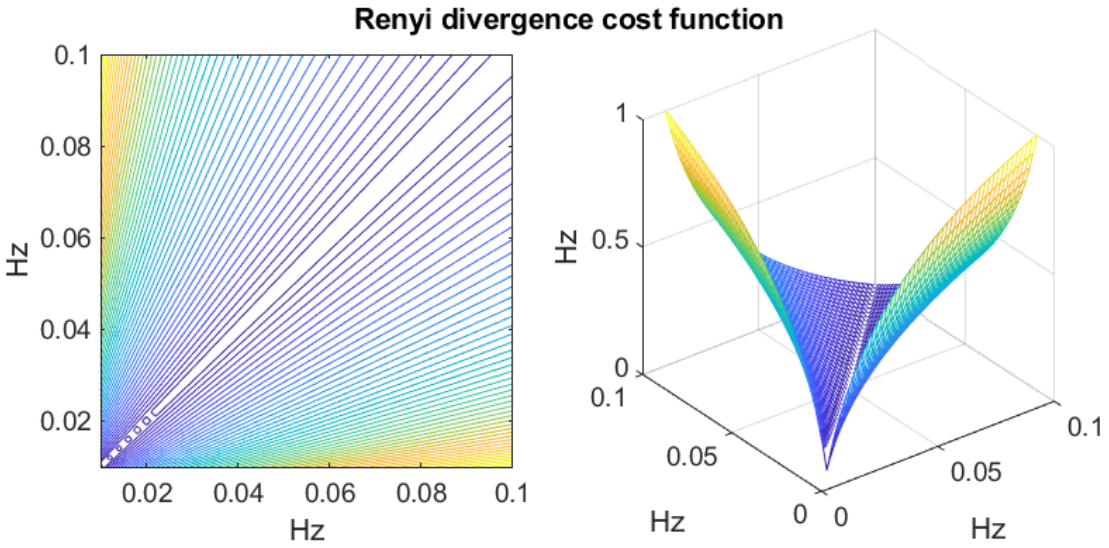

Figure 6.11: Cost function of Rényi divergence: 2D contour (left) and respective 3D plot (right) with α=0.5. The contour lines join points of equal value and between the lines there is an equal increment of height.

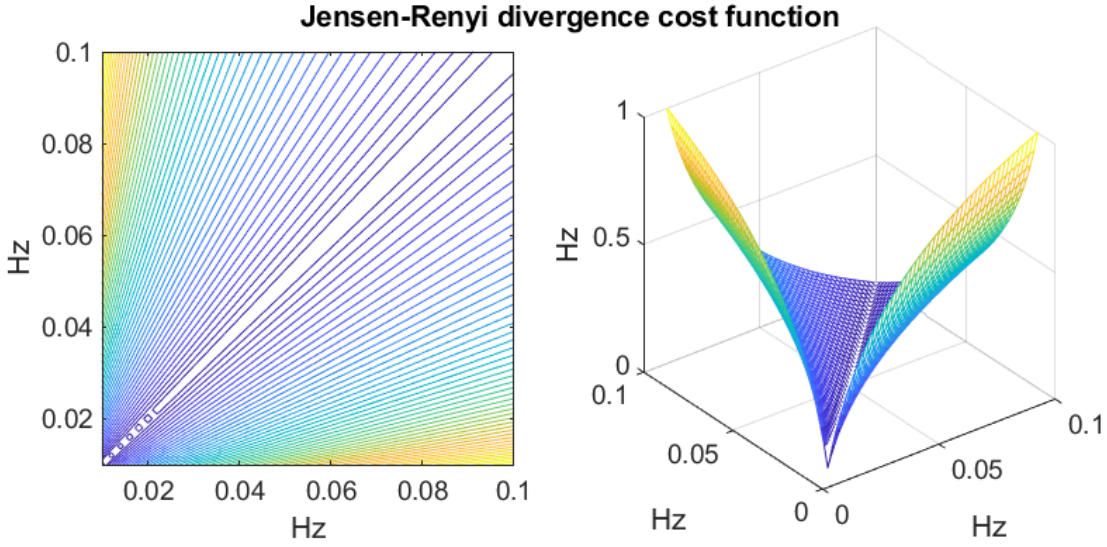

Figure 6.12: Cost function of Jensen-Rényi divergence: 2D contour (left) and respective 3D plot (right) with α=0.5. In this case, the Jensen-Rényi divergence is the same as the Rényi divergence since the α=0.5 makes the Rényi divergence symmetrical.

6.5 Distance Computation

For this purpose, the MATLAB® resident *pdist* command has been used, with a customized option. Four symmetrical distances were considered. The question still remains which of the following symmetrical cost functions with smooth slope should be selected:

- COSH distance, with function *distchpf;*
- Symmetrical Itakura distance, with function *distitpf*
- Jeffrey divergence, with function *KLDiv;*
- Jensen-Rényi divergence, with function *K_q_renyi*.

The *KLDiv* function was adapted in this work since its original version would not allow the comparison of one spectrum against a matrix. To solve this problem a new function was created called *KLDiv_simetric_filipa_v2*. The following adaptations were performed:

- The function returns a symmetrical distance;
- A loop was added to allow the calculation of a distance between a matrix and a single observation.

In order to select one of the four previously mentioned cost functions it has been performed a test using a simulated spectrum with two frequency peaks. The spectral distances will be evaluated between this spectrum and its own 11 displaced versions.

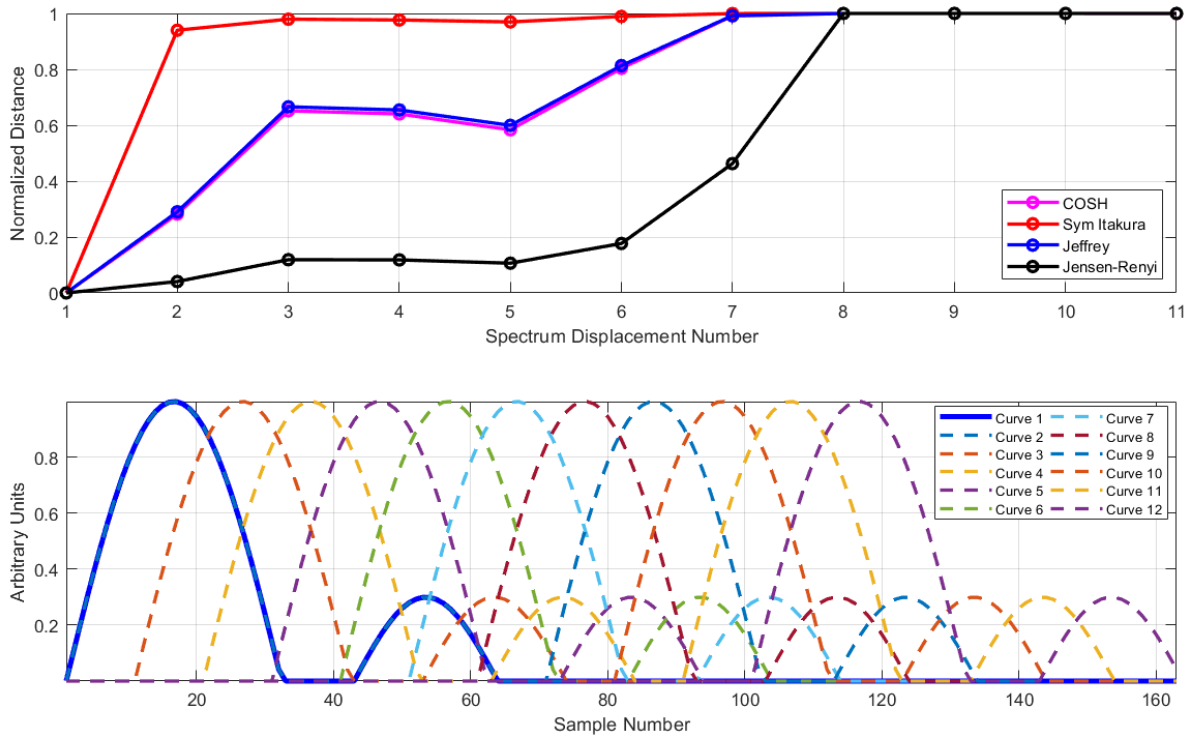

Figure 6.13: On top plot: Spectral distances of the four selected cost functions using a simulated spectrum with two frequency peaks. On bottom plot: The simulated spectrum is shifted several points forward and compared with the blue plot. To each increment a distance is calculated.

As seen in the figure on top the symmetrical Itakura distance displays low sensitivity above the first increment. The Jensen-Rényi divergence displays a similar behavior until the 6th increment. Both the COSH distance and Jeffrey divergence display more increment sensitivity. The COSH distance and the Jeffrey divergence produce therefor similar best results. Both distances were applied to the power spectra of the contractions obtained in both databases. A histogram of the Jeffrey divergence distances and the COSH distances is presented in Figure 6.14 and 6.15, respectively. By analyzing the histograms it is possible to conclude that the COSH distance gives distances in a wider range than the Jeffrey divergence, meaning that some values obtained with the COSH method are very different from the remaining ones. This difference between values could complicate the clustering analysis since these extreme values could be assigned to clusters with only a couple of observations. In this respect the Jeffrey divergence seems to have more balanced results since it presents a smaller range of values. For that reason, the Jeffrey divergence was chosen to be applied in the clustering analysis.

The next step of this work will be the clustering operation of the power spectra, which is presented in the chapter 7.

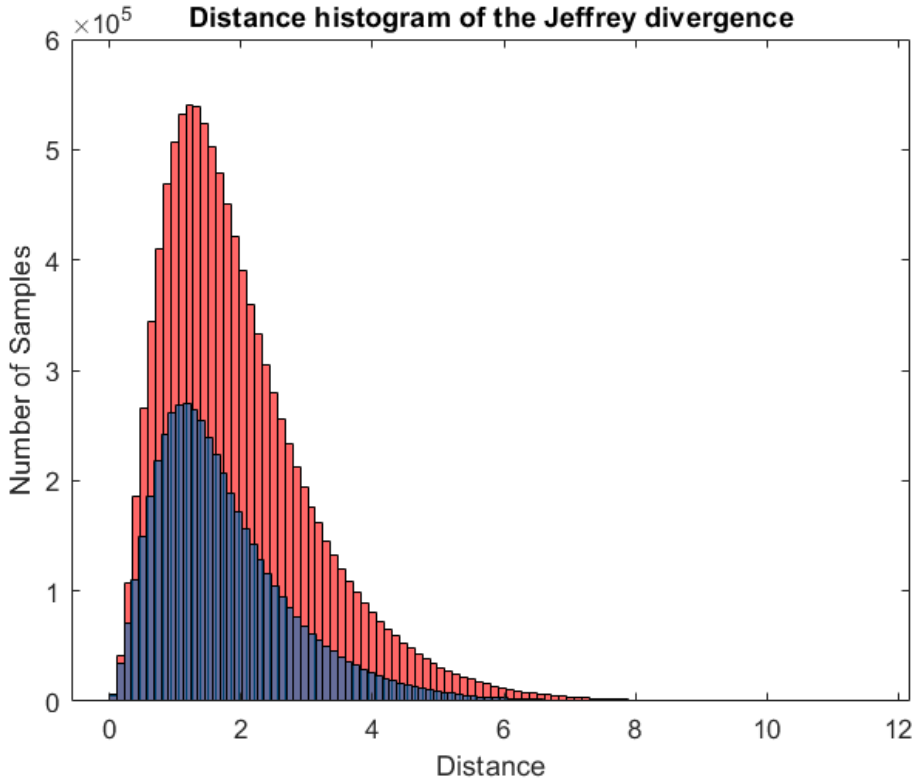

Figure 6.14: Histogram of the distances relative of the spectrum of contractions from the TPEHG database (red) and the Icelandic database (blue), calculated with the Jeffrey divergence.

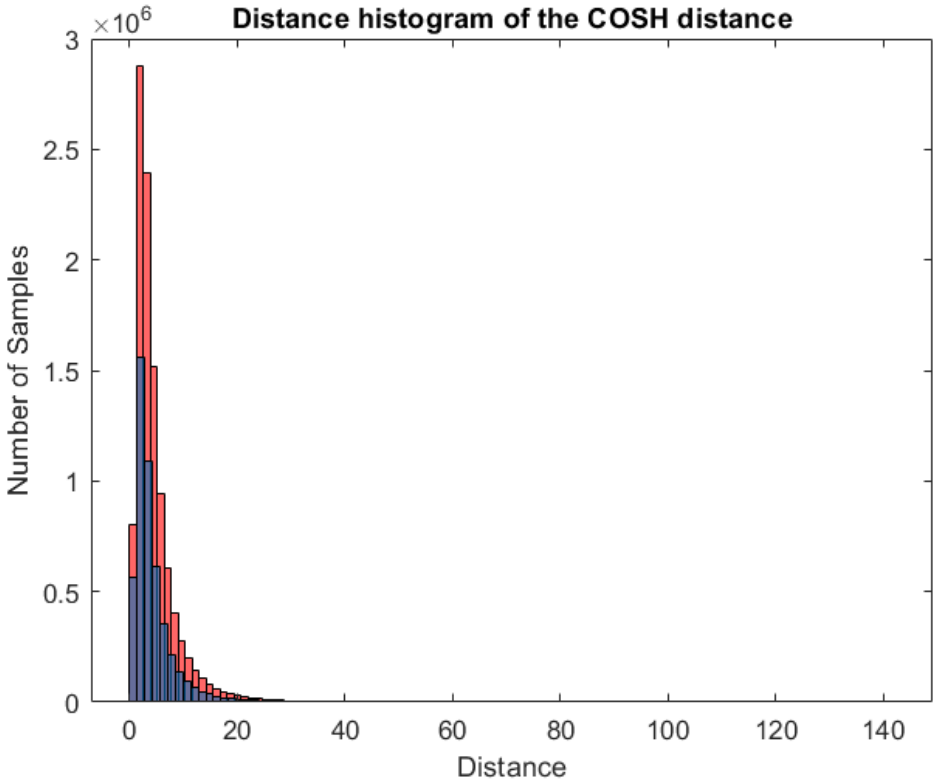

Figure 6.15: Histogram of the distances relative of the spectrum of contractions from the TPEHG database (red) and the Icelandic database (blue), calculated with the COSH divergence.

Chapter 7 – Cluster Analysis

Cluster analysis consists in organizing data into groups so that observations within a cluster are more similar to each other than they are to objects from other clusters.[117] Cluster analysis was introduced in 1939 by Tryon, R..[118] Since then new algorithms for cluster analysis have been developed and its now used in various fields of science.[119] Clustering can be divided in two subgroups: hard clustering and soft clustering. In hard clustering, data is clustered in an exclusive way, meaning that each point of data belongs to only one cluster. In soft clustering each point of data may belong to two or more clusters with different likelihoods.[120] In this thesis only hard clustering is explored. Cluster analysis methods can be divided in several groups but only hierarchical clustering and partitional methods are discussed in this work.

7.1 Linkage Clustering

Hierarchical clustering consists in consecutive aggregation or division of the data, depending if it is a bottom-up or a top-down approach. In the agglomerative method, or bottom-up approach, each observation is assigned to its own cluster and the two most similar cluster are joined and in divisive method, or the top-down approach, the observations are all in the same cluster and are divided in the two less similar clusters.[121] The groups that result from hierarchical clustering are nested and organized in a tree-like structure known as dendrogram. A dendrogram shows how the clusters are linked to each other. It also displays a numeric value that represents the distance between two clusters.[122] In hierarchical clustering it is not necessary to determine the number of groups ahead of time which makes this a good method to explore the data. One of the problems of hierarchical clustering is that it is not possible to split the clusters once they are grouped, meaning that once an object is assigned to one cluster it cannot be reassigned to a "better fitting" cluster.[117,122]

The function *linkage* implements the hierarchical clustering in which are presented 8 possible methods for linkage criteria. These methods are ward, single, complete, average, Mcquitty, median, centroid and custom distance function. Below are the equations of the first 7 methods and a brief explanation of each one. Given a cluster *A* and *B*, the number of objects in each cluster is given by n_A and n_B.

- Ward linkage

The Ward linkage, also called Ward's minimum variance method measures the distance between two clusters by how much the variance will increase when we merge them, that is, it links the two clusters that lead to the minimum increase of within-cluster variance after merging. The within-cluster variance, is defined by[84,121,123]:

$$ESS = \sum_{x_p \epsilon \mathrm{A}} (x_p - \bar{x}\,)^2 \tag{7.1}$$

where x_p is the value of the p-observation and $\bar{x}$ is the mean of the observations. This method is very efficient but can create small size clusters.[121]

- Single linkage

The Single linkage, also known as nearest-neighbor linkage or shortest-distance linkage, measures the distance between clusters and merges groups based on the minimum distance between them. The following equation represents this method[84,124–126]:

$$d_c(A,B) = min\ \{d(x_{Ai}, x_{Bj})\} \tag{7.2}$$

where $d(x_{Ai}, x_{Bj})$ is distance between the observation *i* from group *A* and observation *j* from group *B*. This distance often presents the changing problem, when clusters are created due to single elements being close to each other which could create a cluster with objects that are very distant to each other. Still, this method can effortlessly identify outliers, which will be the last to be merged.[121,127]

- Complete linkage

The Complete linkage or maximum linkage joins groups based on the maximum distance between two objects in two groups, meaning that the distance between clusters *A* and *B* [84,121,126,128,129]:

$$d_c(A,B) = max\ \{d(x_{Ai}, x_{Bj})\} \tag{7.3}$$

where $d(x_{Ai}, x_{Bj})$ is distance between the observation *i* from group *A* and observation *j* from group *B*. This method avoids the chaining problem and tends to find compact clusters of equal diameters. However, a problem of this distance is when the data has outliers since these prevent close clusters to merge together. Nevertheless, complete linkage is not adequate when there is substantial amount of noise in the data.[121,127]

- Average linkage

The average linkage, also called UPGMA (Unweighted Pair Group Method with Arithmetic Mean), calculates the average of all distances between all pairs of objects that belong to both clusters and is defined as[84,126,130]:

$$D(A,B) = \frac{1}{n_A \times n_B} \sum_{x_p \epsilon A} \sum_{x_q \epsilon B} d(x_p, x_q) \tag{7.4}$$

where n_A represents the number of objects in the cluster A and n_B represents the number of objects in the cluster B. The average linkage overcomes the limitations of single and complete linkage and offers a more precise evaluation of the distance between clusters.[127]

- Mcquitty linkage

The Mcquitty linkage, also called WPGMA (Weighted Pair Group Method with Arithmetic Mean), is similar to the average linkage however the distance is calculated as an average. For example, the distance between *A* and *B*, where *B* is composed of B_m and B_n, is[84,121,129]:

$$D((A \cup B), C) = \frac{d(A,C) + d(B,C)}{2} \tag{7.5}$$

This method is recommended when the clusters have different number of objects.[84]

- Centroid linkage

Centroid linkage, also called UPGMC (Unweighted Pair Group Method Centroid), uses centroids to calculate the distances between a cluster and all remaining clusters. This way, when a new cluster is formed a new centroid is assigned. This new centroid is the average of all the objects that constitute it. The centroid equation is given by:[84,121,128]

$$c_A = \frac{1}{n_A} \sum_{x_p \epsilon A} x_p \tag{7.6}$$

where n_A represents the number of objects in the cluster A and c_A is the centroid of the cluster A. The distance by two centroids is[121]:

$$D(A, B) = d(c_A, c_B) \tag{7.7}$$

- Median linkage

The median linkage, also called WPGMC (Weighted Pair Group Method with Arithmetic Centroid), determines the weighted centroid of the cluster as presented [84,121,131]:

$$w_A = \frac{1}{2}(w_m + w_n) \tag{7.8}$$

where $w_m \; and \; w_n$ are the weighted centroids of the clusters M and N and the cluster A is composed by M and N. The distance is given by[121,131]:

$$D(A, B) = d(w_A, w_B) \tag{7.9}$$

This method is similar to Centroid Linkage, however the centroid of the newly fused groups is positioned at the median between the old group centroids.

A study has shown that the Ward's method performs better with the exception where the data contain one or two very large groups and a few other very small groups, in that case average linkage presents better results. This study has also shown that complete linkage and single linkage should not be used when clustering functional data.[126] Another study that compared the complete, average and single linkage concluded that the average linkage was the natural compromise between single and complete linkage since the single linkage is sensible to outliers and the complete linkage is highly influenced by outliers.[127] Generally average linkage performs well, and it maximizes the cophenetic correlation coefficient.[119] For those reasons the average linkage was chosen for the clustering analysis.

7.2 K-means and K-medoids Clustering

Partitional methods, also called optimization methods, were developed to overcome the shortcoming presented by the hierarchical clustering. The K-means and the K-medoids methods are two examples of partitional methods. In partitioning methods, the data is separated into a *k* number of clusters decided previously, each partition represent a cluster. The main advantages of partitional methods are that it only requires the data as input, it is easy to implement and can handle large datasets. However, the main disadvantage is that the number of clusters needs to be predetermined. Partitional methods are also very sensitive to the initial centers and can lead to empty clusters.[117,122]

In the K-means algorithm groups are based on their closeness to each other according to a pre-determined distance, i.e. the Euclidean, Manhattan or correlation distance. This method calculates the cluster center, called centroid, and assigns each object to minimize the sum of squares of distances between the object and the corresponding cluster centroid. The square error sum is defined by[132,133]:

$$Q(P) = \sum_{P_j \in P} \sum_{P_i \in P} d^2(x_i, z_j) \tag{7.10}$$

where $Z = \{z_1, \ldots, z_n\}$ represent the centers of gravity for the classes $P_1, \ldots, P_n$ and x_i represents the data.

To initialize this method the centroid is randomly selected from the data.[134] The K-means algorithm has some disadvantages since it depends on a suitable initialization and on the number of clusters chosen. [132,133]

The K-means algorithm is divided in four key steps:

1. Select the observation assigned as the initial cluster center.
2. Create *k* clusters by assigning each observation to its closest centroid.
3. Calculate the new centroid's values.
4. Repeat step 3 and 4 until convergence.[135,136]

The K-medoids algorithm is similar to the K-means algorithm since both search for *k* representatives in the dataset.[133] The K-medoids follows parallel steps to the K-means except that in step 3 it calculates the medoid of each cluster.[121] The difference between these methods is that K-medoids chooses data points as centers, called medoids, while K-means uses centroids. Medoids are more robust to outliers than the K-means since outliers can affect centroids but hardly affect medoids. [133,134] Studies that performed comparisons between K-means and K-medoids and overall report that K-medoids performs better than K-means.[134,137] For that reason, the K-medoids method was chosen for the clustering analysis.

7.3 Study case

In Chapter 3, the five contraction classes found in literature were addressed. To verify if five is an adequate number of clusters the Upper Tail Rule was applied.

The Upper Tail Rule, also called Elbow method, was developed to determine the number of clusters in hierarchical clustering. In this method the percentage of variance explained by the clusters is plotted against the number of clusters. The first clusters add plenty information but at some point, the marginal gain drops dramatically displaying an angle, called the "Elbow" criteria.[122,138] The *mojenaplot* function from the EDA Toolbox[139] was used to study the Upper Tail Rule and the results are in the Figure 7.1 and Figure 7.2.

Analyzing Figure 7.1, the elbow in the curve seems to indicate that 4 or 5 clusters could be chosen for in the Icelandic database. Analyzing the plot for the TPEHG database, the results are less clear. It could be said that 5 or 6 clusters are adequate for this data. Based in the literature and the Upper Tail Rule the number of clusters chosen was five.

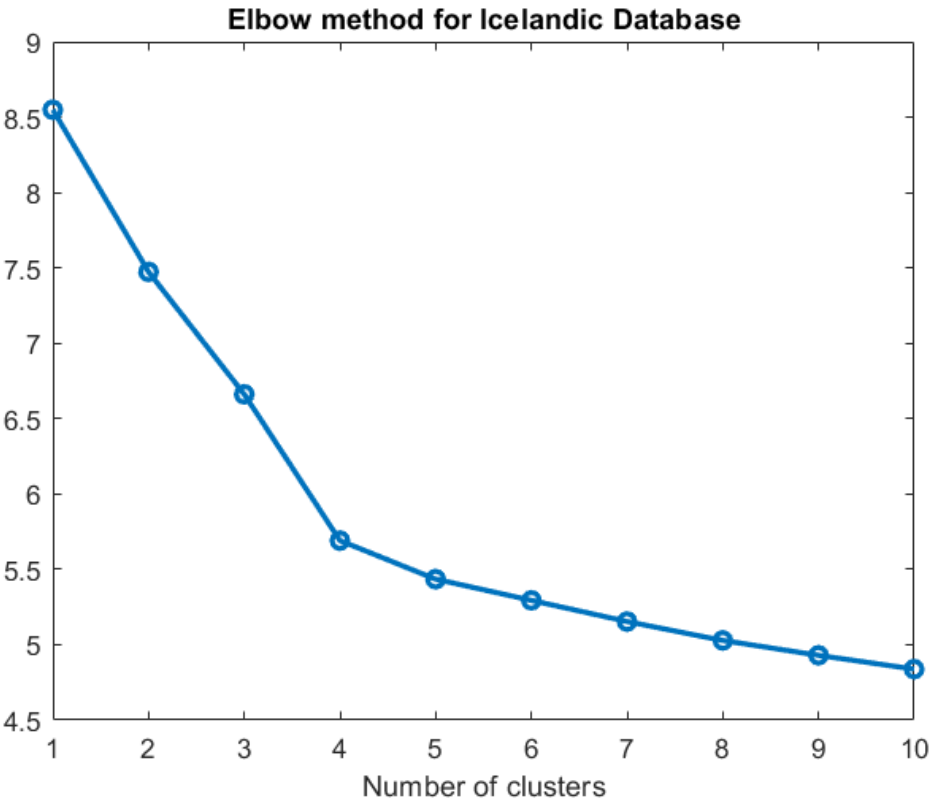

Figure 7.1: Elbow method for the Icelandic database

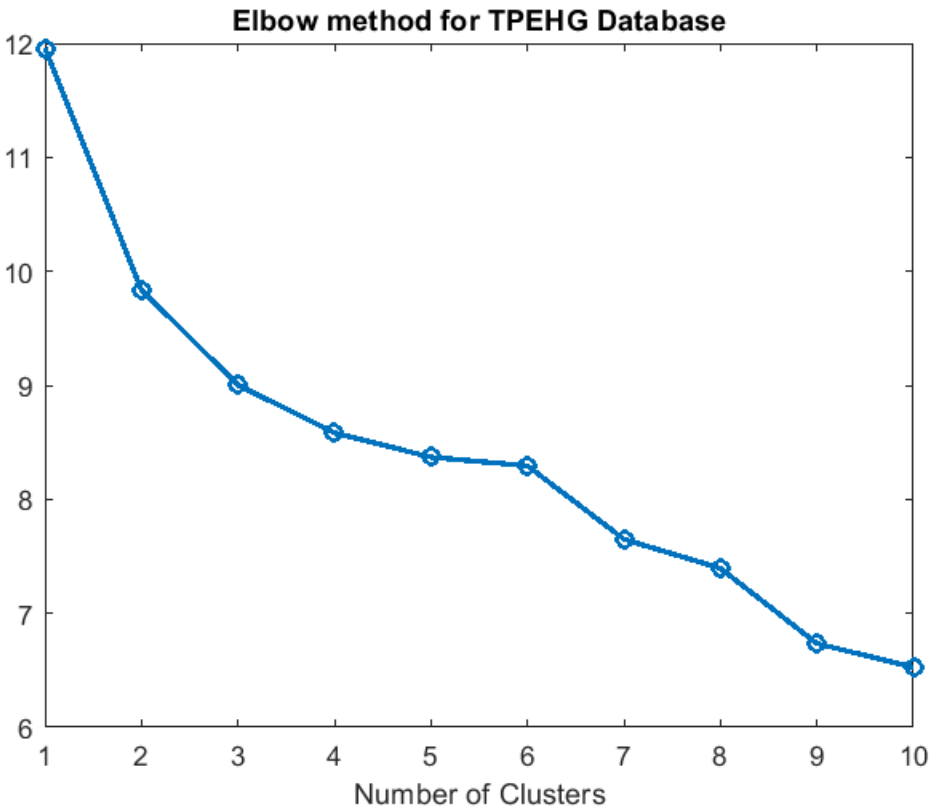

Figure 7.2: Elbow method for the TPEHG database

To perform cluster analysis of the power spectra the function *clustering_dist_pdist_new_v11* was built, Figure 7.3. This function was used for the power spectra of the separated contractions databases of the Icelandic and the TPEHG databases. Upon on evoking this command a pop out menu prompts the user to select a database.

```
>> clustering_dist_pdist_new_v11('welch', 'jeffrey', 'linkage', 'average', 'cityblock', 5, 920)
```

Figure 7.3: Command line of function *clustering_dist_pdist_new_v11*

The inputs of the function *clustering_dist_pdist_new_v11* are:

- *psd_method_name:* string with the name of the chosen PSD method, i.e. 'welch' method;
- *distance_method:* string with the name of the chosen distance method, i.e. 'COSH' distance or 'Jeffrey' divergence;
- *cluster_method:* string with the name of the chosen hierarchical clustering method, i.e. 'linkage' or 'k-medoids';
- *link_method_name:* string with the name of the chosen linkage method, i.e. 'average' or 'complete';
- *kmeans_method_name:* string with the name of the chosen K-means distance, i.e. 'cityblock' or 'sqeuclidean';
- *cluster_number:* number of clusters desired;
- *number_of_samples_for_ldbf:* length of the LDBF wave, in number of samples.

The output of the function *clustering_dist_pdist_new_v11* is:

- *clusters_id*: cell with length of *cluster_number*. Each row corresponds to a cluster. In each cluster is all the information corresponding to the observations assigned to that cluster, Figure 7.5;
- *poss_ldbf:* cell with similar organization of *clusters_id*. All the information corresponding to the contractions with length superior to *number_of_samples_for_ldbf* is included, Figure 7.6;
- *visit_clusters:* table organized per visit of the subject that shows the clusters in which the contractions of the subject were placed in, Figure 7.7;
- *ccoph:* value of the cophenetic correlation coefficient, Figure 8.4 and Figure 8.16;
- *mean_silhouette:* value of the mean silhouette.

The function *clustering_dist_pdist_new_v11* normalizes the power spectra of the chosen PSD method, in this case the Welch method and adds $1e^{-5}$ to each spectrum. A flowchart of the function is displayed in Figure 7.4.

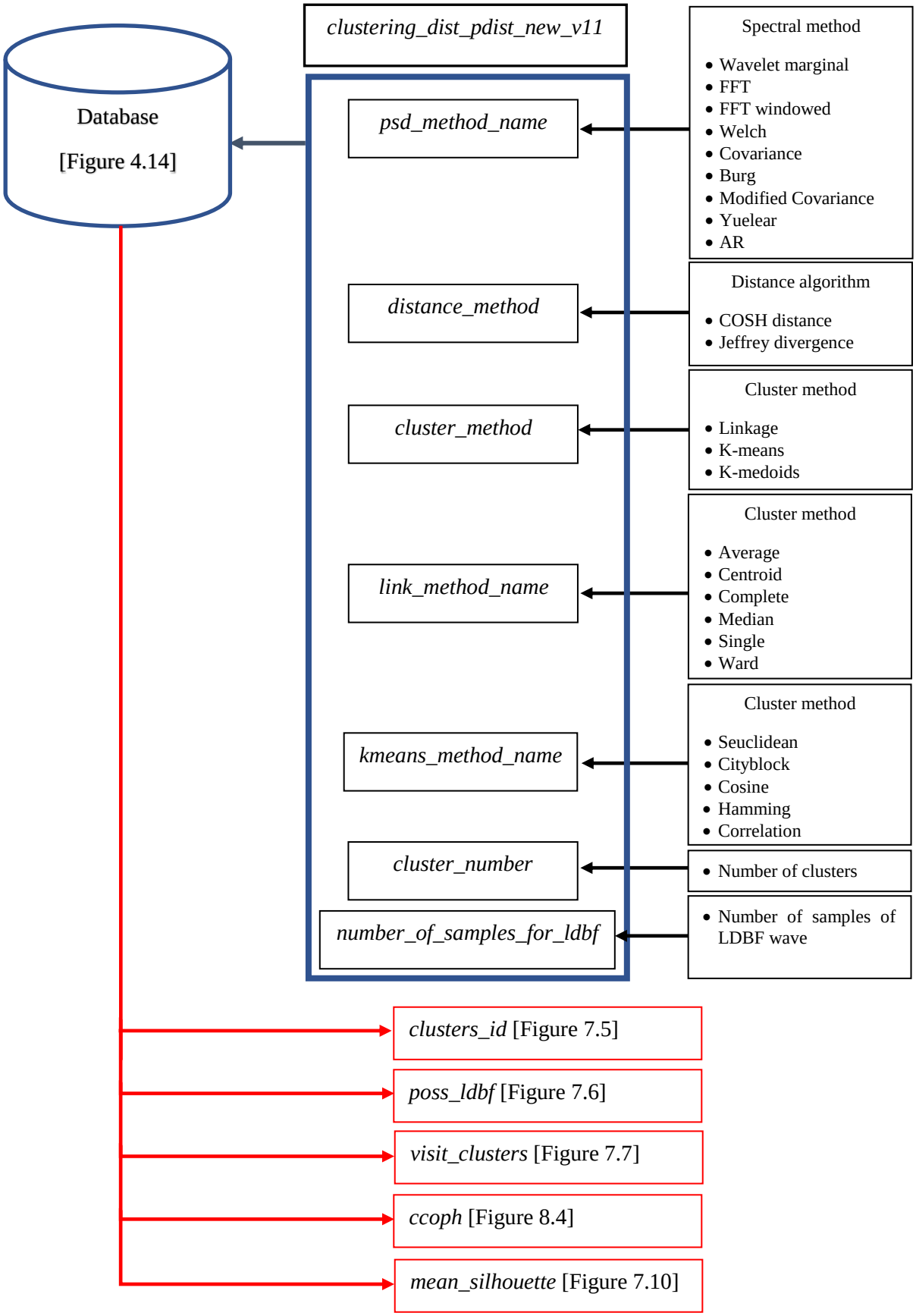

Figure 7.4: Flowchart of function *clustering_dist_pdist_new_v11*. In black are inputs of the function are represented and in red the outputs of the function are represented.

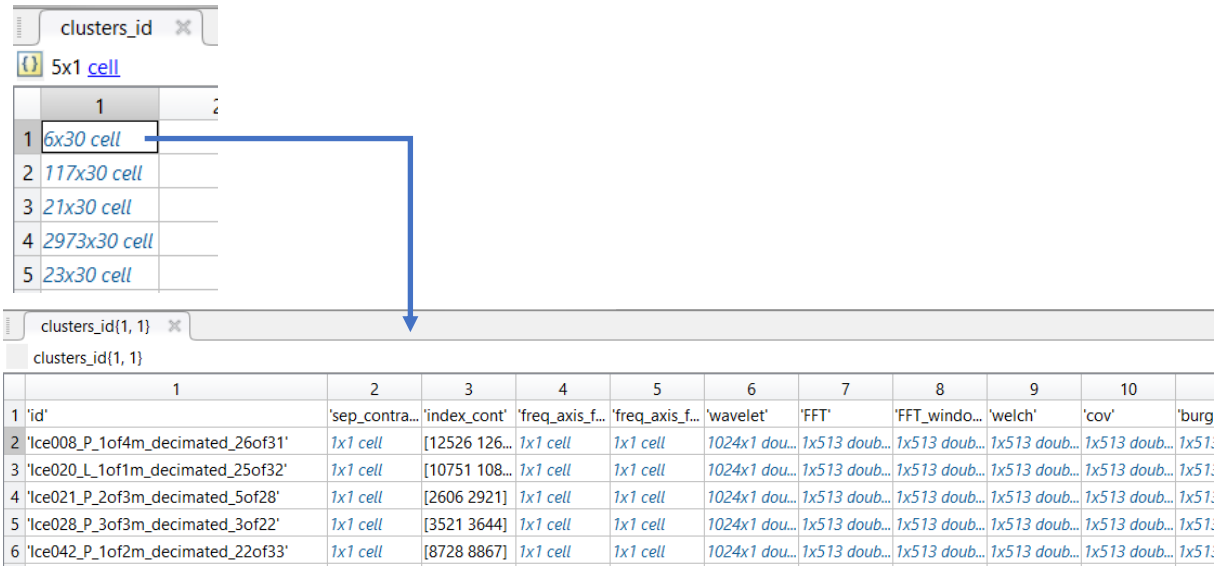

Figure 7.5: *clusters_id* output of the function *clustering_dist_pdist_new_v11* (see text for further explanation)

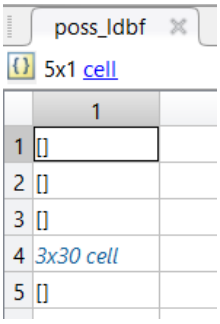

Figure 7.6: *poss_ldbf* output of the function *clustering_dist_pdist_new_v11* (see text for further explanation)

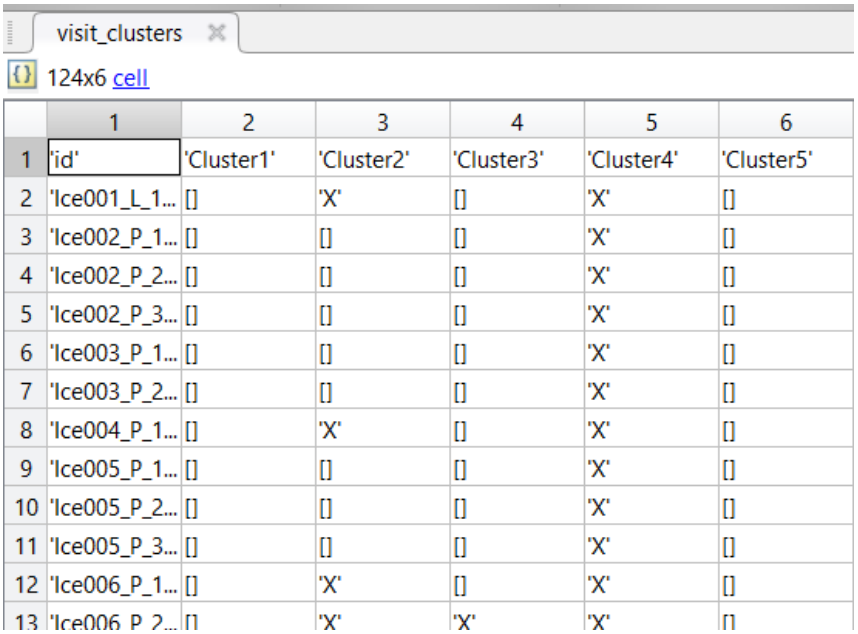

Figure 7.7: *visit_clusters* output of the function *clustering_dist_pdist_new_v1* (see text for further explanation)

The two chosen clustering methods, average linkage and K-medoids, were then implemented for a preliminary analysis of the clusters. To compare the K-medoids and the average linkage an exploratory analysis was performed with 3136 separated contractions from the Icelandic database. The K-medoids is represented in Figure 7.11 and Figure 7.12 and the average linkage is represented in Figure 7.13 and Figure 7.14.

The K-medoids method, Figure 7.11, appears to have a balanced distribution of the number of observations in each cluster. Analyzing the power spectra clustering, Figure 7.12, it is possible to identify some pattern in the power spectra. In cluster 4 there is a peak around 0.12 Hz followed by a decline of the spectrum. In clusters 5, most of the power spectra present a peak between 0.1 and 0.2 Hz. However, there is no distinct feature in any of the clusters.

Analyzing the average linkage method, Figure 7.13, it is possible to observe that this method filled the cluster 5 with only one observation. This object has a duration of around 7 seconds, when the rest of the contractions last at least 45 seconds. In the linkage average clustering of the power spectra, Figure 7.14, the power spectrum of the cluster 5 is significantly different from the others since it only has a small peak at 0.85 Hz. This isolated observation was posteriorly compared to fetal movements images identified in literature, depicted in Figure 1.5. Since the object in cluster 5 presents a fetal movement-like wave form, it was deemed an outlier, and posteriorly removed from the database. For that reason, the database of separated contractions from the Icelandic database has now 3135 objects. Further analysis of Figure 7.14 leads to an observation of distinct peaks in cluster 1 and 3. In cluster 1 the peak is around 0.25 Hz and in cluster 3 the peak is around 0.33 Hz. This discrimination between power spectra is not visible in the K-medoids clustering.

To evaluate both clustering options the silhouette plot was also used. The function that allows it to be implemented in MATLAB® is the *silhouette* function. The silhouette allows the estimation of the number of clusters. The silhouette width for the i^{th} observation is defined by[122]:

$$sw_i = \frac{(b_i - a_i)}{max(a_i, b_i)} \tag{7.11}$$

where a and b represent different clusters. When the silhouette width is large the objects are well clustered. The silhouette width varies between -1 and 1. When the silhouette value is close to 1, then the data is closer to its own cluster than neighboring one. When the silhouette value is close to -1, then the data is not well clustered. When the silhouette value is close to 0, then the object could belong to the assigned cluster or to the nearby one. The silhouette plot allows a quick visualization of the cluster structure.[122,140]

The silhouette plots of K-medoids and average linkage are represented in Figure 7.8 and 7., respectively. The K-medoids method, Figure 7.8, appears to distribute an identical the number of observations in each cluster. In every cluster there is some observations that, according to the silhouette plot, are incorrectly assign to the cluster. Evaluating the Figure 7.9 it is possible to observe that cluster 2 has most of the observations and the remaining clusters have a smaller number of observations. The silhouette plot considers that in cluster 2 there is some observations that are dissimilar to the remaining. However, a small part of the observations presents some dissimilarities to the remaining in each cluster.

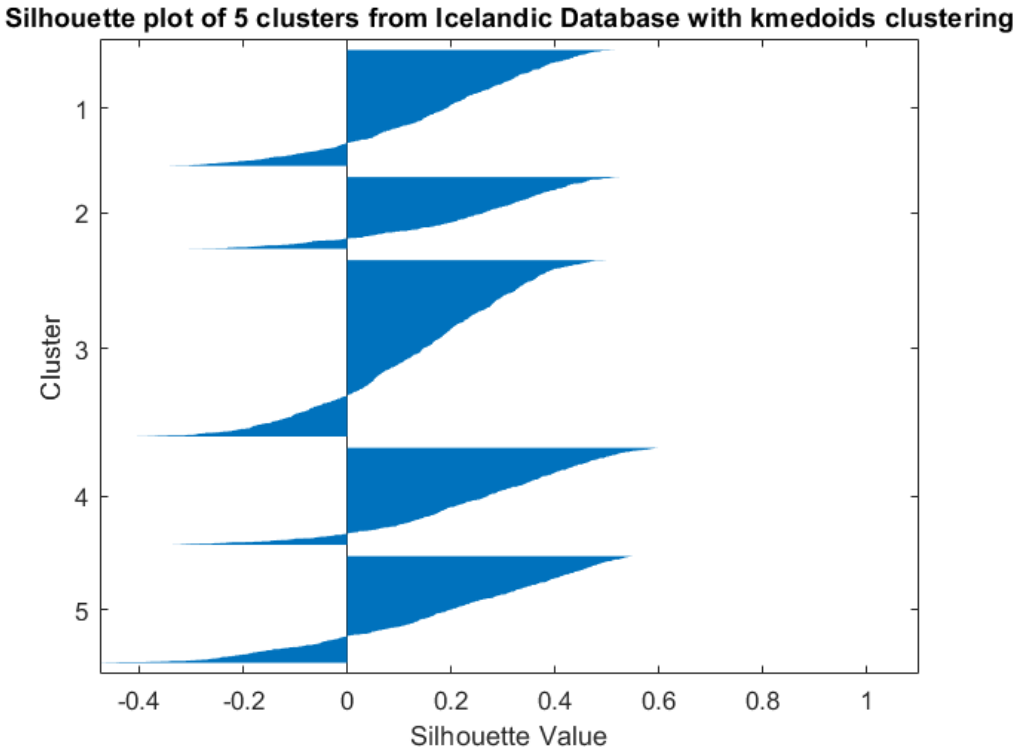

Figure 7.8: Silhouette plot obtained with k-medoids clustering. Silhouette evaluation of the 3136 observations obtained from the Icelandic database.

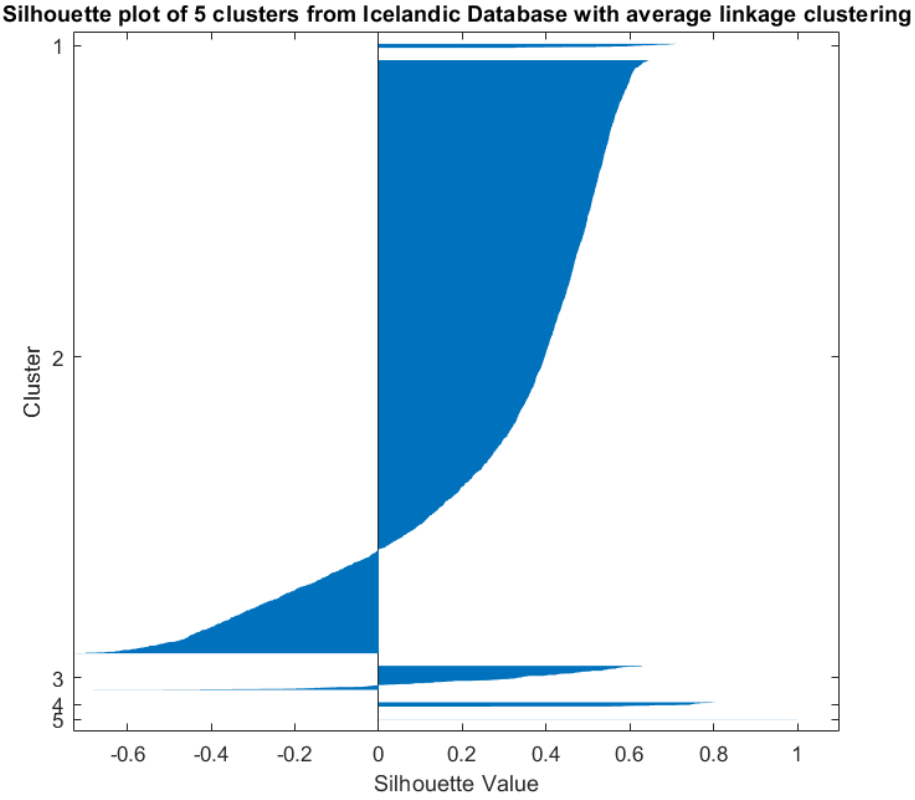

Figure 7.9: Silhouette plot obtained with average linkage clustering. Silhouette evaluation of the 3136 observations obtained from the Icelandic database.

The average silhouette width can also be used to evaluate the cluster number. The average silhouette width is defined by[122]:

$$\overline{sw} = \frac{1}{n}\sum_{i=1}^{n} sw_i \tag{7.12}$$

where sw_i is the silhouette width and n is the number of observations. When the average silhouette width is bigger than 0.5, a reasonable partition of the data was made and when the average silhouette width is less than 0.2, the data does not present cluster structure.[122] The average silhouette width for both clustering methods is presented in Figure 7.10. The average silhouette width obtained with average linkage clustering is higher than the one from K-medoids clustering, implicating that the average linkage clustering performs better with this data than K-medoids.

```
K>> mean_silhouette

mean_silhouette =

    0.2905
```

```
K>> mean_silhouette

mean_silhouette =

    0.1802
```

Figure 7.10: Average silhouette width obtained with average linkage clustering (on the left) and average silhouette width obtained with K-medoids clustering (on the right). Average silhouette width was calculated from the clustering of the 3136 observations obtained from the Icelandic database.

The average linkage method is more sensible to outliers, since it isolated the suspected fetal movement in a cluster. The K-medoids method assigns this observation to cluster 3, which leads to the loss of this distinct observation amid the others. Also, by analyzing both plots of the clustering of the power spectra for K-medoids and for average linkage, it is possible to determine that average linkage identifies power spectra with similar peaks and assigns them to a cluster. In K-medoids the same is not so visible. The average linkage also presents a value of average silhouette width of 0.2905, while K-medoids average silhouette width is 0.1802. According to this method the average linkage would be a more suitable clustering method for this data. For its sensibility to outliers, higher average silhouette width and isolation of power spectra with similar peaks, the linkage average method was chosen to be applied in the clustering analysis.

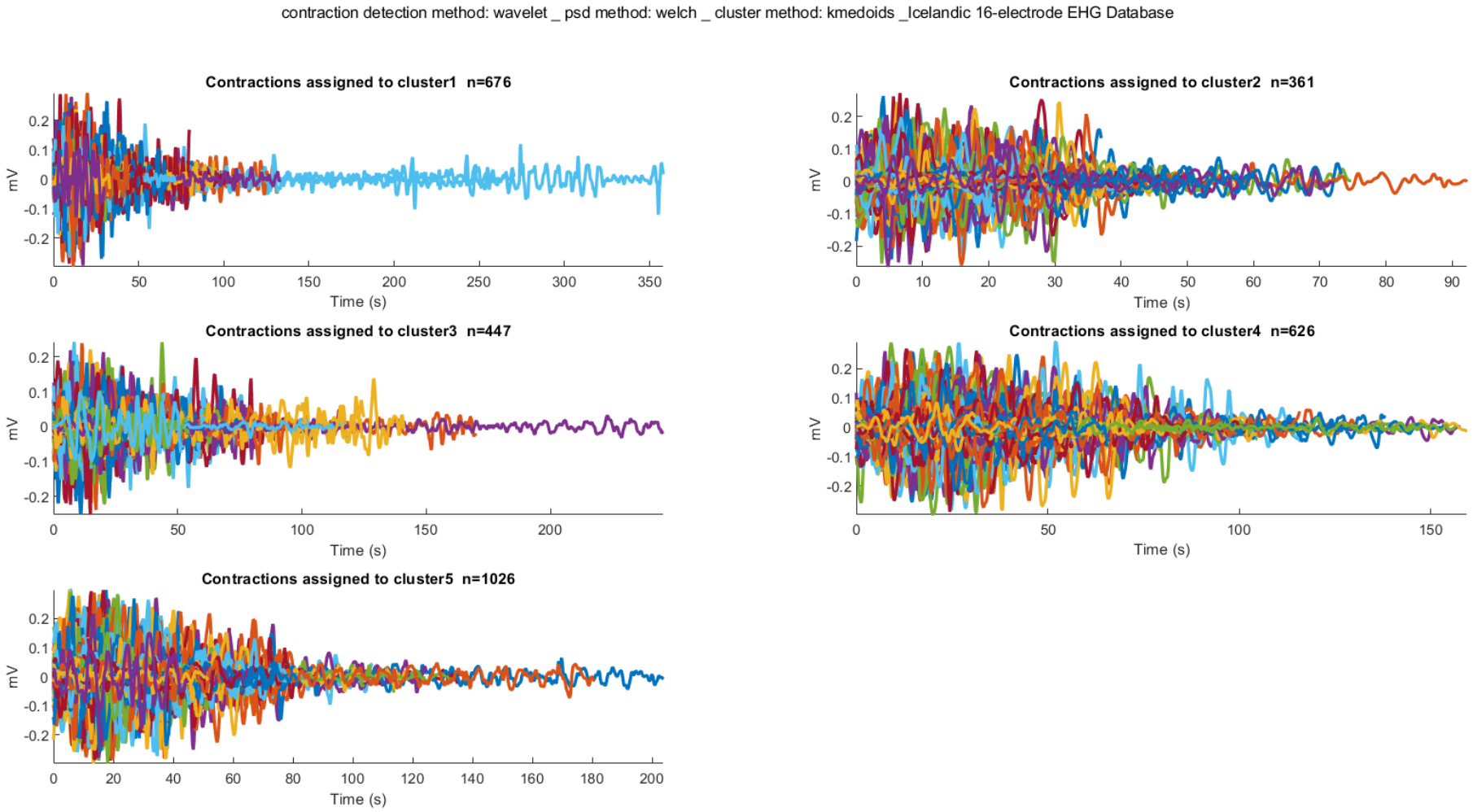

Figure 7.11: Output of the function *clustering_dist_pdist_new_v11*. Clusters of the 3136 separated contractions. The clustering method used was the K-medoids.

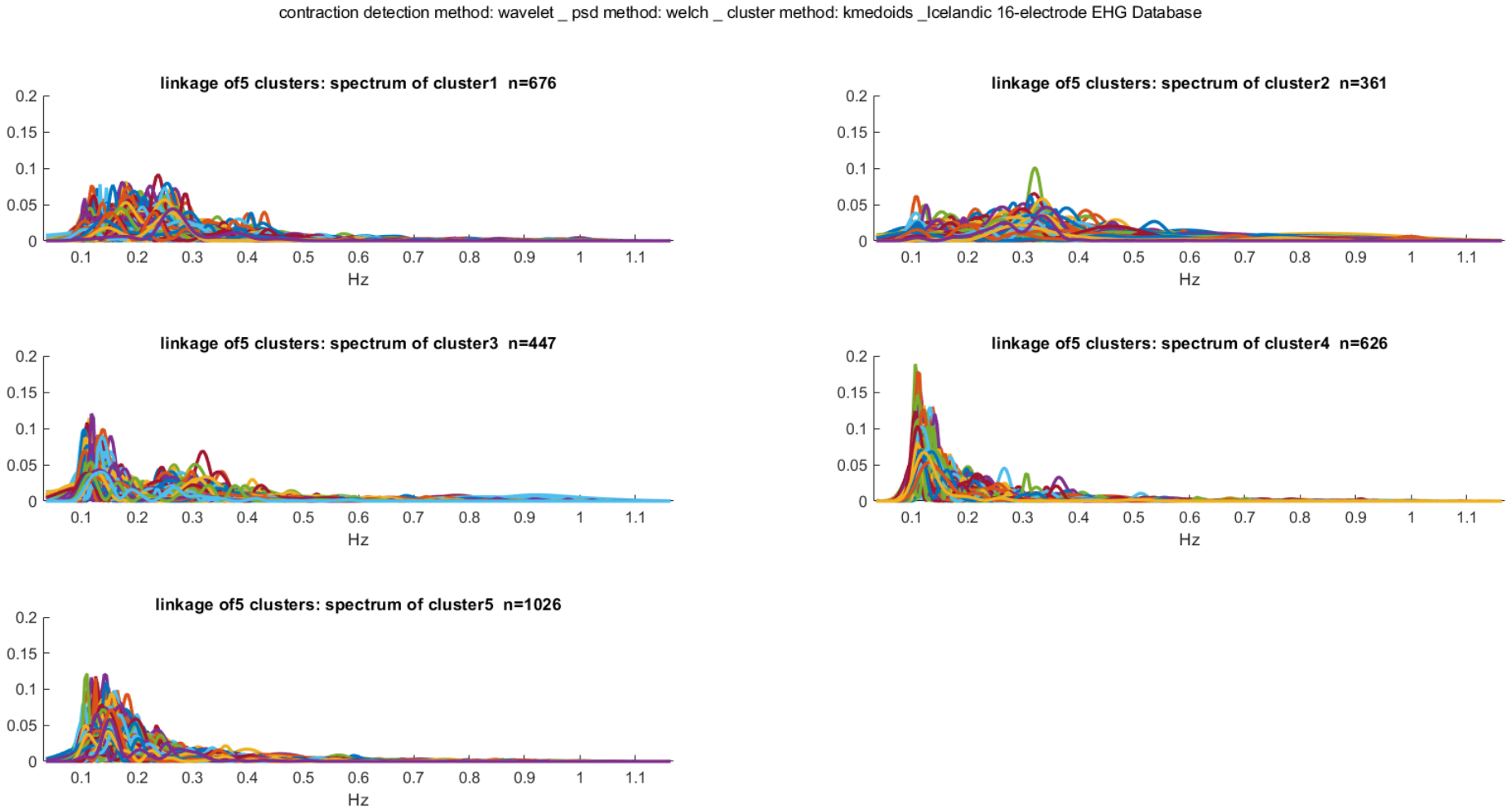

Figure 7.12: Output of the function *clustering_dist_pdist_new_v11*. Clustering of the power spectra of the 3136 separated contractions. The clustering method used was the K-medoids.

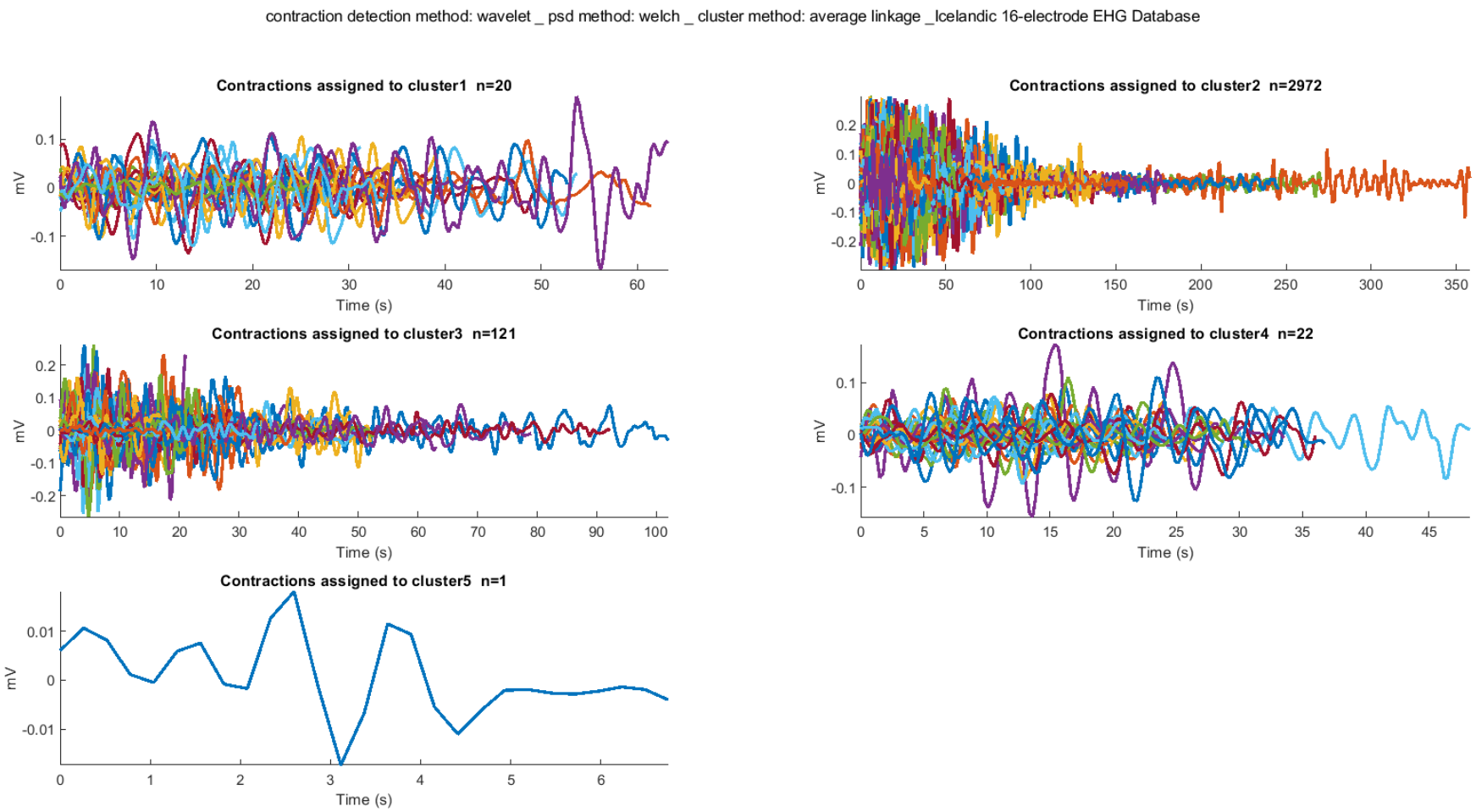

Figure 7.13: Output of the function *clustering_dist_pdist_new_v11*. Clusters of the 3136 separated contractions. The clustering method used was the average linkage. In cluster 5 there is only one observation with a distinct wave form, later identified as a suspected fetal movement.

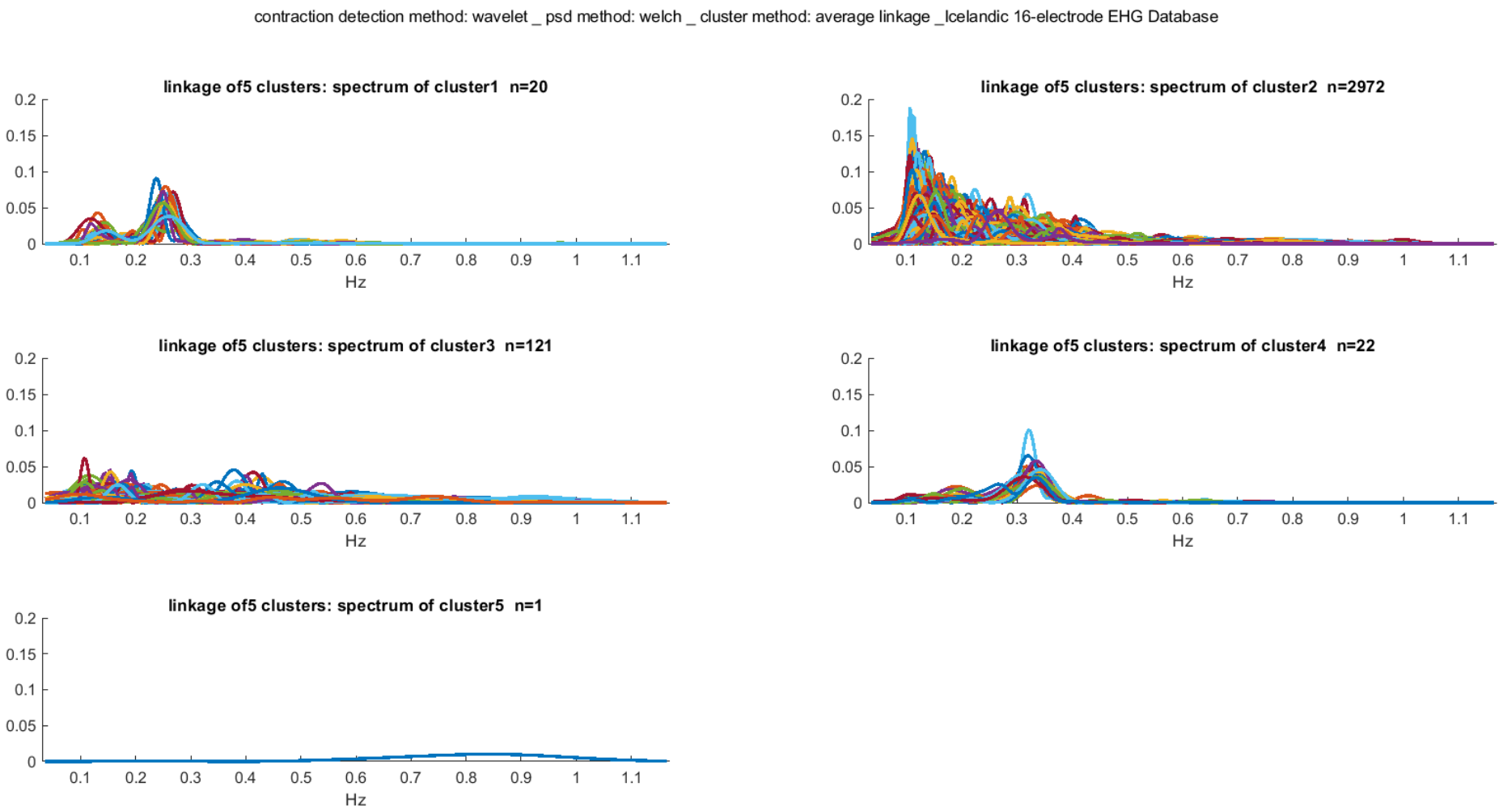

Figure 7.14: Output of the function *clustering_dist_pdist_new_v11*. Clustering of the power spectra of the 3136 separated contractions. The clustering method used was the average linkage. The power spectrum of cluster 5 presents a significant difference from the others since it only has a small peak at 0.85 Hz.

Chapter 8 – Results

The Icelandic and the TPEHG databases clustering analysis results are presented below.

8.1 Icelandic EHG Database Clustering

As it has been mentioned before this are the parameters for the clustering analysis of this database:

1. Contraction detection method: Wavelet energy;
2. PSD estimation method: Welch;
3. Spectral distance method: Jeffrey divergence;
4. Clustering analysis method: Average Linkage;
5. Estimated cluster number: 5.

The only visually recognizable contraction type are the Alvarez waves. The time series shows a short band well behaved oscillatory pattern to which corresponds a frequency peak well isolates in a range of frequencies between 0.2 and 0.4 Hz. Being these components associated with the onset of labor (be it pre-term or not), there is an increase interest regarding their detection.

It has been shown above, that a classification operation with 5 clusters was performed. In the analysis of this database, the clustering was performed for 5 and 6 clusters. The *waterfall* plot for 5 clusters is presented in Figure 8.1 and the *waterfall* plot for 6 clusters is presented in Figure 8.2. The difference between the 5 clusters results and the 6 clusters results are a division of the cluster with more observations. The observations in Cluster 1 in Figure 8.2 come from Cluster 4 in Figure 8.1. Since there was an important separation of this observations from the biggest cluster, the cluster analysis for this database was performed with 6 clusters. A migration of 10 observations from the largest cluster form a new cluster. This new cluster seems to congregate Alverez waves with a higher main peak frequency and increased low frequency component. An experience was made with 7 clusters however the results did not show any improvement.

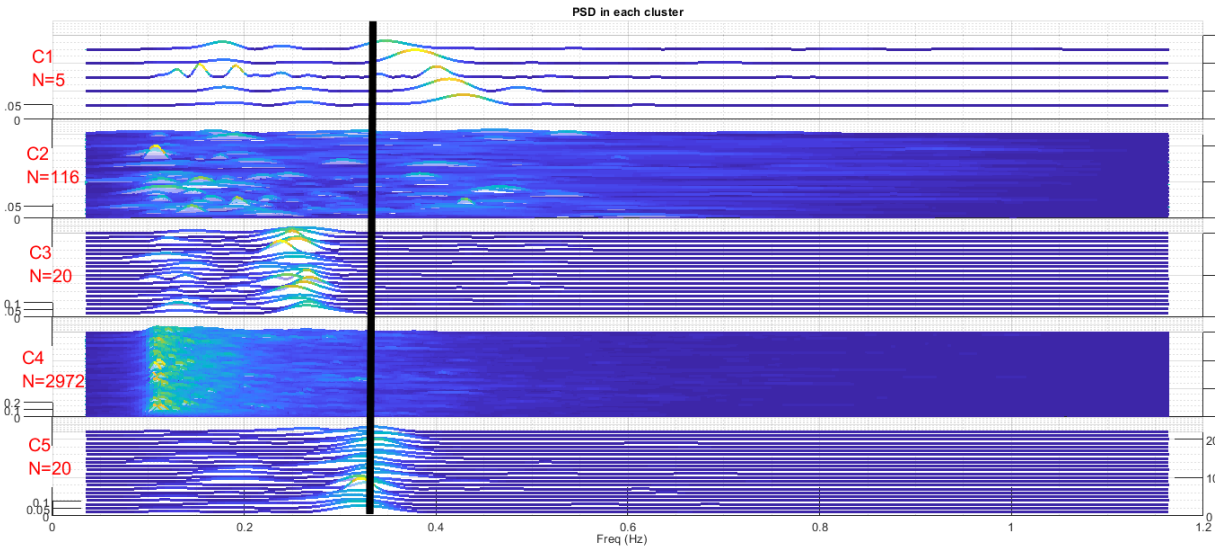

Figure 8.1: Output of the function *clustering_dist_pdist_new_v11*. Clustering of power spectrums with average linkage clustering method with *waterfall* representation for 5 clusters. The black line represents the 0.35 Hz.

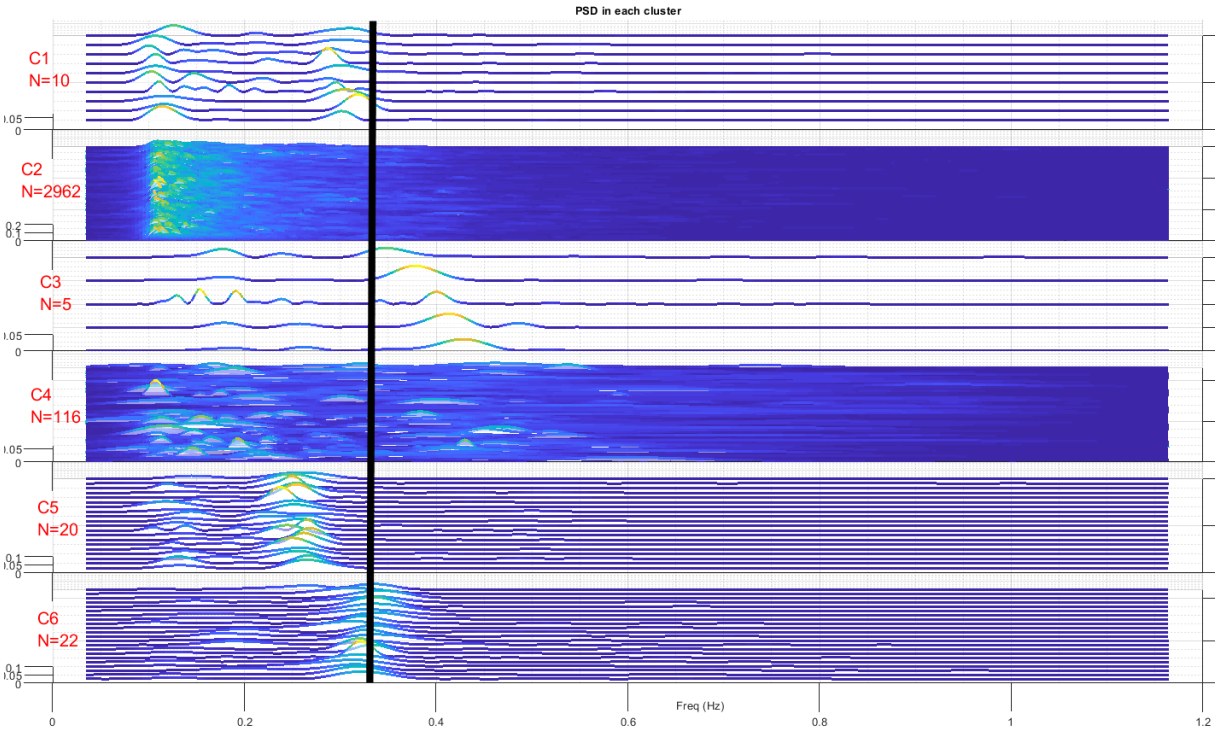

Figure 8.2: Output of the function *clustering_dist_pdist_new_v11*. Clustering of power spectrums with average linkage clustering method with *waterfall* representation for 6 clusters. The black line represents the 0.35 Hz.

The linkage average clustering was applied to the Icelandic database and the following dendrogram was obtained.

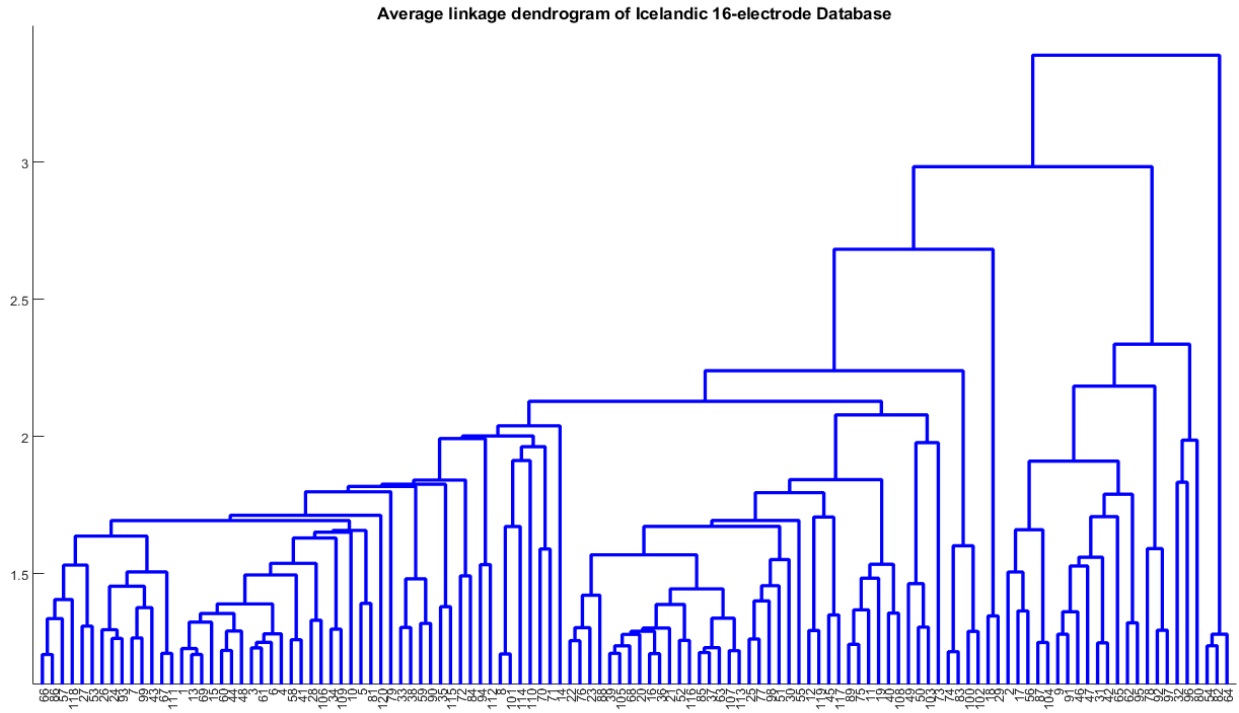

Figure 8.3: Dendrogram of the 3135 observations from Icelandic database obtained with average linkage clustering. The vertical axis represents the dissimilarity between clusters.

Analyzing the dendrogram it is clear there is some chaining, which was expected since most of the observations are gathered in one cluster. In Figure 8.3, the observations on the right side of the dendrogram are significantly different from the rest of the data. The dissimilarity reaches the value 8 when most of the data only present a dissimilarity between 2 and 4.

The cophenetic correlation coefficient can be used to evaluate hierarchical clustering techniques. The cophenetic correlation coefficient determines the distance between two objects as it calculates the height of the node at which these two objects are first joined together in the dendrogram.[136] If the value of the coefficient is closer to 1 then the dendrogram faithfully represents the pairwise distances between the original data.[141] The cophenetic correlation coefficient is defined as[141]:

$$c = \frac{\sum_{i<j}(Y_{ij} - y)(Z_{ij} - z)}{\sqrt{\sum_{i<j}(Y_{ij} - y)^2 \sum_{i<j}(Z_{ij} - z)^2}} \tag{8.1}$$

where Y_{ij} is the distance between the objects i and j in Y, Z_{ij} is the is the cophenetic distance between the objects i and j and y and z are the average of Y and Z.[141]

The cophenetic correlation coefficient was calculated for the Icelandic and TPEHG databases for the average linkage clustering with the MATLAB® function *cophenet*. The result is presented in Figure 8.4. The cophenetic correlation coefficient of the Icelandic database for 6 clusters was 0.5939 which indicates a good performance according to this criterion.

```
>> ccoph

ccoph =

    0.5939
```

Figure 8.4: Cophenetic correlation coefficient of the Icelandic database for 6 clusters.

Figure 8.6 represents the contractions time series organized cluster wise. The following considerations are relevant:

1. Cluster 2 represents the large majority of the contractions. It is observed that smaller contractions have higher amplitude which explains the bell shape in the cluster plot. There is no clear scientific explanation for this behavior. As far as energy balance is concerned it makes sense: longer contractions should have lower amplitude to keep the energy balance off the myometrium tissue. This is a topic that certainly deserves some further research and has not been found in the current literature.
2. Cluster 2 includes the longer contractions normally associated to uterine hypertonia (LDBF) which in this work has been accepted as contractions over 4 minutes. In this way it becomes apparent that LDBF waves should be detected using the duration feature as its main characteristic. In a section below more considerations will be made about LDBF automatic detection.
3. It is clear that the contraction time series may not be used for visually classification. The signals are non-stationary in nature.
4. Upon zooming on Cluster 5 and Cluster 6 the smooth oscillatory pattern is recognizable. Cluster 1 also presents components which visually could be associated with Alvarez waves with heavy low frequency (Slow Wave) contamination.

Figures 8.7 and 8.2 show the spectra clustering results using Welch method. The following considerations are relevant:

1. Cluster 2 (2962 observations) which comprises most of the contractions has in average a spectral shape with a frequency peak around 0.15 Hz followed by a consistent decay for the higher frequencies. This is of course an average behavior. This cluster should comprise either Braxton-Hicks or Alvarez. Being Alvarez low amplitude waves, unlike Braxton-Hicks, this cluster includes therefor the former and the latter events. In this respect ideally, the clustering process would be accurate enough to include only these events in this cluster. This is not however the case. Closer observation some atypical Alvarez waves were found in this cluster. So far it is not known the spectral characteristics of Braxton-Hicks contractions.
2. Given the nature of Alvarez waves, mentioned earlier in this work, one would expect that their spectra have a short band frequency peak almost mono component like. Cluster 6 (22 observations) shows such a spectrum with a peak frequency consistently around 0.35 Hz. Lower frequency peaks are also present which might represent Slow Wave interference. So, in this way, it is here considered that this cluster represents the Alvarez contractions. The question rouse why so few (22 observations) were actually detected when it is known that Alvarez contractions are very prevalent in EHG recordings. The explanation is twofold: the contraction algorithm missed probably most of the Alvarez waves, due to lack of energy, and the some of the detected ones fell in cluster number 2. An evident solution for this problem will be presented in the further below.
3. Cluster 5 (20 observations) is similar to cluster 6 with a main peak frequency around 0.25 Hz. Comparing with cluster 5 the main peak frequency consistently shows around 0.25

Hz and the lower frequency peak in average have higher amplitude than the Alvarez waves. This clusters seems to comprise Alvarez waves with higher Slow Wave contamination level.

4. Cluster 3 (5 observations) stands out as showing the higher frequency peak dominance compared to the lower frequency ones. It is actually the cluster with higher frequency with components around 0.4 Hz. It is not clear which wave type this cluster refers to.

5. Cluster 4 (116 observations) represents broad band spectra with apparent no distinct peak frequency.

6. Cluster 1 (10 observations) resembles Cluster 6 however Cluster 1 presents an evident peak around 0.1 Hz. Despite this fact, these components seem to belong the Alvarez set, since the costumery frequency peak in the interval [0.2 - 0.4] Hz is present. Further comments on this will follow below.

It becomes evident that the clustering operation was able to differentiate, in average, spectrum the most evident are cluster 2,5 and 6.

It will be shown below that Alvarez components were wrongly classified in Cluster 2 and possibly Cluster 4. A possible explanation will be provided. In Figure 8.10, an Alvarez wave and its spectrum are represented. The Alvarez wave is affected by a Slow Wave component, which affects the PSD estimation. The spectrum has two peaks, the first at 0.1 Hz, caused by the Slow Wave, and the second at 0.32 Hz. Similar spectra to the one represented can be found in Cluster 2. It is possible that, due to the Slow Wave influence, several Alvarez waves were wrongly assigned to Cluster 2.

Alvarez waves detection was not ideal since these waves have low amplitude. In Figure 8.12 an EHG signal from subject 22 is represented. Two Alvarez waves were detected by the Wavelet method however, between the detected Alvarez waves is an undetected one. A visual verification was performed to assess the extension of this phenomenon and several EHG signals with undetected Alvarez waves were found.

An alternative method to detect Alvarez waves is proposed in Figure 8.5. The Alvarez waves should be detected based in a frequency feature, such as Instantaneous Frequency, instead of using an energy-based method. After the Instantaneous Frequency is calculated for each wave, the main peak of the spectrum must be found. The main peak must be between 0.2 to 0.4 Hz. If the main peak is indeed between the mentioned frequencies, it should be compared to the second highest peaks of the spectrum. If the main peak is two times higher the second highest peak, then an Alvarez wave was detected.

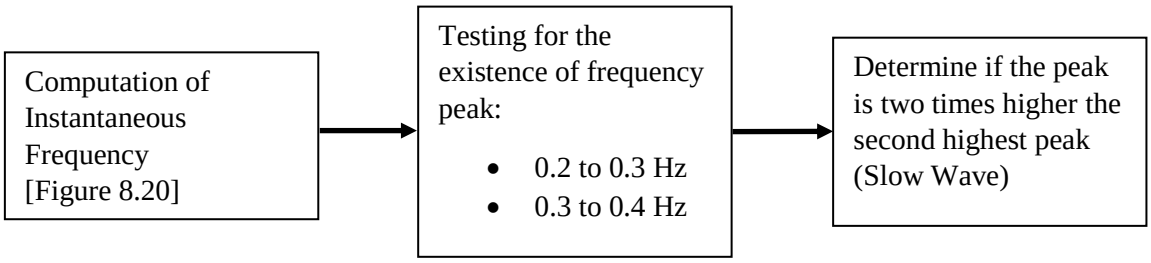

Figure 8.5: Flowchart of proposed method to detect Alvarez wave.

Figure 8.13 (a) represents an EHG signal with an Alvarez wave followed by a Braxton-Hicks contraction. Analyzing the PSD of both components, the difference in the spectrum is clear. The Alvarez wave has a distinct peak between 0.3 and 0.4 Hz, and 75 % of its energy is between 0.17 and 0.4 Hz. The contraction main peak is around 0.1 Hz and 75 % of its energy is between 0.17 and 0.35 Hz.

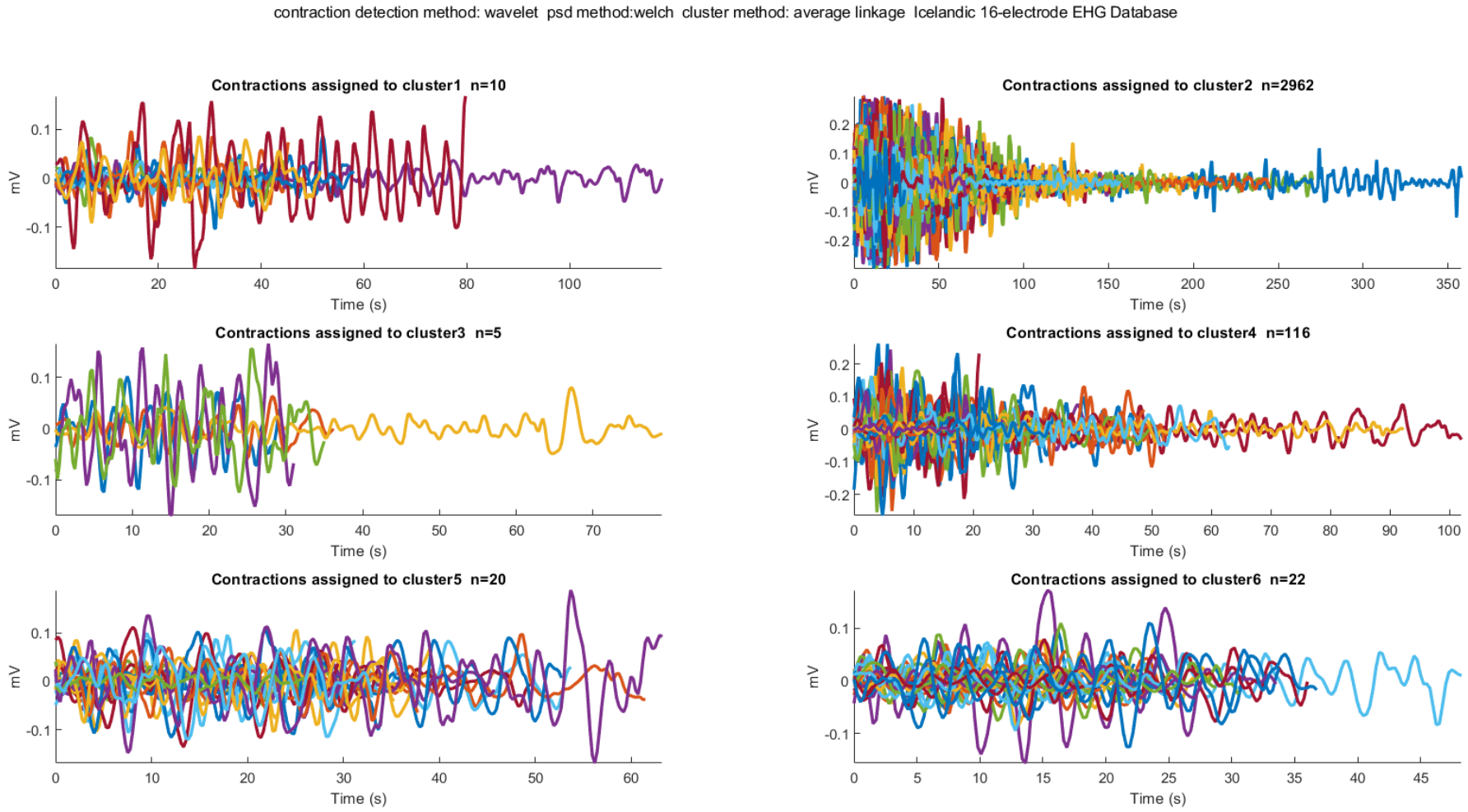

Figure 8.6: Output of the function *clustering_dist_pdist_new_v11*. Clusters of the 3135 separated contractions from the Icelandic database. Clustering method: average linkage.

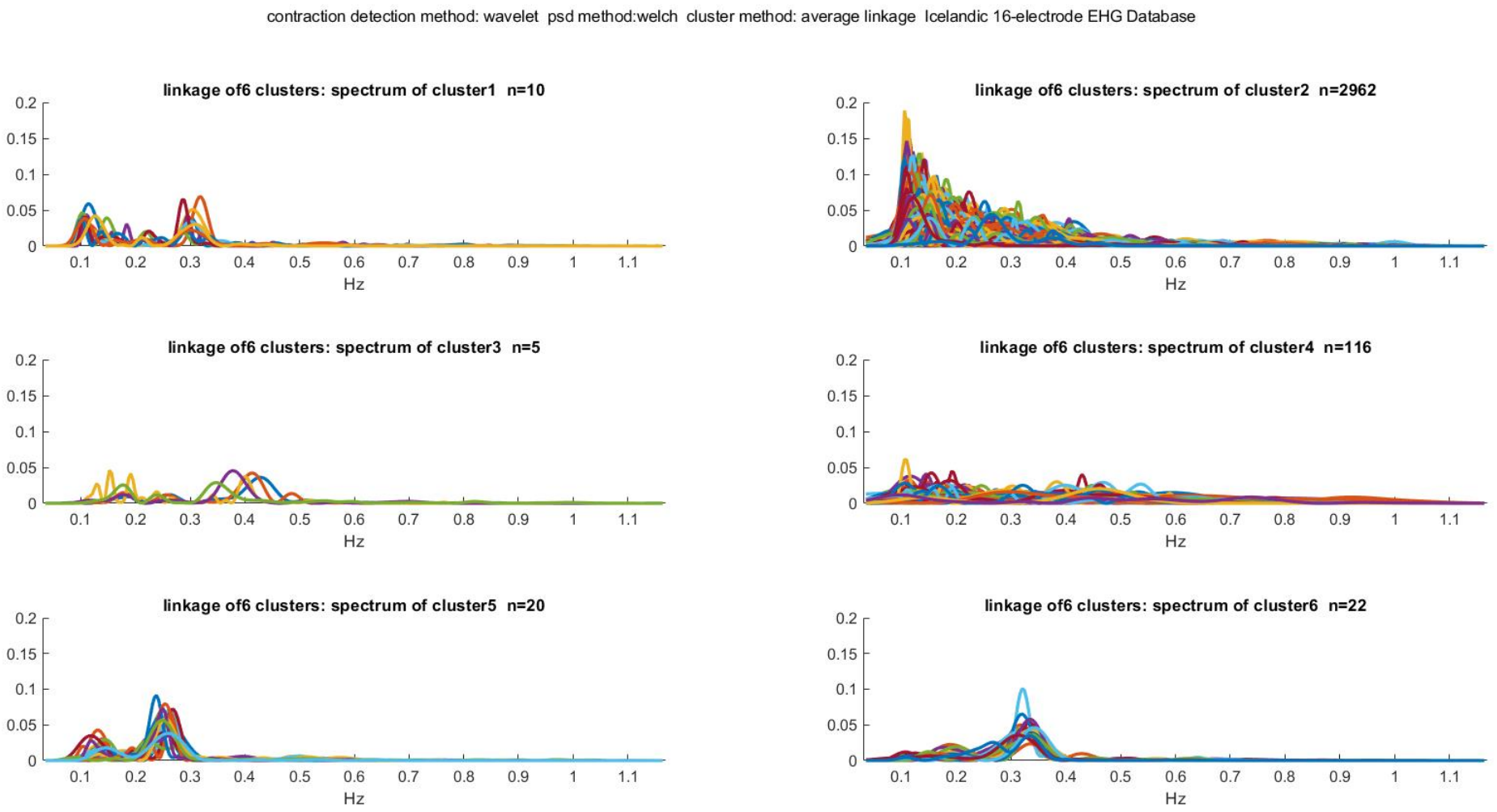

Figure 8.7: Output of the function *clustering_dist_pdist_new_v11*. Clustering of power spectra with average linkage clustering method. In cluster 5 and 6 it is possible to identify distinct peaks in the power spectra. The power spectra were obtained from the 3135 separated contractions of the Icelandic database.

In the next step the scatter plot of the Icelandic Database has been used to be overlapped with the cluster subject cases in an attempt to find any recognizable patterns namely the Alvarez components, Figure 8.8. The following considerations are pertinent:

1. Alvarez waves, which are a recognized marker of preterm delivery and labor closeness, seem to be distributed over the database scatter with possibly an increased presence in the higher GA's (Gestational Age) which should be expected. However, this might just represent the database distribution which favors higher gestational weeks recordings. This should prompt all EHG database developers to evenly distribute the acquisitions gestational weeks' time points, which is not the case in the Icelandic database. Moreover, as it has been mentioned before, the Alvarez components are present from the 20th GA onwards, so it comes as no surprise that it is found in lower GA's. However, one should expect that, at least the higher GA should contain Alvarez and those being represented in cluster 6. An explanation for this incongruence has been provided above.
2. As has been mentioned above, Cluster 2 should represent the Braxton-Hicks contractions that are spread throughout pregnancy with possible activity reduction before labor. To be able to detect this gap it would be necessary a more comprehensive database, as far as number of recordings is concerned and its even distribution over the GA interval. Of course, the building of such database is a significantly complex task requiring enough human resources and organization.
3. Regarding the Alvarez components not predominantly showing in the higher GA in cluster 6 it has been anticipated that components could have leaked to Cluster 2. Upon research it was found that cluster 2 has a significant number of Alvarez components that show an additional characteristic: a relatively high peak frequency (albite below the main peak). This lower frequency component which might be an effect of slow wave interference which got the clustering algorithm classification process confused leading to a misclassification of a component that should be present in Cluster 6. Figure 8.9 shows four of these components that were found in Cluster 2 and should be in Cluster 6. In this figure it is clearly shown the typical Alvarez peak frequency component at around 0.35 Hz. However, a low frequency component with significant energy is also present. It is hypothesized here that these components should be alien to the Alvarez wave itself and it is no more than an interference. This is represented in Figure 8.10 where a multi component Alvarez is shown on the top as well as is baseline feature which was obtained through the application of a low pass filter with a cut-of frequency of 0.2 Hz. In the bottom plot it is represented the PSD of the Alvarez, where it is clearly shown the low frequency peak corresponding to the baseline.
4. LDBF components are important since they represent uterine hypotonic action as mentioned earlier. From the observation of Figure 8.6 it is not clear in which cluster this component ended up. Since uterine hypertonic is associated with abnormally longer contractions it is therefore plausible that a detection criterion based in this feature should be applied instead, or at least before any clustering process. The decision was made to isolate contractions with durations above 4 minutes followed by the observation of the respected PSD estimations, which is represented in Figure 8.11 for three different LDBF components. It is observed that the PSD spectrum is quite different from the ones that have been observed in all clusters. There are abundant peaks periodically spread over the spectrum. Several frequency peaks can be detected in the spectrum. The question arises why such a particular spectrum was not isolated in a separated cluster. That raised the suspicion the distance function for this clustering operation (Jeffrey divergence) might not be ideal for spectra with multicomponent sharp peaks. One has to keep in mind that this distance function has been successfully applied in audio processing and is being for the first time applied in EHG processing, which are two different phenomena.

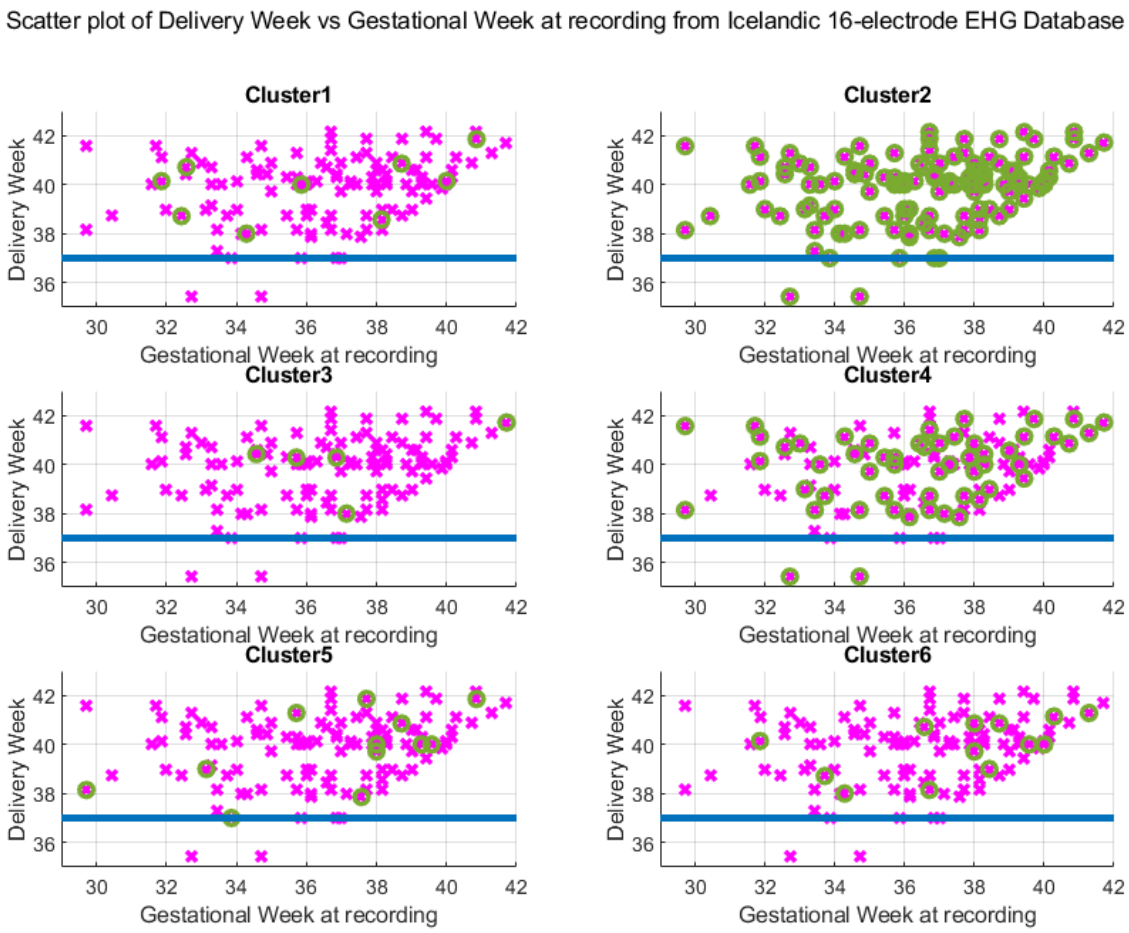

Figure 8.8: Output of the function *clustering_dist_pdist_new_v11*. Relation of the Delivery week vs Recording week with the average linkage clustering for the Icelandic database. The blue line represents the 37 weeks of gestation. In pink is represented the whole database and in green is represented the observations in each cluster.

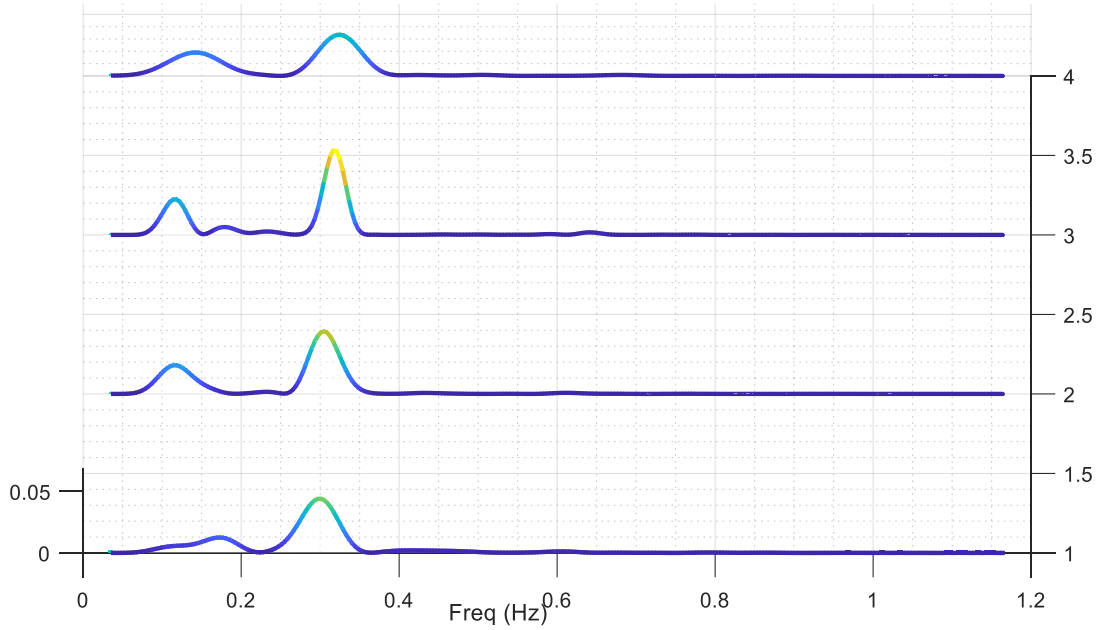

Figure 8.9: Four observations found in Cluster 2 that were misclassified. Representation of the PSD with the *waterfall* function of MATLAB®. The observations show a peak around 0.35 Hz.

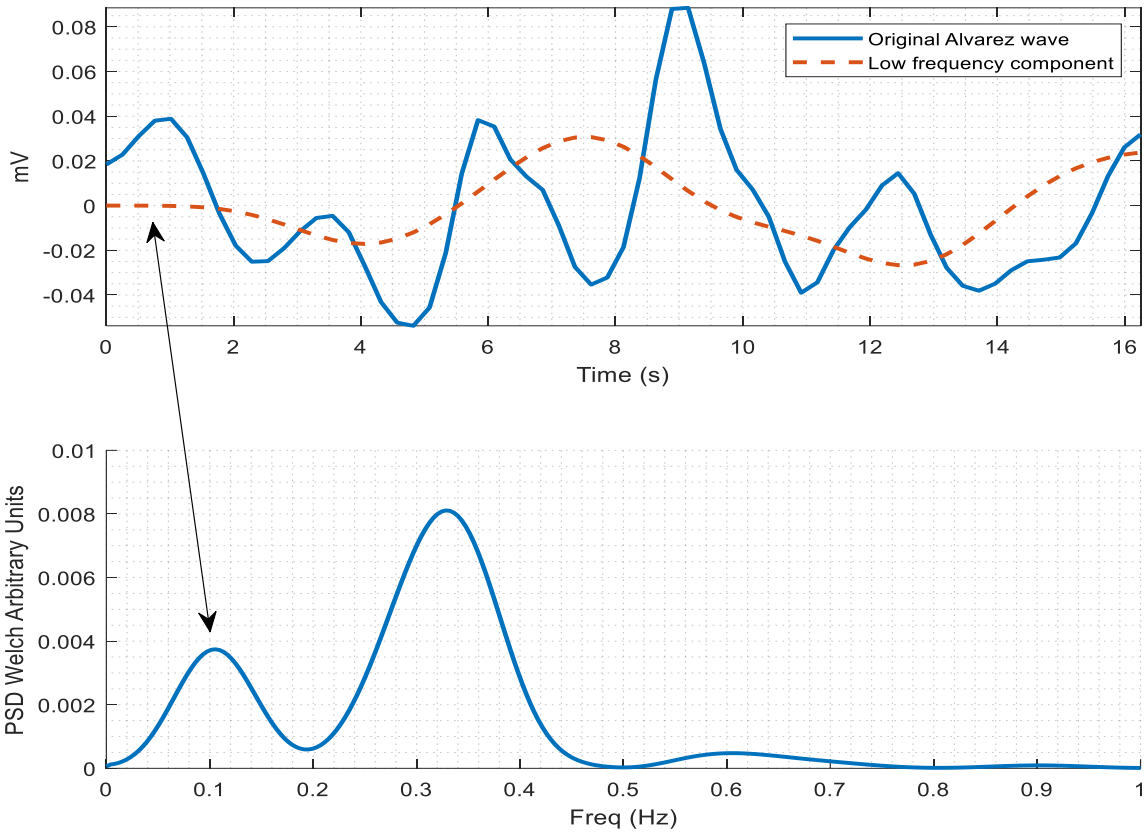

Figure 8.10: On top: Alvarez wave is represented in blue and the low frequency component of the Alvarez wave is represented in orange. On Bottom: PSD of the Alvarez wave. The low frequency component is responsible for the first peak in the spectrum.

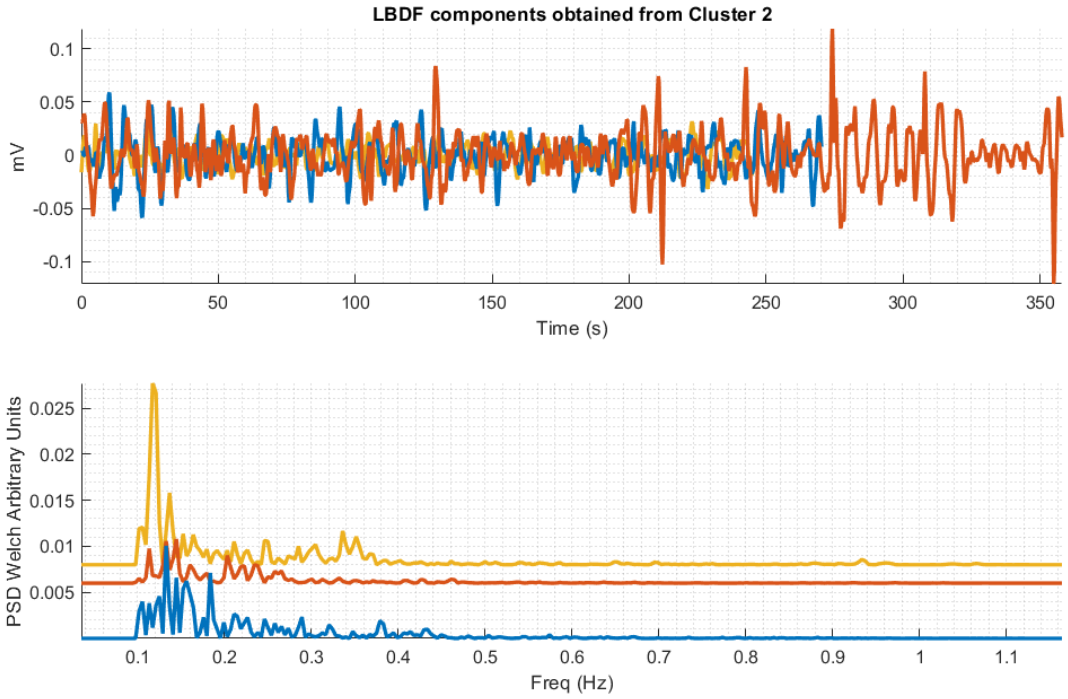

Figure 8.11: On top: LDBF waves with more than 4 minutes from the Iceland database. On Bottom: Respective PSD from the LDBF waves represented above.

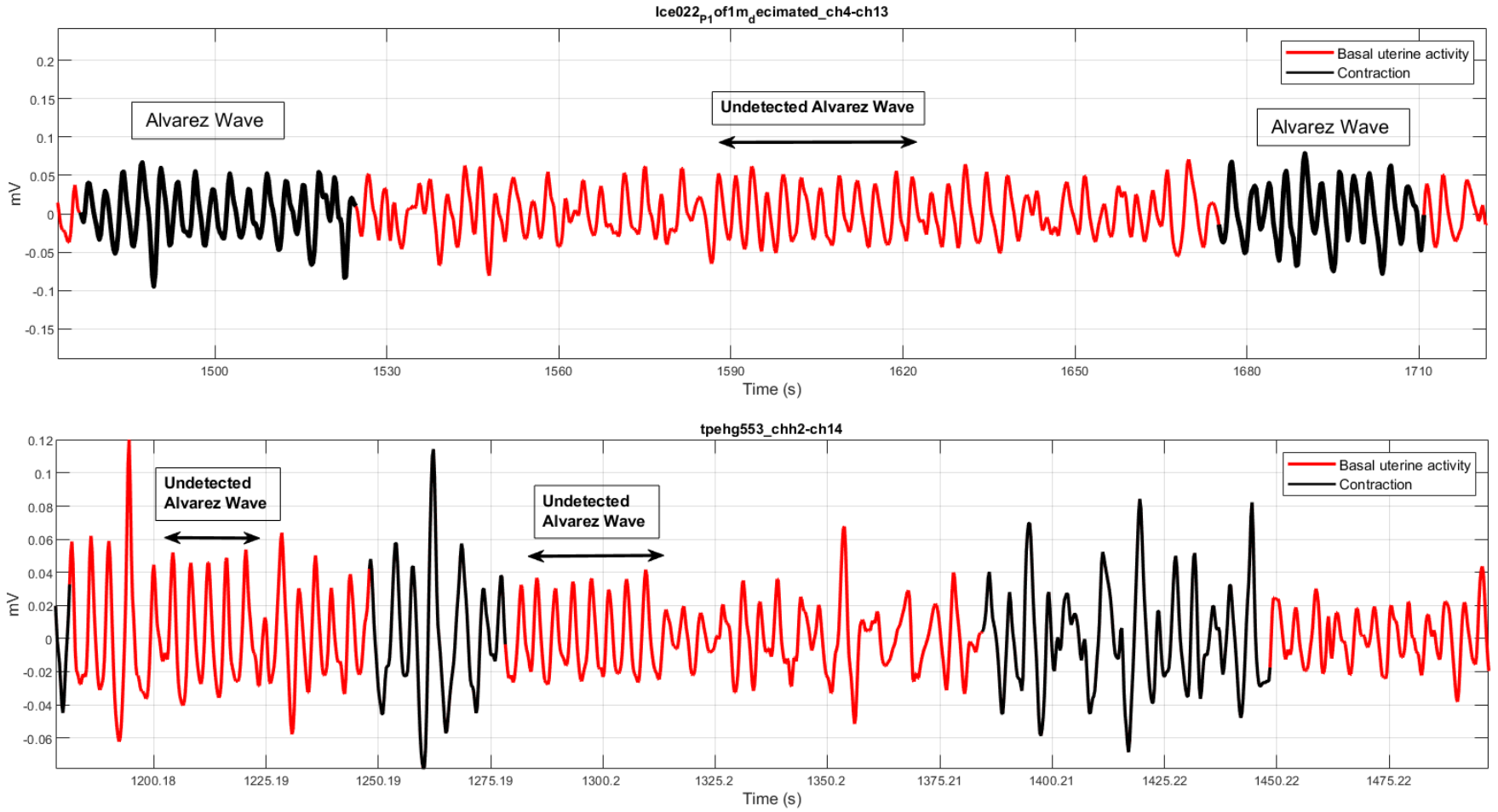

Figure 8.12: On top: EHG signal from the subject 22 of the Icelandic database with undetected Alvarez waves. The detected Alvarez waves are represented in black. On bottom: EHG signal from the subject 553 of the TPEHG database with undetected Alvarez waves. The black arrow represents an undetected Alvarez wave.

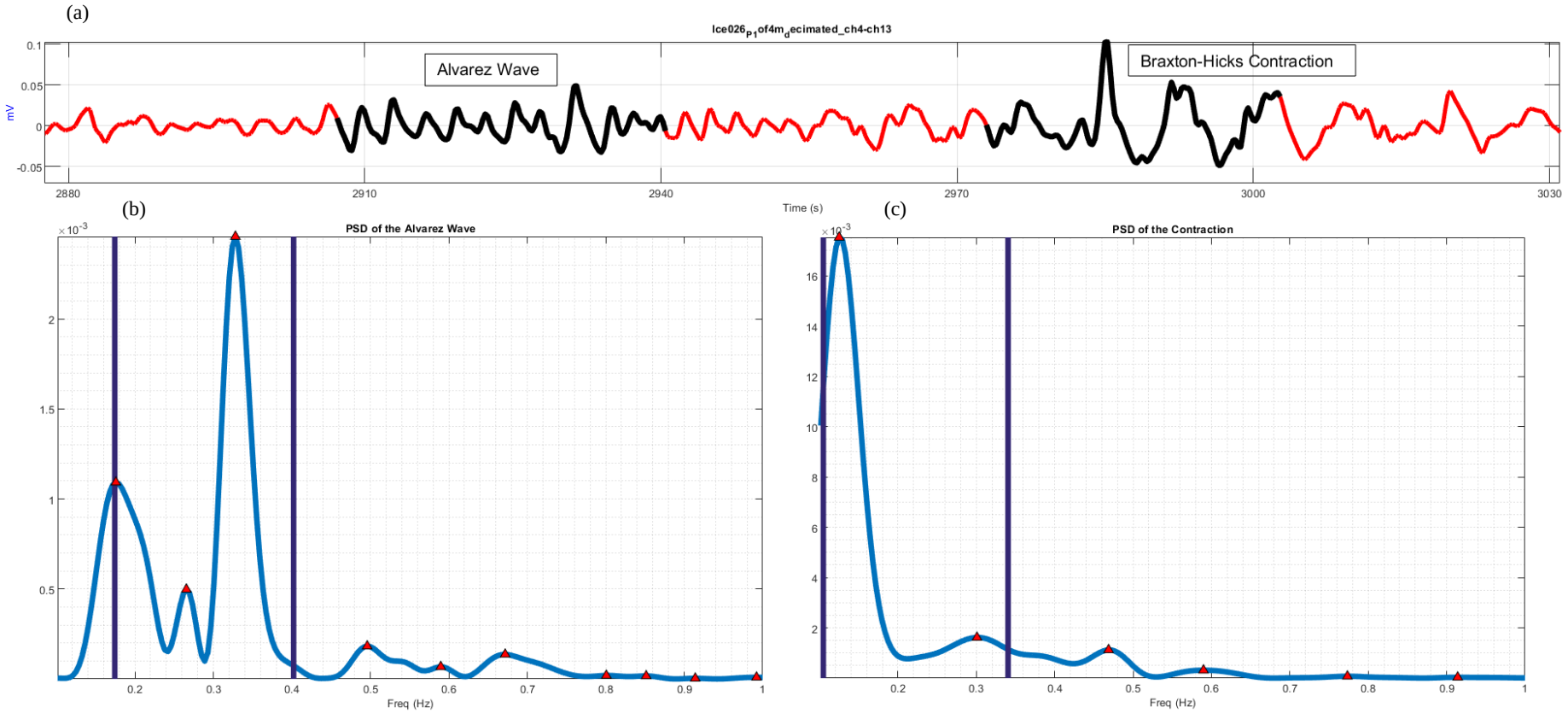

Figure 8.13: EHG signal from the subject 26 of the Icelandic database with an Alvarez wave and a contraction.

(a) The Alvarez wave and the Contraction are represented in black and the EHG signal in red.
(b) Power spectrum of the Alvarez wave. The blue lines represent where 75% of the PSD energy is. The power spectrum the highest peak between 0.3 Hz and 0.4 Hz.
(c) Power spectrum of the Contraction. The blue lines represent where 75% of the PSD energy is. The contraction's power spectrum has the highest peak at a lower frequency than the Alvarez wave.

8.2 TPEHG Database Clustering

As it has been mentioned before this are the parameters for the clustering analysis of this database:

1. Contraction detection method: Wavelet energy;
2. PSD estimation method: Welch;
3. Spectral distance method: Jeffrey divergence;
4. Clustering analysis method: Average Linkage;
5. Estimated cluster number: 5;

In the analysis of this database, the clustering was performed for 5 and 6 clusters however the results from 6 clusters did not show any improvement, so the chosen cluster number was 5. It is expected that similar results to the Icelandic database would be found since all the parameters are equal. In Figure 8.14 the *waterfall* representation of the 5 clusters is shown.

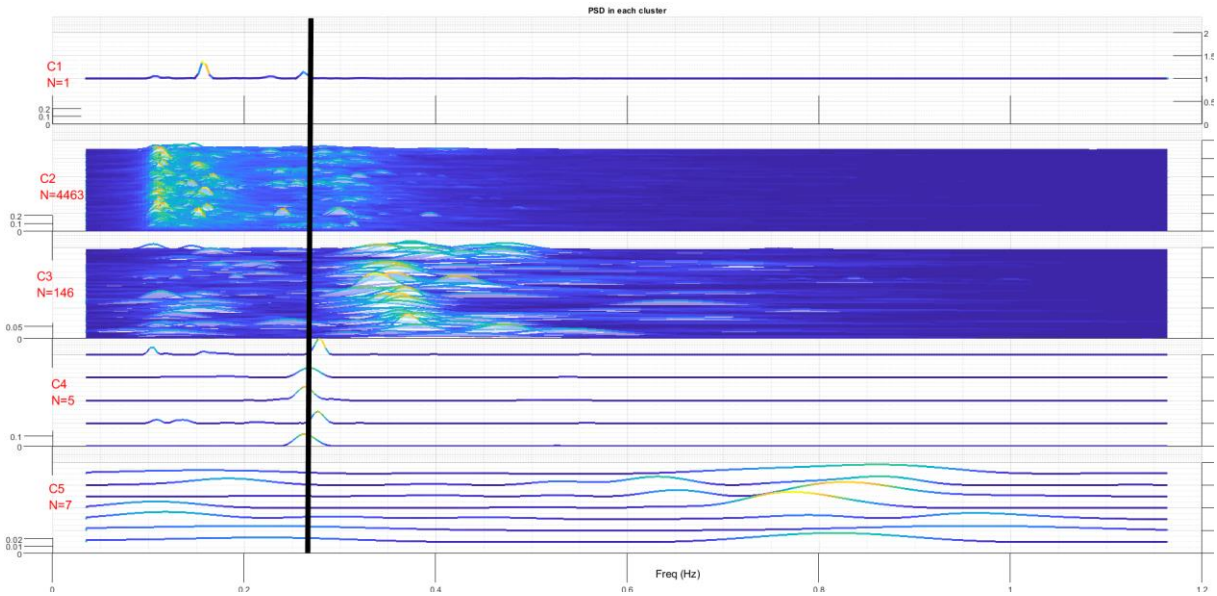

Figure 8.14: Output of the function *clustering_dist_pdist_new_v11*. Clustering of power spectrums with average linkage clustering method with *waterfall* representation for 5 clusters. The black line represents the 0.26 Hz.

The linkage average clustering was applied to the TPEHG database and the following dendrogram was obtained.

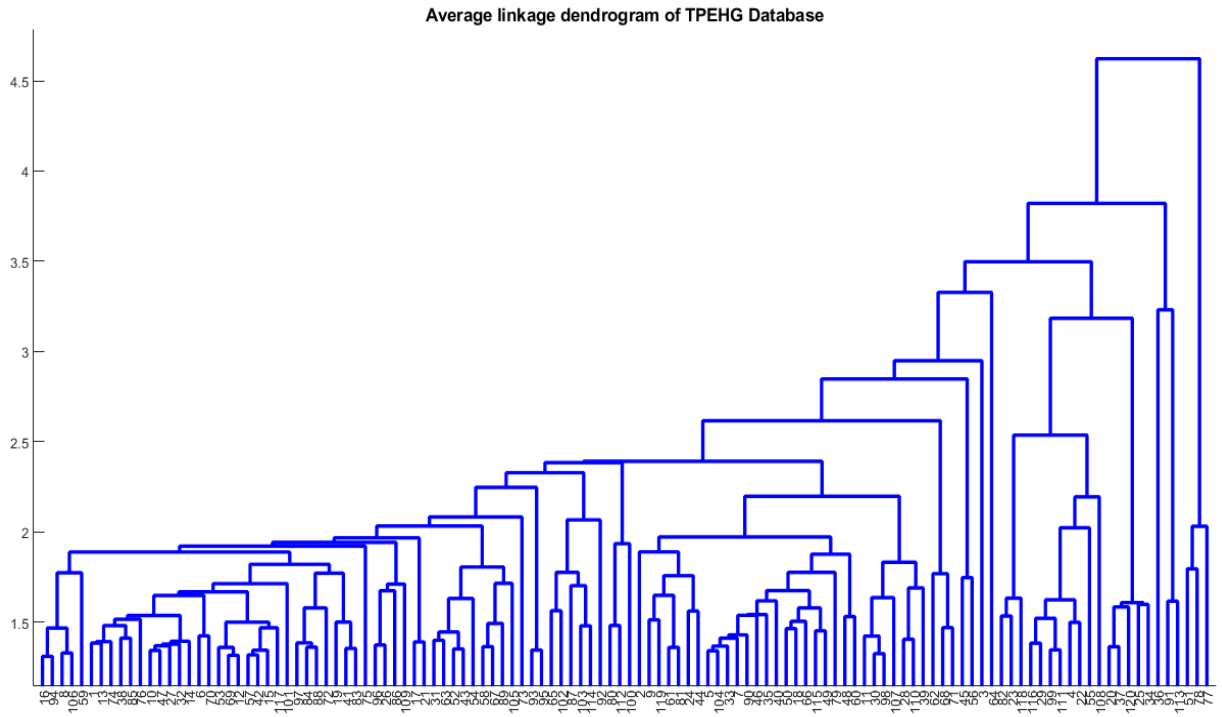

Figure 8.15: Dendrogram of the 4622 observations from the TPEHG database obtained with average linkage clustering. The vertical axis represents the dissimilarity between clusters.

Analyzing the dendrogram, there is some chaining in the TPEHG database, which was expected since most of the observations are gathered in one cluster. In Figure 8.15, clustering presents low dissimilarity values. On the right side of the dendrogram there is two clear isolated groups of observations. The cophenetic correlation coefficient was calculated for TPEHG database for the average linkage clustering with the MATLAB® function *cophenet*. The results are presented in Figure 8.16. The cophenetic correlation coefficient of the TPEHG database was 0.5939, which indicates a good performance according to this criterion. This value is identical to the Icelandic database.

```
ccoph =

    0.5939
```

Figure 8.16: Cophenetic correlation coefficient of the TPEHG database for 5 clusters

It can be considered that, for Braxton-Hicks and Alvarez waves the clustering results for this database are similar to the Icelandic database: Cluster 2 gathers the Braxton-Hicks contractions and the Cluster 4 comprises the Alvarez waves. However, a particularity for this case is relevant. Cluster 5 shows components with higher frequency around 0.8 Hz which is not expected. One should have in mind that the applied filter frequency was 1 Hz. So, the question arises, where is this high energy coming from. The only explanation that seems to be reasonable is that this cluster comprises some sort of interference noise with no biologic origin. Maybe it is due to the equipment or other external source.

The results regarding GA, Figure 8.19, for this database are coincident with the ones found in the Icelandic database.

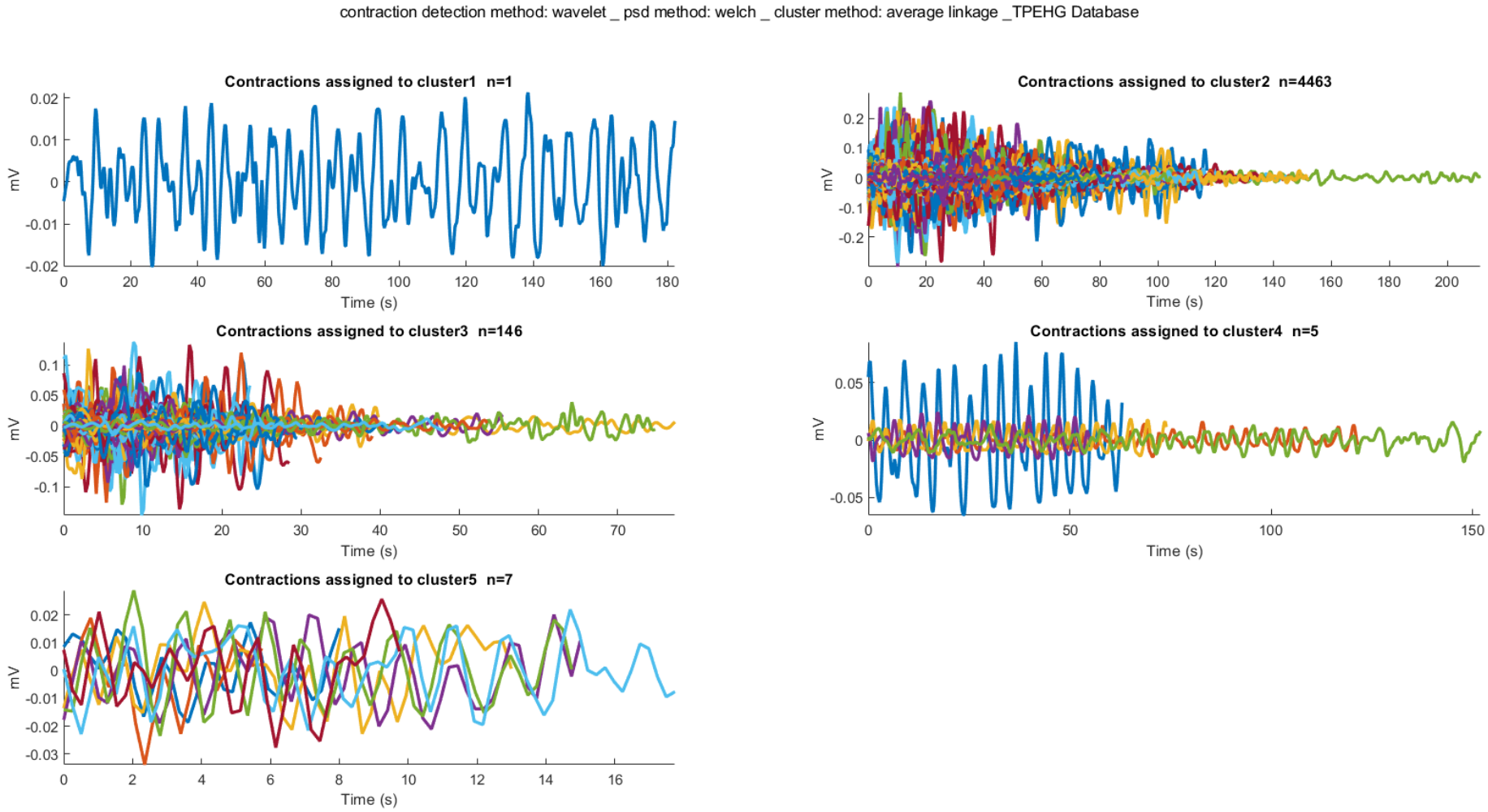

Figure 8.17: Output of the function *clustering_dist_pdist_new_v11*. Clusters of the 4622 separated contractions from the TPEHG database. Clustering method: average linkage.

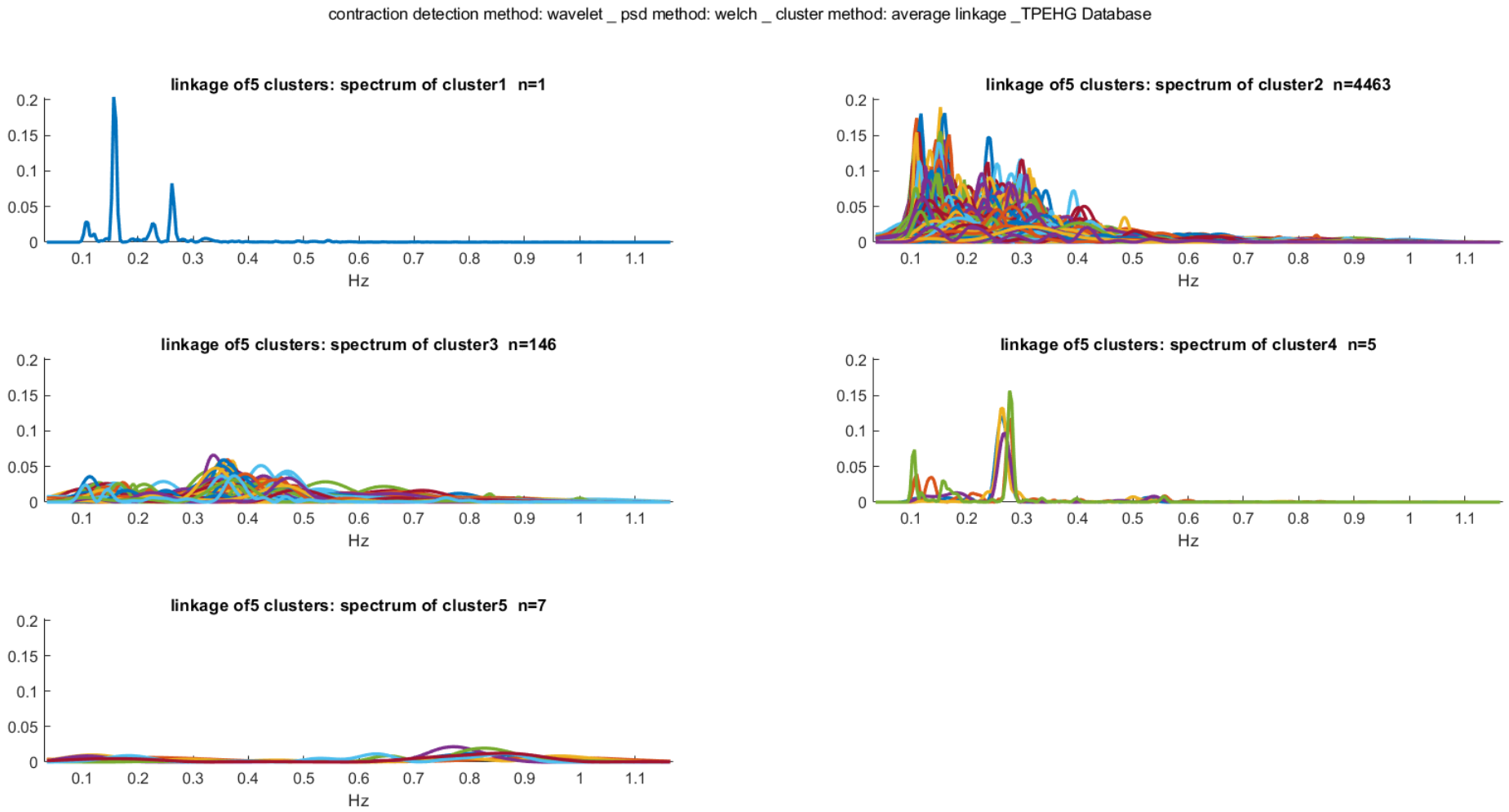

Figure 8.18: Output of the function *clustering_dist_pdist_new_v11*. Clustering of power spectra with average linkage clustering method. In cluster 3 and 5 it is possible to identify distinct peaks in the power spectra. The power spectra were obtained from the 4622 separated contractions of the TPEHG database.

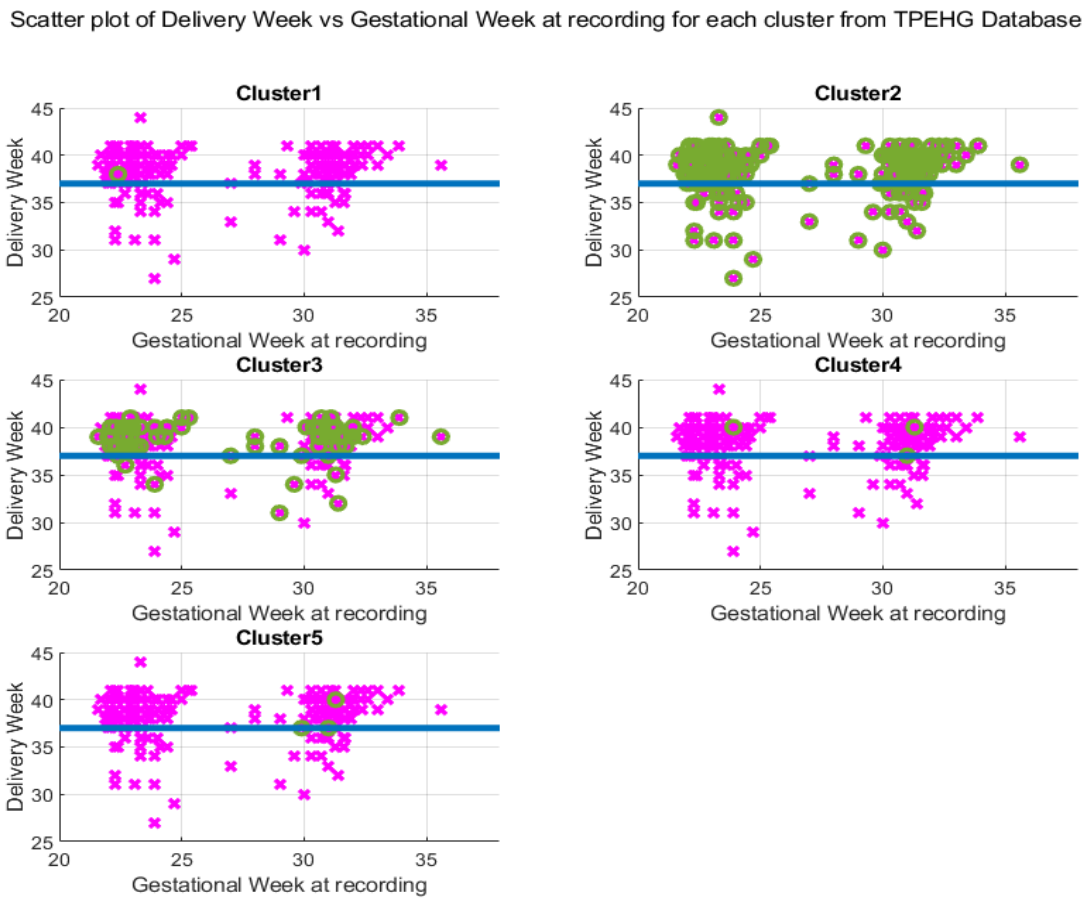

Figure 8.19: Output of the function *clustering_dist_pdist_new_v11* Relation of the Delivery week vs Recording week with the average linkage clustering for the TPEHG database. The blue line represents the 37 weeks of gestation. In pink is represented the whole database and in green is represented the observations in each cluster.

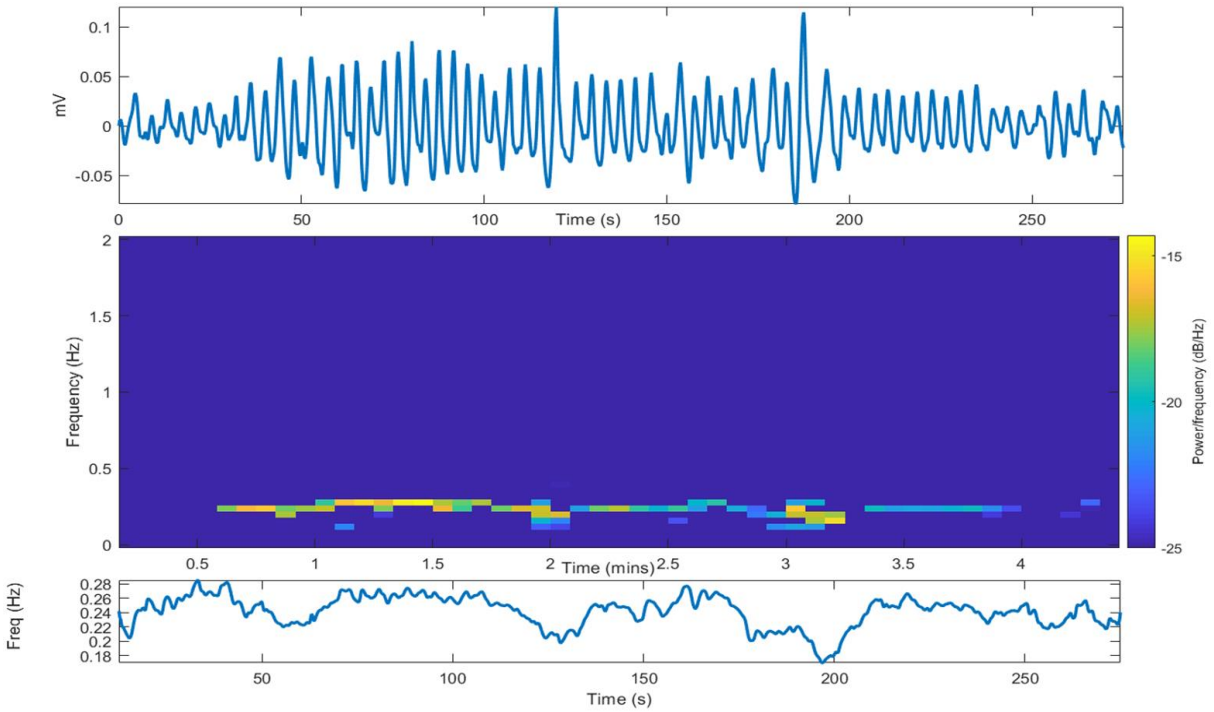

Figure 8.20: (a) – EHG signal from subject 553 from the TPEHG database with Alvarez wave;
(b) – Spectrogram of the signal represented in (a);
(c) – Instant Frequency of signal represented in (a).

Chapter 9 – Conclusions and Future Work

9.1 Conclusions

The Icelandic and the TPEHG database were used in this work to automatically separate contractions. After pre-processing and filtering the EHG signal, four databases were built:

- Table for each subject of the Icelandic database with function *read_Iceland_Database_v13_append_psd_contract_fm_v9_bipolar*;
- Table for each subject of the TPEHG database with function *read_Iceland_Database_v13_append_psd_contract_fm_v9_bipolar*;
- Database with separated contractions for the Icelandic database with function *create_database_cont_bipolar_v2*;
- Database with separated contractions for the TPEHG database with function *create_database_cont_bipolar_v2_tpehg*;

The four databases are available for future work. The parameters used in this work are:

1. Contraction detection method: Wavelet energy;
2. PSD estimation method: Welch;
3. Spectral distance method: Jeffrey divergence;
4. Clustering analysis method: Average Linkage;
5. Estimated cluster number: 6 for the Icelandic database and 5 for the TPEHG database.

The cluster analysis was performed over the complete contraction spectra which is an innovative method. It was demonstrated that it is computational feasible to use the whole contraction spectra for classification, using a common personal computer. Classification has typically been made based on low size features such as: entropy, frequency peaks locations and amplitudes.

It was anticipated that any clustering method would separate at least 3 contraction classes: Braxton-Hicks, Alvarez waves and LDBF waves. It was demonstrated that the clustering analysis was able to separate these classes. However, the following deviant behavior was demonstrated:

- The Braxton-Hicks contractions were found mostly in one single cluster (#2). However, this cluster also displays other events such as the Alvarez components and LDBF. This leakage is due, as mentioned before, to the cost function limited differentiation accuracy.
- Other cluster (#6) exclusive contained recognizable Alvarez waves (22 events in the Icelandic database, peak frequency around 0.35 Hz)
- Other cluster (#5) contained 20 Alvarez waves with a lower frequency peak (around 0.25 Hz)
- Other cluster (#1) contained what seems to be Alvarez waves with increased Slow wave component (10)
- A cluster (#4) with 116 events contains the components with the higher frequency content above 0.5 Hz.
- A cluster (#3) with 5 events also contains higher frequency events, which could represent a leakage from cluster #4.

- The system was able to successfully cluster the two main events in the EHG (Alvarez and Braxton-Hicks). Cluster #3 and #4 contain unidentified events that should be the target of further investigation.
- Regarding the LDBF components, that correspond to pregnancy risks, it has been shown that the clustering process was unable to create a separated class for these events despite the typical spectrum. This might be explained by the used distance function inability to differentiate these pluri-component spectra with sharp peaks. So, the path is open to try other distance functions or perhaps to detect using their most outstanding feature, the time duration which leads to a straight forward detection process.
- 52 Alvarez waves were clustered in the Icelandic database and 5 in the TPEHG database. Surely the number of the events present in these databases is much higher. As explained, this is explained by the used energy-based contraction detector having massively missed to detect this low energy event. Thus, a recommendation is made to detect these events using the instantaneous frequency feature. The other culprit is the misclassification in the clustering process due to the Alvarez wave contamination with Slow Wave. This reinforces the recommendation of using the instantaneous frequency feature of these contractions for detection, exclusively.

Other conclusions of this work are:

- No relation was found between the contractions and the GA;
- The shorter contractions have higher amplitude than longer ones;
- The Alvarez waves can be periodic and have similar spectrum features;
- Most of the Alvarez waves' spectrum has values close to zero. It is possible that the distance cost function chosen in this work is not the more adequate to deal with this factor, which is illustrated in the silhouette plots;
- In the distance calculation, the proximity of the PSD to zero and the constant added to avoid this problem have a significant impact in the obtained results.

It has been demonstrated that any work to establish standards in the EHG cluster analysis requires a comprehensive database which should include the following features:

- The GA recording should be evenly distributed along the pregnancy period and begin as early as 20 weeks of gestation for which only a certain type of contraction event would exist, in normal cases;
- A representative number of preterm cases should exist to be able to investigate the EHG as a preterm risk evaluation tool;
- A representative number of pre-labor cases should exist in order to be able to investigate the EHG as a marker of impending labor;
- The subject's perception as far as contraction discomfort and intensity is concerned, should also be registered by the database operator. This annotation will contribute for the evaluation of the contraction classification used methodology. The Icelandic database contains this annotation, using a two-scale grade: strong and weak. Basically, the subject perception of the Braxton-Hicks, Alvarez and Fetal Movements will contribute to the assessment of the automatic classification method. The decision should be made as whether the subject is allowed to drowse/sleep.

Despite the two databases used in this project being excellent research data tools that have been used and validated by the EHG research community, thus providing an important contribution in this research field, the above-mentioned topics are somehow an improvement that other prospective EHG database developers could follow. The *Maternidade Alfredo da Costa* database that is under development, addresses these subjects.

Regarding pre-term risk evaluation, using the databases scatter plot (Delivery Week versus Recording week) it was found that no cluster was assigned to the preterm cases, namely in the TPEHG database which contains a larger number of preterm cases. It should not be concluded that this clustering operation is not the adequate tool for this task since it is demonstrated that significantly number of Alverez events are not present in the target database because the contraction detector algorithm missed them. It is reasonable to assume that hundreds of these events are missing if it is taken in consideration that they are the most common event along with Braxton-Hicks, and only about 52 (5) are present in the Icelandic (TPEHG) databases.

As far as this thesis work plan is concerned, if there was a previous knowledge of this fact, it would have been made a provision for the development of the adequate algorithms for the Alvarez waves based on the instantaneous frequency. The mentioned constraint was only evident after the clustering process was complete. The idea was to develop an unsupervised classification methodology.

The clustering process heavily relies on code development and optimization. A great deal of coding was necessary to reach the proposed goals. This system is open source code that may be used for future implementations, for instance trying new distance functions, different PSD method or other clustering parameters. The main strategy is therefor in place for future work in the Uterine Explorer project. Code optimization is always a matter of improvement however it has been found that the developed code is reasonably optimized. For instance, a clustering process of 3135 contractions takes 6 minutes with a computer with the following specifications: Windows 10, Intel Core i5 (3.1 GHz) and 8 Gb of RAM. It should be noticed however that the database feeding the clustering algorithm may have higher developing times. In this work the contraction database was developed for further use with all the contractions spectra and respective headers. The databases were made for bipolar channels using the wavelet method as a contraction detector. This process depends directly on the contraction detection accuracy which is part of an ongoing work. The selected contraction detector method produced good results but was unable to detect properly the Alvarez events, for which has been presented a solution.

The work presented in this project is the first step for the EHG contractions sequencing that will eventually lead to an accurate preterm risk evaluation and term time prediction. The contractions sequencing method is essential to understand if there is specific sequence of contractions conductive to labor triggering. In this method the following features should be considered: contraction type and time gap between the considered contractions. A statistic algorithm could be applied to differentiate contractions sequences. In fact, references[54] pointed out for this possible uterine electrophysiological behavior. Warkentin, B.[142] referred that Alvarez waves represent 70 to 80% of all the contractions and Creasy, R.[55] concluded that Alvarez waves lead to contractions of higher intensity, which could induce labor. The high occurrence rate of the Alvarez waves probably is not the root of preterm birth since the low amplitude of these waves can only contribute to larger contractions that can trigger labor.

9.2 Future Work

For future work the following suggestions are made:

- Apply different methods of energy estimation of the EHG signal to increase the accuracy of the contraction detector;
- Being the EHG a known non-stationary signal the contraction delineation (onset/off set) cannot be clearly determined even by the expert visual classification, unlike the Electrocardiography signal

case. It is expected some inter-expert definition variation in this matter. Perhaps some common ground decision maker rules should be set. In one case only some general rules were lay down about this subject, but the criteria are too vague.[3] However one should keep in mind that the delineation accuracy of the contraction is not critical within reasonable limits;

- The Alvarez waves detection must be performed with frequency features;
- Use other non-parametric as well as parametric methods of PSD;
- Explore different distance functions less influenced by zero proximity;
- Different cluster analysis methods can be applied to the power spectra or other features such as main peak frequency or median frequency;
- Database improvements regarding including annotations of the subject perceptions regarding the contractions. Fetal ECG detection that would contribute to Braxton-Hicks contraction detection, since the fetal heart rate decreases when these event happen[57];
- Contraction sequencing is the next step of in the EHG research since it would help determining a relation between different types of contractions and preterm and term pregnancies.

References

1. Hadar E, Biron-Shental T, Gavish O, Raban O, Yogev Y. A comparison between electrical uterine monitor, tocodynamometer and intra uterine pressure catheter for uterine activity in labor. *J Matern Neonatal Med*. 2015;28(12):1367-1374. doi:10.3109/14767058.2014.954539

2. MacOnes GA, Cahill A, Stamilio DM, Odibo A. A new method for assessing uterine activity: Haran et al. *Am J Obstet Gynecol*. 2012;206(5):449. doi:10.1016/j.ajog.2012.03.019

3. Alberola-Rubio J, Prats-Boluda G, Ye-Lin Y, Valero J, Perales A, Garcia-Casado J. Comparison of non-invasive electrohysterographic recording techniques for monitoring uterine dynamics. *Med Eng Phys*. 2013;35(12):1736-1743. doi:10.1016/j.medengphy.2013.07.008

4. Preterm birth. http://www.who.int/news-room/fact-sheets/detail/preterm-birth. Accessed May 23, 2018.

5. Preterm Birth | Maternal and Infant Health | Reproductive Health | CDC. https://www.cdc.gov/reproductivehealth/maternalinfanthealth/pretermbirth.htm. Accessed May 23, 2018.

6. Estatística IN De. *Estatísticas Demográficas 2016*. (Instituto Nacional de Estatística I, ed.). Lisboa: Instituto Nacional de Estatística, IP; 2017.

7. Kandil M, Emarh M, Ellakwa H. Abdominal electromyography in laboring and non-laboring pregnant women at term and its clinical implications. *Arch Gynecol Obstet*. 2013;288(2):293-297. doi:10.1007/s00404-013-2757-4

8. Fele-Žorž G, Kavšek G, Novak-Antolič Ž, Jager F. A comparison of various linear and non-linear signal processing techniques to separate uterine EMG records of term and pre-term delivery groups. *Med Biol Eng Comput*. 2008;46(9):911-922. doi:10.1007/s11517-008-0350-y

9. Alexandersson A, Steingrimsdottir T, Terrien J, Marque C, Karlsson B. The Icelandic 16-electrode electrohysterogram database. *Sci Data*. 2015;2:1-9. doi:10.1038/sdata.2015.17

10. Ye-Lin Y, Garcia-Casado J, Prats-Boluda G, Alberola-Rubio J, Perales A. Automatic identification of motion artifacts in EHG recording for robust analysis of uterine contractions. *Comput Math Methods Med*. 2014;2014. doi:10.1155/2014/470786

11. Hill MG, Wood SL, Anyaegbunam U, Cohen WR, Hayes-gill B. Performance of a condensed electrode patch compared to a diffuse array for transabdominal fetal heart rate monitoring. *Reprod Sci*. 2014;21(3):252A.

12. Garfield RE, Maner WL. Physiology and electrical activity of uterine contractions. *Semin Cell Dev Biol*. 2007;18(3):289-295. doi:10.1016/j.semcdb.2007.05.004

13. Marque C, Duchene JMG, Leclercq S, Panczer GS, Chaumont J. Uterine EHG Processing for Obstetrical Monitoring. *IEEE Trans Biomed Eng*. 1986;BME-33(12):1182-1187. doi:10.1109/TBME.1986.325698

14. Newman RB, Gill PJ, Campion S, Katz M. Antepartum ambulatory tocodynamometry: the significance of low-amplitude, high-frequency contractions. *Obstet Gynecol*. 1987;70(5):701-705. http://www.ncbi.nlm.nih.gov/pubmed/3658276.

15. Roberts WF, Perry KG, Naef RW, Washburne JF, Morrison JC. The irritable uterus: A risk factor for preterm birth? *Am J Obstet Gynecol*. 1995;172(1 PART 1):138-142. doi:10.1016/0002-9378(95)90102-7

16. Khalil M, Duchene J. Uterine EMG analysis: a dynamic approach for change detection and classification. *IEEE Trans Biomed Eng*. 2000;47(6):748-756. doi:10.1109/10.844224

17. Chendeb M. Détection et classification des signaux non stationnaires par utilisation des

ondelettes. Application aux signaux électromyographiques utérins. 2006.

18. Marque C, Gondry J, Rossi J, Baaklini N, Duchêne J. Surveillance des grossesses à risque par électromyographie utérine. *RBM-News*. 1995;17(1):25-31. doi:10.1016/S0222-0776(00)88906-3

19. Sousa C. Electrohysterogram Signal Component Cataloging with Spectral and Time-Frequency Methods. 2015;(October). http://hdl.handle.net/10362/16081.

20. Chendeb M, Khalil M, Hewson D, Duchêne J. Classification of non stationary signals using multiscale decomposition. *J Biomed Sci Eng*. 2010;3(February):193-199. doi:10.4236/jbise.2010.32025

21. Braxton Hicks J. On the contractions of the uterus throughout pregnancy. Their physiological effects and their value in the diagnosis of pregnancy. *Trans Obstet Soc London*. 1872;123(4):216–231. doi:10.1016/S0002-9378(16)33445-7

22. Novii Wireless Patch System | Fetal Monitoring | Monica Healthcare. http://www.monicahealthcare.com/products/labour-and-delivery/monica-novii-wireless-patch-system. Accessed September 22, 2018.

23. Nemo Healthcare. https://nemohealthcare.com/en/. Accessed September 22, 2018.

24. Shier D, Lewis R, Butler J. *Human Anatomy & Physiology*. 11th ed. McGraw-Hill; 2007.

25. Hassan M. Analysis of the Propagation of Uterine Electrical Activity Applied To Predict Preterm Labor. 2015. http://hdl.handle.net/1946/13098.

26. Boron W, Boulpaep E. *Medical Physiology*. 2nd ed. Saunders; 2012.

27. Lawrence-Watt D, Montgomery J, Johnston M. Applied anatomy and imaging of the uterus, vagina, ovaries and breast. In: Fiander A, Thilaganathan B, eds. *MRCOG Part One*. Cambridge: Cambridge University Press; 2017:41-50. doi:10.1017/CBO9781107587519.004

28. Pregnancy process design Vector | Free Download. https://www.freepik.com/free-vector/pregnancy-process-design_1095964.htm. Accessed June 27, 2018.

29. Hall JE. *Textbook of Medical Physiology*. 12th ed. (Elsevier, ed.). Saunders; 2010.

30. Abbas K, Monaghan SD, Campbell I. Uterine physiology. *Anaesth Intensive Care Med*. 2011;12(3):108-110. doi:10.1016/j.mpaic.2010.11.004

31. Alotaibi M. The physiological mechanism of uterine contraction with emphasis on calcium ion. *Calcium Signal*. 2014;1(2):70-75.

32. Buhimschi C, Garfield RE. Uterine contractility as assessed by abdominal surface recording of electromyographic activity in rats during pregnancy. *Am J Obstet Gynecol*. 1996;174(2):744-753. doi:10.1016/S0002-9378(96)70459-3

33. La Rosa PS, Eswaran H, Preissl H, Nehorai A. Multiscale forward electromagnetic model of uterine contractions during pregnancy. *BMC Med Phys*. 2012;12(1). doi:10.1186/1756-6649-12-4

34. Howson C, Kinney M, Lawn J. *Born Too Soon: The Global Action Report on Preterm Birth*. (WHO, Dimes M of, PMNCH, Children S the, eds.). Geneva; 2012.

35. Blencowe H, Cousens S, Oestergaard MZ, et al. National, regional, and worldwide estimates of preterm birth rates in the year 2010 with time trends since 1990 for selected countries: A systematic analysis and implications. *Lancet*. 2012;379(9832):2162-2172. doi:10.1016/S0140-6736(12)60820-4

36. American College of Obstetricians and Gynecologists. Extremely Preterm Birth - ACOG.

https://www.acog.org/Patients/FAQs/Extremely-Preterm-Birth#preterm. Published 2016. Accessed August 18, 2018.

37. Loftin RW, Habli M, Snyder CC, Cormier CM, Lewis DF, DeFranco EA. Late Preterm Birth. *Rev Obstet Gynecol*. 2010;3(1):10-19. doi:10.3909/riog0098

38. WHO. Maternal and newborn health. August 2018. http://www.euro.who.int/en/health-topics/Life-stages/maternal-and-newborn-health/maternal-and-newborn-health. Accessed August 18, 2018.

39. Galal M, Symonds I, Murray H, Petraglia F, Smith R. Postterm Pregnancy. *FVV Obgyn*. 2012;4(3):175-187. doi:10.1002/9781119979449.ch23

40. Léman H, Marque C, Gondry J. Use of the electrohysterogram signal for characterization of contractions during pregnancy. *IEEE Trans Biomed Eng*. 1999;46(10):1222-1229. doi:10.1109/10.790499

41. Higby K, Xenakis EM-J, Pauerstein CJ. Do tocolytic agents stop preterm labor? A critical and comprehensive review of efficacy and safety. *Am J Obstet Gynecol*. 1993;168(4):1247-1259. doi:10.1016/0002-9378(93)90376-T

42. Bajlekov GI, Rabotti C, Oei SG, Mischi M. Electrohysterographic detection of uterine contractions in term pregnancy. In: *2015 37th Annual International Conference of the IEEE Engineering in Medicine and Biology Society (EMBC)*. IEEE; 2015:5851-5854. doi:10.1109/EMBC.2015.7319722

43. Bhong SS, Lokhande SD. Monitoring of Unborn Babies Using Bluetooth. 2013;4(5):2182-2185.

44. Alvarez H, Caldeyro-Barcia R. The normal and abnormal contractile waves of the uterus during labour. *Gynaecologia*. 1954;138(2):190-212. doi:10.1159/000308198

45. Rabotti C, Mischi M, Van Laar JOEH, Oei GS, Bergmans JWM. Estimation of internal uterine pressure by joint amplitude and frequency analysis of electrohysterographic signals. *Physiol Meas*. 2008;29(7):829-841. doi:10.1088/0967-3334/29/7/011

46. PhD MM, RNC. *Antepartal and Intrapartal Fetal Monitoring: Third Edition*. Vol 8.; 2006. https://books.google.com/books?id=_4jYJUGG56cC&pgis=1.

47. Maul H, Maner WL, Saade GR, Garfield RE. The physiology of uterine contractions. *Clin Perinatol*. 2003;30(4):665-676. doi:10.1016/S0095-5108(03)00105-2

48. Horoba K, Jezewski J, Wrobel J, Graczyk S. Algorithm for detection of uterine contractions from electrohysterogram. In: *2001 Conference Proceedings of the 23rd Annual International Conference of the IEEE Engineering in Medicine and Biology Society*. Vol 3. IEEE; 2001:2161-2164. doi:10.1109/IEMBS.2001.1017198

49. Yang Z, Yang R, Lu Y. Estimation of intrauterine pressure from electrohysterography using hilbert phase slips and statistics method. *J Mech Med Biol*. 2017;17(06):1750089. doi:10.1142/S0219519417500890

50. Fergus P, Cheung P, Hussain A, Al-Jumeily D, Dobbins C, Iram S. Prediction of Preterm Deliveries from EHG Signals Using Machine Learning. *PLoS One*. 2013;8(10). doi:10.1371/journal.pone.0077154

51. Parra CB, Tendero AI, Ye-Lin Y, et al. Feasibility of Labor Induction Success Prediction based on Uterine Myoelectric Activity Spectral Analysis. 2017;4(Biostec):70-77. doi:10.5220/0006649400700077

52. Batista AG, Najdi S, Godinho DM, et al. A multichannel time–frequency and multi-wavelet toolbox for uterine electromyography processing and visualisation. *Comput Biol Med*.

2016;76:178-191. doi:10.1016/j.compbiomed.2016.07.003

53. Alvarez H, Caldeyro-Barcia R. Contractility of the human uterus recorded by new methods. *Surg Gynecol Obstet*. 1950;91(1):1-13. http://www.ncbi.nlm.nih.gov/pubmed/15442821.

54. Colditz P. *Multiple Pregnancy: Epidemiology, Gestation, and Perinatal Outcome*. Vol 9. 2nd ed. (Press C, ed.).; 2006. http://journals.cambridge.org/abstract_S1832427400006162.

55. Creasy RK. Preterm birth prevention: Where are we? *Am J Obstet Gynecol*. 1993;168(4):1223-1230. doi:10.1016/0002-9378(93)90373-Q

56. Devedeux D, Marque C, Mansour S, Germain G, Duchêne J. Uterine electromyography: A critical review. *Am J Obstet Gynecol*. 1993;169(6):1636-1653. doi:10.1016/0002-9378(93)90456-S

57. Mulder EJH, Visser GHA. Braxton Hicks' contractions and motor behavior in the near-term human fetus. *Am J Obstet Gynecol*. 1987;156(3):543-549. doi:10.1016/0002-9378(87)90047-0

58. Diab A. Study of the nonlinear properties and propagation characteristics of the uterine electrical activity during pregnancy and labor. 2015.

59. Chandraharan E. *Handbook of CTG Interpretation*. (Chandraharan E, ed.). Cambridge University Press; 2017. doi:10.1017/9781316161715

60. Diab MO, Moslem B, Khalil M, Marque C. Classification of uterine EMG signals by using normalized wavelet packet energy. *Proc Mediterr Electrotech Conf - MELECON*. 2012:335-338. doi:10.1109/MELCON.2012.6196443

61. Diab A, Hassan M, Marque C, Karlsson B. Quantitative performance analysis of four methods of evaluating signal nonlinearity: Application to uterine EMG signals. *Proc Annu Int Conf IEEE Eng Med Biol Soc EMBS*. 2012:1045-1048. doi:10.1109/EMBC.2012.6346113

62. AMBOSS. Childbirth. https://www.amboss.com/us/knowledge/Childbirth. Accessed September 16, 2018.

63. Goldberger AL, Amaral LAN, Glass L, et al. PhysioBank, PhysioToolkit, and PhysioNet : Components of a New Research Resource for Complex Physiologic Signals. *Circulation*. 2000;101(23):e215-e220. doi:10.1161/01.CIR.101.23.e215

64. Conference AI, Boston IE. Classification of Multichannel Uterine EMG Signals. 2011:2602-2605.

65. Thomas BE, John SK, Abe S. Power Spectral Density Computation using Modified Welch Method. *Int J Sci Technol Eng*. 2015;2(4):145-152.

66. Alamedine D, Khalil M, Marque C. Comparison of different EHG feature selection methods for the detection of preterm labor. *Comput Math Methods Med*. 2013;2013(March 2014):1-9. doi:10.1155/2013/485684

67. Alamedine D, Diab A, Muszynski C, Karlsson B, Khalil M, Marque C. Selection algorithm for parameters to characterize uterine EHG signals for the detection of preterm labor. *Signal, Image Video Process*. 2014;8(6):1169-1178. doi:10.1007/s11760-014-0655-2

68. Alamedine D, Khalil M, Marque C. Parameters extraction and monitoring in uterine EMG signals. Detection of preterm deliveries. *Irbm*. 2013;34(4-5):322-325. doi:10.1016/j.irbm.2013.08.003

69. Parhi KK, Ayinala M. Low-Complexity Welch Power Spectral Density Computation. *IEEE Trans Circuits Syst I Regul Pap*. 2014;61(1):172-182. doi:10.1109/TCSI.2013.2264711

70. Solomon OM. PSD Computations Using Welch ' s Method. 1991;(December).

71. Brahmani K, Kumar BA, Ramesh KS, Rao SK, Chandra TV. Estimation of power spectral density of seismic data using welch method. *Int J Pure Appl Math*. 2017;114(10 Special Issue):211-219.

72. Smrdel A, Jager F. Separating sets of term and pre-term uterine EMG records. *Physiol Meas*. 2015;36(2):341-355. doi:10.1088/0967-3334/36/2/341

73. Oliveira A, Ferreira J, Ferreira J. Eletromiografia Uterina e os Movimentos Fetais. 2017.

74. Itakura F, Saito S. Analysis synthesis telephony based on the maximum likelihood method. *Proc 6th Int Congr Acoust*. 1968:17–20.

75. Chavan K, Gawande U. Speech recognition in noisy environment, issues and challenges: A review. *Proc IEEE Int Conf Soft-Computing Netw Secur ICSNS 2015*. 2015. doi:10.1109/ICSNS.2015.7292420

76. Wiriyarattanakul S, Eua-anant N. Pitch segmentation of speech signals based on short-time energy waveform. *Int J Speech Technol*. 2017;20(4):907-917. doi:10.1007/s10772-017-9459-4

77. Wang Z, Bi G. A Voice Activity Detector Based on Noise Spectrum Adaptation and Discrimination Information for Automatic Speech Recognition System. *2014 5th Int Conf Intell Syst Model Simul*. 2014:301-305. doi:10.1109/ISMS.2014.57

78. Ryu J, Park C. Time-Frequency Analysis of Electrohysterogram for Classification of Term and Preterm Birth. 2015;4(2).

79. Verdenik I, Pajntar M, Leskos B, Leskošek B. Uterine electrical activity as predictor of preterm birth in women with preterm contractions. *Eur J Obstet Gynecol Reprod Biol*. 2001;95(2):149-153. doi:10.1016/S0301-2115(00)00418-8

80. Lucovnik M, Maner WL, Chambliss LR, et al. Noninvasive uterine electromyography for prediction of preterm delivery. *Am J Obstet Gynecol*. 2011;204(3):228.e1-228.e10. doi:10.1016/j.ajog.2010.09.024

81. Vitányi PMB. Information distance in multiples. *IEEE Trans Inf Theory*. 2011;57(4):2451-2456. doi:10.1109/TIT.2011.2110130

82. Gray A, Markel J. Distance measures for speech processing. *IEEE Trans Acoust*. 1976;24(5):380-391. doi:10.1109/TASSP.1976.1162849

83. Arkhangel'skii AV, Pontryagin LS. *General Topology I*. Vol 17. 1st ed. (Arkhangel'skii A V., Pontryagin LS, eds.). Berlin, Heidelberg: Springer Berlin Heidelberg; 1990. doi:10.1007/978-3-642-61265-7

84. Wierzchoń S, Kłopotek M. *Modern Algorithms of Cluster Analysis*. Vol 34. Cham: Springer International Publishing; 2018. doi:10.1007/978-3-319-69308-8

85. Shumway RH. Time-frequency clustering and discriminant analysis. *Stat Probab Lett*. 2003;63(3):307-314. doi:10.1016/S0167-7152(03)00095-6

86. Zhang Z, Ooi BC, Parthasarathy S, Tung AKH. Similarity Search on Bregman Divergence: Towards Non-Metric Indexing. *Proc VLDB Endow*. 2009;2(1):13-24. doi:10.14778/1687627.1687630

87. Soong FK, Sondhi MM. A Frequency-Weighted Itakura Spectral Distortion Measure and Its Application to Speech Recognition in Noise. *IEEE Trans Acoust*. 1988;36(1):41-48. doi:10.1109/29.1487

88. Gao B, Bai L, Woo WL, Tian G. Thermography pattern analysis and separation. *Appl Phys Lett*. 2014;104(25). doi:10.1063/1.4884644

89. Iser B, Minker W, Schmidt G. *Bandwidth Extension of Speech Signals*.; 2008. doi:10.1007/978-0-387-68899-2

90. Banerjee A, Merugu S, Dhillon IS, Ghosh J. Clustering with Bregman Divergences. *J Mach Learn Res*. 2005;6:1705-1749. doi:10.1007/s10994-005-5825-6

91. Wang W. *Machine Audition: Principles, Algorithms and Systems (Premier Reference Source)*. IGI Global; 2010.

92. Nielsen F, Nock R. Bregman sided and symmetrized centroids. *2008 19th Int Conf Pattern Recognit*. 2008;55(6):2882-2904. doi:10.1109/ICPR.2008.4761794

93. Bregman LM. The relaxation method of finding the common point of convex sets and its application to the solution of problems in convex programming. *USSR Comput Math Math Phys*. 1967;7(3):200-217. doi:10.1016/0041-5553(67)90040-7

94. Acharyya S, Banerjee A, Boley D. Bregman Divergences and Triangle Inequality. In: *Proceedings of the 2013 SIAM International Conference on Data Mining*. Philadelphia, PA: Society for Industrial and Applied Mathematics; 2013:476-484. doi:10.1137/1.9781611972832.53

95. Brooks M. VOICEBOX: Speech Processing Toolbox for MATLAB. http://www.ee.ic.ac.uk/hp/staff/dmb/voicebox/voicebox.html. Published 1997. Accessed May 24, 2018.

96. Itakura F. Minimum prediction residual applied to speech recognition. *IEEE Trans Acoust Speech Signal Process*. 1975;23(1):67-72.

97. Ebrahimi F, Mikaili M, Estrada E, Nazeran H. Assessment of itakura distance as a valuable feature for computer-aided classification of sleep stages. *Annu Int Conf IEEE Eng Med Biol - Proc*. 2007:3300-3303. doi:10.1109/IEMBS.2007.4353035

98. Kullback S, Leibler RA. On Information and Sufficiency. *Ann Math Stat*. 1951;22(1):79-86. doi:10.1214/aoms/1177729694

99. Ponti M, Kittler J, Riva M, Campos T de, Zor C. A decision cognizant Kullback–Leibler divergence. *Pattern Recognit*. 2017;61:470-478. doi:10.1016/j.patcog.2016.08.018

100. Kullback S. *Information Theory and Statistics*. 2nd ed. Dover Publications; 1968.

101. Georgiou TT, Lindquist A. Kullback-Leibler approximations of spectral density functions. *IEEE Trans Inf Theory*. 2003;49(11):2910-2917. doi:10.1109/TIT.2003.819324

102. De Domenico M, Biamonte J. Spectral Entropies as Information-Theoretic Tools for Complex Network Comparison. *Phys Rev X*. 2016;6(4):34-37. doi:10.1103/PhysRevX.6.041062

103. Martin F, Carballeira J, Moreno L, Garrido S, Gonzalez P. Using the jensen-shannon, density power, and itakura-saito divergences to implement an evolutionary-based global localization filter for mobile robots. *IEEE Access*. 2017;5:13922-13940. doi:10.1109/ACCESS.2017.2724199

104. Budka M, Gabrys B, Musial K. On accuracy of PDF divergence estimators and their applicability to representative data sampling. *Entropy*. 2011;13(7):1229-1266. doi:10.3390/e13071229

105. Szabó Z. Information Theoretical Estimators Toolbox. *J Mach Learn Res*. 2014;15:283-287. https://bitbucket.org/szzoli/ite/.

106. Legrand L, Grivel E. Jeffrey's divergence between moving-average models that are real or complex, noise-free or disturbed by additive white noises. *Signal Processing*. 2017;131:350-363. doi:10.1016/j.sigpro.2016.08.026

107. Fass D. KLDIV - File Exchange - MATLAB Central. https://www.mathworks.com/matlabcentral/fileexchange/13089-kldiv. Published 2016. Accessed June 22, 2018.

108. Rényi A. On measures of entropy and information. *Fourth Berkeley Symp Math Stat Probab*. 1961;1:547–561.

109. van Erven T, Harremoës P. Rényi Divergence and Kullback-Leibler Divergence. *IEEE Trans Inf Theory*. 2012;60(7):3797-3820. doi:10.1109/TIT.2014.2320500

110. Leonenko N, Pronzato L, Savani V. A class of rényi information estimators for multidimensional densities. *Ann Stat*. 2008;36(5):2153-2182. doi:10.1214/07-AOS539

111. He Y, Hamza A Ben, Krim H. A generalized divergence measure for robust image registration. *IEEE Trans Signal Process*. 2003;51(5):1211-1220. doi:10.1109/TSP.2003.810305

112. Wang F, Syeda-Mahmood T, Vemuri BC, Beymer D, Rangarajan A. Closed-form Jensen-Renyi divergence for mixture of Gaussians and applications to group-wise shape registration. *Lect Notes Comput Sci (including Subser Lect Notes Artif Intell Lect Notes Bioinformatics)*. 2009;5761 LNCS(PART 1):648-655. doi:10.1007/978-3-642-04268-3_80

113. Singh J, Darpe AK, Singh SP. Bearing damage assessment using Jensen-Rényi Divergence based on EEMD. *Mech Syst Signal Process*. 2017;87(October):307-339. doi:10.1016/j.ymssp.2016.10.028

114. Aviyente S. Information processing on the time-frequency plane. In: *2004 IEEE International Conference on Acoustics, Speech, and Signal Processing*. Vol 2. ; 2004. doi:10.1109/ICASSP.2004.1326333

115. Zeyong Shan, Aviyente S. Jensen-Rényi Divergence for Source Separation on the Time-Frequency Plane. In: *2006 IEEE International Conference on Acoustics Speed and Signal Processing Proceedings*. Vol 3. IEEE; 2006:III-424-III-427. doi:10.1109/ICASSP.2006.1660681

116. Wenye G. shannon and non-extensive entropy - File Exchange - MATLAB Central. https://www.mathworks.com/matlabcentral/fileexchange/18133-shannon-and-non-extensive-entropy. Published 2008. Accessed June 22, 2018.

117. Hair JF, Black W. Cluster analysis. *Read Underst MORE Multivar Stat*. 2000:147-206.

118. Tryon RC. *Cluster Analysis: Correlation Profile and Orthometric (Factor) Analysis for the Isolation of Unities in Mind and Personality*.; 1939.

119. van Vark GN, Howells WW. *Multivariate Statistical Methods in Physical Anthropology*. (Van Vark GN, Howells WW, eds.). Dordrecht: Springer Netherlands; 1984. doi:10.1007/978-94-009-6357-3

120. Bora DJ, Gupta DAK. A Comparative study Between Fuzzy Clustering Algorithm and Hard Clustering Algorithm. *Int J Comput Trends Technol*. 2014;10(2):108-113. doi:10.14445/22312803/IJCTT-V10P119

121. Abu-Jamous B, Fa R, Nandi AK. *Integrative Cluster Analysis in Bioinformatics*. Chichester, UK: John Wiley & Sons, Ltd; 2015. doi:10.1002/9781118906545

122. Martinez WL, Martinez AR, Solka JL. *Exploratory Data Analysis with MATLAB*. 2nd ed.; 2012.

123. Ward JH. Hierarchical Grouping to Oprimize an Objective Function. *J Am Stat Assoc*. 1963;58(301):236-244. doi:10.1080/01621459.1963.10500845

124. Venables WN, Ripley BD. Exploratory Multivariate Analysis. *Mod Appl Stat with S*. 2002:301-

330. doi:10.1007/978-0-387-21706-2

125. Sneath PHA. The Application of Computers to Taxonomy. *J Gen Microbiol*. 1957;17(1):201-226. doi:10.1099/00221287-17-1-201

126. Ferreira L, Hitchcock DB. A comparison of hierarchical methods for clustering functional data. *Commun Stat Simul Comput*. 2009;38(9):1925-1949. doi:10.1080/03610910903168603

127. Yim O. Hierarchical Cluster Analysis : Comparison of Three Linkage Measures and Application to Psychological Data. 2017;(February 2015):7-21. doi:10.20982/tqmp.11.1.p008

128. SNEATH PHA, SOKAL RR. Numerical Taxonomy. *Nature*. 1962;193(4818):855-860. doi:10.1038/193855a0

129. McQuitty LL. Hierarchical Syndrome Analysis. *Educ Psychol Meas*. 1960;20(2):293-304. doi:10.1177/001316446002000209

130. Sokal RR, Michener CD. *A Statistical Method for Evaluating Systematic Relationships*. Vol 38. 22nd ed. (Kansas U of, ed.).; 1958.

131. Sneath PHA, Sokal RR. Numerical Taxonomy : The Principles and Practice of Numerical Classification. *J Am Stat Assoc*. 1973;70(352):962.

132. Cleuziou G. A Generalization of k -Means for Overlapping Clustering. 2007.

133. Wyld DC, Wozniak M. *Advances in Computing and Information Technology*. Vol 198. (Wyld DC, Wozniak M, Chaki N, Meghanathan N, Nagamalai D, eds.). Berlin, Heidelberg: Springer Berlin Heidelberg; 2011. doi:10.1007/978-3-642-22555-0

134. Arora P, Varshney S. Analysis of K-Means and K-Medoids Algorithm For Big Data. *Procedia - Procedia Comput Sci*. 2016;78(December 2015):507-512. doi:10.1016/j.procs.2016.02.095

135. Panda B, Sahoo S, Patnaik SK. A Comparative Study Of Hard and Soft Clustering Using Swarm Optimization. 2013;4(10):785-790.

136. Tan P-N, Steinbach M, Kumar V. Chap 8 : Cluster Analysis: Basic Concepts and Algorithms. *Introd to Data Min*. 2005. doi:10.1016/0022-4405(81)90007-8

137. Arbin N, Suhaimi NS, Mokhtar NZ, Othman Z. Comparative Analysis between K-Means and K-Medoids for Statistical Clustering. In: *2015 3rd International Conference on Artificial Intelligence, Modelling and Simulation (AIMS)*. IEEE; 2015:117-121. doi:10.1109/AIMS.2015.82

138. Bholowalia P, Kumar A. EBK-Means: A Clustering Technique based on Elbow Method and K-Means in WSN. *Int J Comput Appl*. 2014;105(9):975-8887. doi:10.5120/18405-9674

139. EDA Toolbox Contents. http://cda.psych.uiuc.edu/martinez/edatoolbox/Docs/Contents.htm. Accessed September 16, 2018.

140. Rousseeuw PJ. Silhouettes: A graphical aid to the interpretation and validation of cluster analysis. *J Comput Appl Math*. 1987;20:53-65. doi:10.1016/0377-0427(87)90125-7

141. Saraçli S, Doğan N, Doğan I. Comparison of hierarchical cluster analysis methods by cophenetic correlation. *J Inequalities Appl*. 2013;2013:1-8. doi:10.1186/1029-242X-2013-203

142. Warkentin B. Uterine activity in late pregnancy. *Z Geburtshilfe Perinatol*. 1976;180(3):225-229. http://www.ncbi.nlm.nih.gov/pubmed/960964. Accessed September 24, 2018.

143. Naeem SM, Seddik AF, Eldosoky MA. New technique based on uterine electromyography nonlinearity for preterm delivery detection. *J Eng Technol Res*. 2014;6(7):107-114, November 2014. doi:10.5897/JETR2013.0332

144. Fergus P, Idowu I, Hussain A, Dobbins C. Advanced artificial neural network classification for detecting preterm births using EHG records. *Neurocomputing*. 2016;188:42-49. doi:10.1016/j.neucom.2015.01.107

145. Lemancewicz A, Borowska M, Kuć P, et al. Early diagnosis of threatened premature labor by electrohysterographic recordings - The use of digital signal processing. *Biocybern Biomed Eng*. 2016;36(1):302-307. doi:10.1016/j.bbe.2015.11.005

146. Acharya UR, Sudarshan VK, Rong SQ, et al. Automated detection of premature delivery using empirical mode and wavelet packet decomposition techniques with uterine electromyogram signals. *Comput Biol Med*. 2017;85(April):33-42. doi:10.1016/j.compbiomed.2017.04.013

147. Borowska M, Brzozowska E, Kuć P, Oczeretko E, Mosdorf R, Laudański P. Identification of preterm birth based on RQA analysis of electrohysterograms. *Comput Methods Programs Biomed*. 2018;153:227-236. doi:10.1016/j.cmpb.2017.10.018

148. Altini M, Rossetti E, Rooijakkers M, Penders J. Combining Electrohysterography and Heart Rate Data to Detect Labour Combining Electrohysterography and Heart Rate Data to Detect Labour. 2017;(January):149-152.

149. Diab MO, Marque C, Khalil M. An unsupervised classification method of uterine electromyography signals: Classification for detection of preterm deliveries. *J Obstet Gynaecol Res*. 2009;35(1):9-19. doi:10.1111/j.1447-0756.2008.00981.x

150. Hassan M, Terrien J, Karlsson B, Marque C. Application of wavelet coherence to the detection of uterine electrical activity synchronization in labor. *Irbm*. 2010;31(3):182-187. doi:10.1016/j.irbm.2009.12.004

151. Alamedine D, Khalil M, Marque C. Comparison of different EHG feature selection methods for the detection of preterm labor. *Comput Math Methods Med*. 2013;2013(March 2014). doi:10.1155/2013/485684

152. Diab A, Falou O, Hassan M, Karlsson B, Marque C. Effect of filtering on the classification rate of nonlinear analysis methods applied to uterine EMG signals. *Proc Annu Int Conf IEEE Eng Med Biol Soc EMBS*. 2015;2015-Novem:4182-4185. doi:10.1109/EMBC.2015.7319316

153. Chen L, Hao Y. Feature Extraction and Classification of EHG between Pregnancy and Labour Group Using Hilbert-Huang Transform and Extreme Learning Machine. 2017;2017. doi:10.1155/2017/7949507

Attachment 1 – Publications with complete EHG signal

Document	Research purpose	Used data	Band-pass and Fs	Methods and features	Results
Fele-Zorz et al., 2008[8]	Separate term and pre-term deliveries using linear and non-linear EMG signals	TPEHG dataset: 300 EHG signals (262 term and 38 preterm)	Band-pass: - 0.08 to 4 Hz - 0.3 to 4 Hz - 0.3 to 3 Hz Fs: 20 Hz	- RMS (Root Mean Square) - Peak Frequency - Median Frequency - Autocorrelation zero-crossing - Maximal Lyapunov exponent - Correlation dimension - SE (Sample Entropy)	Median Frequency: - before the 26th week (p value=0.03) - between all term and all preterm delivery records (p value=0.012) SE: - before the 26th week (p value=0.035) - between all term and all preterm delivery records (p value=0.011)
Rabotti et al., 2008[45]	Estimation of IUP (Intrauterine Pressure) through EHG signal analysis	- Bipolar signals - 9 women during labor	- Anti-aliasing filtering at 5 Hz Fs: 1000 Hz	- RMS - Optimal linear filtering - WT (Wavelet Transform) - Time–Frequency Distribution - Polynomial model	Correlation coefficient: - Optimal linear filtering: 0.5 ± 0.16 - RMS: 0.36 ± 0.16 - Polynomial model: 0.73 ± 0.11
Lucovnik et al., 2011[80]	Compare EMG power spectrum and EMG propagation velocity against current methods to predict preterm delivery	EMG was recorded in 116 patients (20 preterm labor, 68 preterm nonlabor, 22 term labor, 6 term nonlabor)	Band-pass: - 0.34 to1.00 Hz Fs: 100 Hz	- Peak Frequency - Median Frequency - Propagation velocity - ROC (Receiver Operating Characteristic) curves	Combined propagation velocity and PS peak frequency predicted preterm delivery within 7 days with AUC (Area Under Curve) of 0.96
Fergus et al., 2013[50]	EHG classification to determine whether delivery will be preterm or	TPEHG dataset: 300 EHG signals (262 term and 38 preterm)	Band-pass: - 0.34 to 1 Hz Fs: 20 Hz	- SMOTE (Synthetic Minority Over-sampling Technique) - WT and FT (Fourier Transform)	Polynomial Classifier: - Sensitivity: 96.67% - Specificity: 90.00%

Document	Research purpose	Used data	Band-pass and Fs	Methods and features	Results
	term			Features: - RMS; Median Frequency - SE; Peak Frequency	- AUC: 0.95 - Global error: 8%
Ye-Lin et al., 2014[10]	Develop an automatic system of segmenting EHG recordings to distinguish between uterine contractions and artifacts	Twelve women in first stages of labor (277 EHG artifacts and 422 non-artifacts) - Only the segments in which the classification of both experts agreed were included in the design and test of the automatic classifier - Bipolar signals	Band-pass: - 0.1 to 4 Hz Fs: 4 Hz	- LDA (Linear Discriminant Analysis) - Quadratic Discriminant Analysis - SVM using RBF (Radial Basis Function) Features: - Standard Deviation; Relative Amplitude - Normalized Maximum Derivative - TR (Time Reversibility); Kurtosis	Quadratic Discriminant Analysis: - Sensitivity: 84.3% - Specificity: 97.0% - Positive predictive value: 94.8 % - Negative Predictive Value: 90.6%
Naeem et al., 2014[143]	Compare linear parameters and non-linear parameters with neural networks	TPEHG database: 300 records of pregnant subjects (262 term and 38 preterm)	Band-pass: - 0.3 to 3 Hz	- Mean power frequency - RMS - Peak and median frequencies of the power spectrum - Time reversibility - Approximate entropy - Correlation dimension - ANN (Artificial Neural Network)	With ANN features the non-linear parameters present a better performance than the linear ones
Fergus et al., 2015[144]	Detect preterm births through EHG signals	TPEHG database: 300 records of pregnant subjects (262 term and 38 preterm)	Band-pass: - 0.34 to 1 Hz. Fs: 20 Hz	- SMOTE - Radial Basis Function Neural Network, using Linear Discriminant Analysis Forward Features: - SE; Waveform Length	Radial Basis Function Neural Network: - 85% sensitivity - 80% specificity - 90% AUC - 17% mean error rate

Document	Research purpose	Used data	Band-pass and Fs	Methods and features	Results
				- Log Detector; Variance	
Smrdel et al., 2015[72]	Estimate EHG signal with AAR (Adaptive Autoregressive) method	TPEHG dataset: 300 EHG signals (262 term and 38 preterm)	Band-pass: - 0.08 to4 Hz; - 0.3 to 4 Hz - 0.3 to 3 Hz; - 0.34 to 1 Hz Fs: 20 Hz	- AAR - Mean power spectrum - Median frequency	Accuracy: 86 % for all records
Lemancewicz et al., 2016[145]	Compare results from FFT (Fast Fourier Transform), WT and AR (Autoregressive modeling)	60 patients between the 24th and 34th week of pregnancy	Band-pass: - 0.24 to 4 Hz Fs: 200 Hz	- FFT - WT - AR - Peak Frequency Features: - Approximate Entropy - Lempel–Ziv complexity measure	Dominant frequencies: - FFT: 0.359 – 0.886 Hz - WT: 0.317 – 0.824 Hz - AR: 0.317 - 0.824 Hz
Acharya et al., 2017[146]	Predict preterm births using EMG signals	TPEHG dataset: 300 EHG signals (262 term and 38 preterm)	Band-pass: - 0.3 to 3 Hz - first and last 180 s length of signals were removed Fs: 20 Hz	Empirical Mode Decomposition and Wavelet Packet Decomposition - SMOTE - SVM using RBF - Adaptive Synthetic Sampling Approach for Imbalanced Learning Features: - Mean Absolute Deviation - Mean Energy - Mean Teager-Kaiser Energy - SE; Standard Deviation	SVM RBF Classifier: - Accuracy: 96.25% - Sensitivity: 95.08% - Specificity: 97.33% - AUC: 0.962
Borowska et al., 2017[147]	- Evaluating the performance	20 patients between the 24th and the 28th week	No pre-processing Fs: 500 Hz	- Recurrence Quantification Analysis	Recurrence Quantification Analysis with SVM:

Document	Research purpose	Used data	Band-pass and Fs	Methods and features	Results
	Of Recurrence Quantification Analysis to predict the risk of threatening preterm birth - Finding a feature extractor that generates a feature vector from the EHG signals - Applying PCA to map the data set to a feature set	of pregnancy with threatened preterm labor		- PCA (Principal Component Analysis) - SVM classifications (multiclass SVM) - Mann-Whitney test	- Accuracy: 79.27% PCA-SVM: - Accuracy: 83.32%
Altini et al., 2017[148]	Detect labor combining EHG and HR (Heart Rate) data	37 women (19 labor and 18 non-labor)	Band-pass: - 0.1 to 4 Hz Fs: 128 Hz	- Random forests Features: - RMS - Mean of EHG and HR - Power of EHG signal - GA (Gestational Age)	Accuracy: - With EHG, GA and HR data: 87 % - EHG features: 71 % - HR features: 71 % - EHG and HR features: 82 %

Attachment 2 – Publications with contractions signals

Document	Research purpose	Used data	Band-pass and Fs	Methods and features	Contractions detection method	Results
Diab et al., 2009 [149]	Unsupervised classification method applied to the EMG signal of uterine contractions for the detection of preterm birth	102 contractions from 25 women: 7 with term deliveries and 18 with preterm deliveries	Band-pass: - 0.2 to 8 Hz Fs: 16 Hz	- Wavelet decomposition - USCM (Unsupervised Statistical Classification Method) - Competitive Neural Network Method - Fisher's test	Wavelet decomposition	USCM: - 83.3% of separation between preterm deliveries and term deliveries
Hassan et al., 2010[150]	Analyze the synchronization of uterine electrical activity by using the "wavelet coherence" method	3 women in labor - Bipolar signal	Band-pass: -low pass cut-off frequency of 100 Hz. Fs: 200 Hz	- Wavelet coherence method - Multiple Window Time Frequency Analysis - Frequency-dependent correlation coefficient - Time Varying Causal Coherence Function based on the multivariate autoregressive model	Manual segmentation	Wavelet coherence successfully detected the correlations of EHG activity and separated them from the uncorrelated baseline noise recorded between bursts
Moslem et al., 2011[64]	Classification of multichannel EMG	32 women: - 22 during pregnancy - 7 during labor - 3 during both pregnancy and labor - Vertical bipolar signals	Band-pass: - 0.1 to 3 Hz - Signals were normalized into same amplitude Fs: 200 Hz	- ANN (Artificial Neural Network) based on RBF Features: - Power of the contraction - Median Frequency	Manual segmentation	Overall classification accuracy: 82.65 % Correct Classification Rate: - Pregnancy contractions: 93% - Labor contractions: 72.3%

Document	Research purpose	Used data	Band-pass and Fs	Methods and features	Contractions detection method	Results
Diab et al., 2012[61]	Study of sensitivity analyses and robustness of non-linearity measures	49 women: - 36 during pregnancy - 13 during labor	Fs: 200 Hz (signals from Iceland) and 256 Hz (signals from France)	- TR - SE - Lyapunov Exponents - Delay Vector Variance	Manual segmentation (115 labor bursts and 174 pregnancy bursts)	TR: - AUC: 0.842 - Specificity: 0.721 - Sensitivity: 0.860
Diab et al., 2012[60]	Detect labor by classifying EMG signals into 2 classes: pregnancy and labor	213 uterine EMG signals (137 pregnancy and 76 labor signals)	Band-pass: - 0.1 to 3 Hz Fs: 200 Hz	- Normalized Wavelet Packets Energies - Wavelet Packet Transform - PCA - ANN with a Gaussian RBF kernel	Manual segmentation	Correct Classification Rate: - Pregnancy contractions: 96.3% - Labor contractions: 71.0 % - All contractions: 87.3 %
Alberola-Rubio et al., 2013[3]	- Study the signal quality obtained from monopolar, bipolar and Laplacian techniques in EHG recordings - Assess the ability to detect uterine contractions	22 recordings on women hospitalized for spontaneous or induced labor - Bipolar signals	Band-pass: - 0.05 to 35 Hz Fs: 500 Hz	- Contraction Consistency Index - Signal-to-noise ratio - Rules of manual segmentation: - Significant rise in signal amplitude with respect to the basal period. - Duration longer than 30 s. - Signal morphology typical of electrophysiological changes.	Manual segmentation	Contraction Consistency Index: - TOCO: 63.77% - Monopolar EHG recordings (M1): 93.39% - Laplacian EHG recordings: 89.3% Signal-to-noise ratio: - Mean values: 5.1-7.6 dB

Document	Research purpose	Used data	Band-pass and Fs	Methods and features	Contractions detection method	Results
Alamedine et al., 2013[151]	Reduce the number of features in the contraction's classification	48 women: - 32 during pregnancy - 16 during labor - Vertical bipolar signals (Only Vb7 was used)	Band-pass: - 0.16 to 3 Hz Fs: 200 Hz	- LDA - QDA (Quadratic Discriminant Analysis) - SFS (Sequential Forward Selection) - Binary Particle Swarm Optimization - K-Nearest Neighbors	Manual segmentation based on the tocodynamometer signal recorded simultaneously (133 contractions bursts and 133 labor bursts)	Correct classification using LDA: - SFS with QDA: 84.96% - SFS with K-Nearest Neighbors: 84.96% Correct classification using QDA: - BPSO with QDA: 87.47%
Alamedine et al., 2014[67]	Selection method to choose the best parameters to classify contractions EHG signal for the detection of preterm labor	27 women: - 16 during pregnancy - 11 during labor - Vertical bipolar signals	Band-pass: - 0 to 3.125 Hz Fs: 200 Hz	- Wavelet packet decomposition - Jeffrey divergence - Time reversibility - SE - H^2 (Nonlinear Correlation coefficient) - Lyapunov Exponents - VarEn (Variance entropy)	Manual segmentation (106 contractions bursts and 106 labor bursts)	- Mean: 0.1852 - Standard deviation: 0.1055 Methods selected: - Threshold1: H^2, SE, VarnEn and decile 1 - Threshold2: VarEn
Diab et al., 2015[152]	Effects of signal filtering on the sensitivity of TR, SE, LE and DVV	49 women - Vertical bipolar signal	Band-pass: - 0.1 to 0.3 Hz - 0.3 to 1 Hz - 0.3 to 3 Hz Fs: 200 Hz	- TR - SE - LE (Lyapunov Exponents) - DVV (Delay Vector Variance)	Manual segmentation (174 contractions bursts and 155 labor bursts)	AUC: No filtering: - TR: 0.862; - SE: 0.481 - LE: 0.757; - DVV: 0.632 Band-pass [0.1-0.3 Hz]: - TR: 0.874; - SE: 0.780 - LE: 0.603; - DVV: 0.725

Document	Research purpose	Used data	Band-pass and Fs	Methods and features	Contractions detection method	Results
Bajlekov et al., 2015[42]	Improve the reliability of contraction detection	9 women (Data from two patients were discarded due to artifacts in the EHG or IUP measurements)	Fs: 20 Hz	- Gaussian likelihood function - Template-matching algorithm - Teager energy	Manual segmentation	Krippendorff's α coefficient: α = 0.999
Chen et al., 2017[153]	Method for feature extraction and classification of EHG between pregnancy and labor group	Icelandic 16-electrode EHG Database: 122 EHG recordings (112 pregnancy recordings and 10 labor recordings)	Band-pass: - 0.1 to 3 Hz Fs: 200 Hz	- HHT (Hilbert-Huang Transform) - Extreme learning machine - Intrinsic Mode Functions Features: - Maximum amplitude	Manual segmentation (150 contractions bursts and 150 labor bursts)	Extreme learning machine with Intrinsic Mode Functions: - Accuracy: 88.00% - Sensitivity: 91.30% - Specificity: 85.19% - ROC: 0.88
Altini et al., 2017[148]	Detect labor combining EHG and HR data	37 women (19 labor and 18 non-labor)	Band-pass: - 0.1 to 4 Hz Fs: 128 Hz	- Random forests Features: - RMS - Mean of EHG and HR - Power of EG signal - GA	Features representative of labor (windows of 20 minutes)	Accuracy: - With EHG, GA and HR data: 87 % - EHG features: 71 % - HR features: 71 % - EHG and HR features: 82 %
Benalcazar Parra et al., 2017[51]	Characterize and compare the response of uterine myoelectrical activity to labor induction drugs for different labor induction outcomes	72 women	Band-pass: - 0.1 to 4 Hz Fs: 20 Hz	- Welch PSD in the range of 0.2 to 1 Hz	Manual segmentation	Shift of the EHG-Bursts energy content toward higher frequencies was identified vaginal delivery and cesarean section after achieving active phase of labor groups for all deciles

Attachment 3 – Evolution of pregnancy throughout the gestational weeks. Survival rate of preterm infants and birth classification according to GA (Miscarriage, Extremely preterm, Very preterm, Late preterm, term and Post-term)[19]

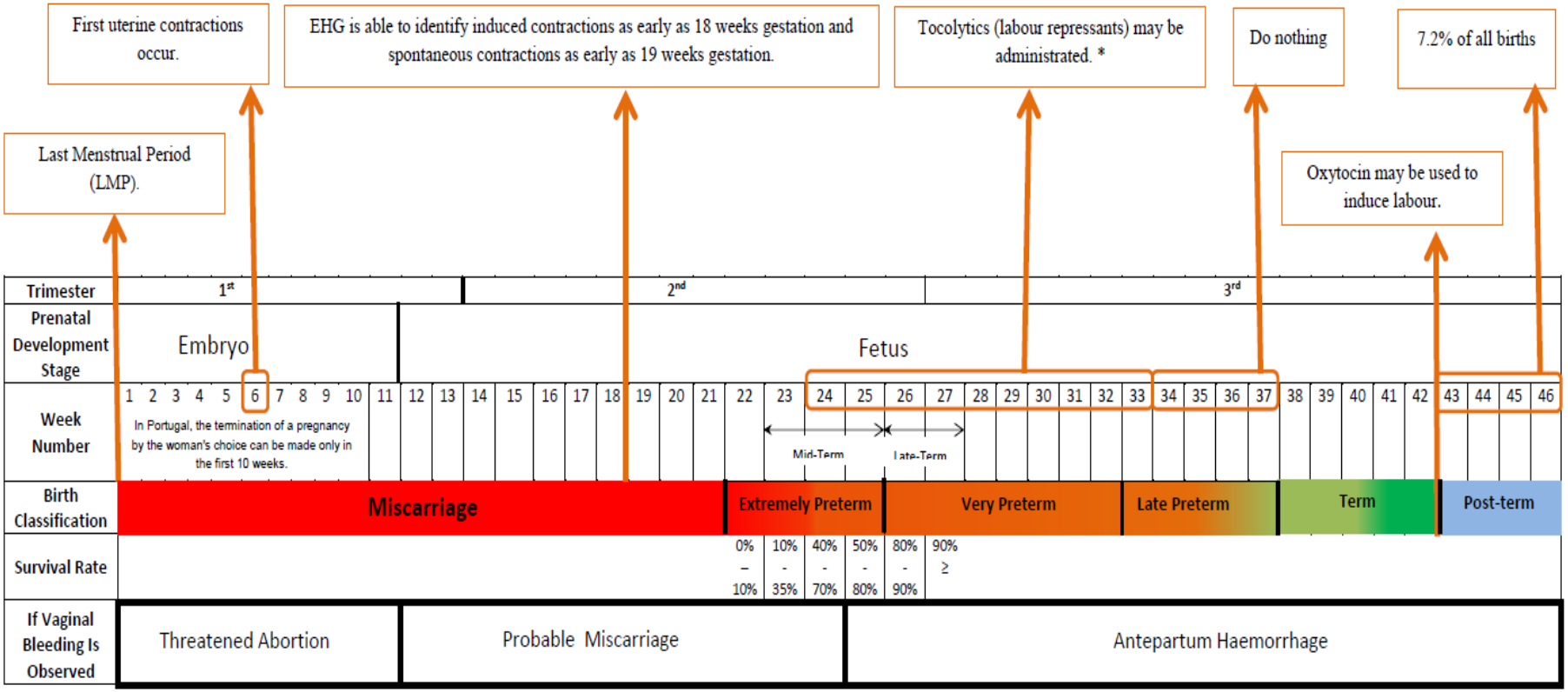

*Labour repressants (Tocolytics): These oxytocin antagonists delay delivery by 2-7 days but carry side effects. To avoid respiratory distress syndrome in the fetus, glucocorticoids may be used to stimulate the production of surfactant in the lungs.

Attachment 4 – Table of uterine contractions characteristics adapted from AMBOSS[62]. The text highlighted in grey is not part of the original table

		Occurrence	Characteristics
Uterine contractions during pregnancy	**Alvarez waves**	Physiological; occurs after 20 weeks of pregnancy	• Low intensity, high occurrence rate • As the frequency of the Braxton-Hicks contractions increases, the Alvarez waves between them decrease • Occurrence: 1 or 2 per minute • Localized in the tissue focus where it was generated • Difficult to detect using TOCO[53] • Associated with normal uterine activity and uterine hyperactivity[18]
	Braxton Hicks contractions	Physiological; occur after 20 weeks of pregnancy	• High intensity • Tetanic (sustained muscle contraction) in nature • Diffuse abdominal tightening • Last for 1 minute at the most • Occurrence: typically ≤ 2 times / hour; may become more frequent near term (false labor) • May occur unnoticed and are usually not painful • Usually considered as myometrium training for labor • May be induced by physical and sexual activity, touch, fetal movements • Associated with a decrease in the fetal hear rate[57]
	LDBF waves	Physiological; occur after 20 weeks of pregnancy	• Long duration (> 4 minutes) • Low occurrence rate • Associated with uterine hypertonia • Uterine hypoxia inductor[56]
	Leman waves	Unknown	• Frequency spectrum similar to the contractions but with lower amplitude • Normally ignored in the EHG studies[17]

False labor		3–4 weeks before birth	• Uncoordinated uterine contractions of moderate intensity (helps with fetal positioning) • Cervical changes are absent • Contractions do not increase in occurrence, intensity, or duration • Easily relieved with analgesia
Pre-labor		3–4 days before birth	• Irregular contractions of high intensity, which occur every 5–10 min shortly before phase 1 begins. They are responsible for correctly positioning the fetal head in the pelvis.
Labor	**Stage 1: cervical dilation and effacement**	Onset of normal childbirth.	• Coordinated, regular, rhythmic contractions of high intensity; occur approximately every 10 minutes. Shortly before stage 2, they occur every 2–3 min. These contractions are responsible for cervical dilation.
	Stage 2: fetal expulsion	After complete cervical dilation and effacement	• Coordinated and regular contractions of high intensity; occur approximately every 4–10 min and are responsible for fetal expulsion. Towards the end of the stage, they occur very often (every 2–3 minutes) and are of higher intensity (pressure greater than 200 mm Hg).
Stage 3: placental expulsion or afterbirth		Several minutes after childbirth	• Irregular contractions of very low intensity, which force the placenta through the vaginal canal within 30 min after fetal expulsion
Afterpains		Several days after childbirth	• Irregular contractions of varying intensity, which cause uterine involution and bleeding cessation